Divergent patterns of healthy aging across human brain regions at single-cell resolution reveal links to neurodegenerative disease

Megan F. Duffy[1], Jinhui Ding[2], Rebekah G. Langston[1], Syed I. Shah[3,4], Mike A. Nalls[3,4], Sonja W. Scholz[5,6], D. Thad Whitaker[1], Pavan K. Auluck[7], Stefano Marenco[7], J. Raphael Gibbs[2], Mark R. Cookson[1]*

[1] Cell Biology and Gene Expression Section, Laboratory of Neurogenetics, National Institute on Aging, National Institutes of Health, Bethesda, Maryland, USA 20892

[2] Computational Biology Group, Laboratory of Neurogenetics, National Institute on Aging, National Institutes of Health, Bethesda, Maryland, USA 20892

[3] Data Tecnica International LLC, Washington, DC, USA

[4] Center for Alzheimer's and Related Dementias, National Institutes of Health, Bethesda, MD, USA

[5] Neurodegenerative Diseases Research Unit, National Institute of Neurological Disorders and Stroke, Bethesda, MD, USA

[6] Department of Neurology, Johns Hopkins University Medical Center, Baltimore, MD, USA

[7] Human Brain Collection Core, Division of Intramural Research, National Institute of Mental Health, NIH, Bethesda, MD, 20892, USA

* Correspondence: cookson@mail.nih.gov

Graphical Abstract

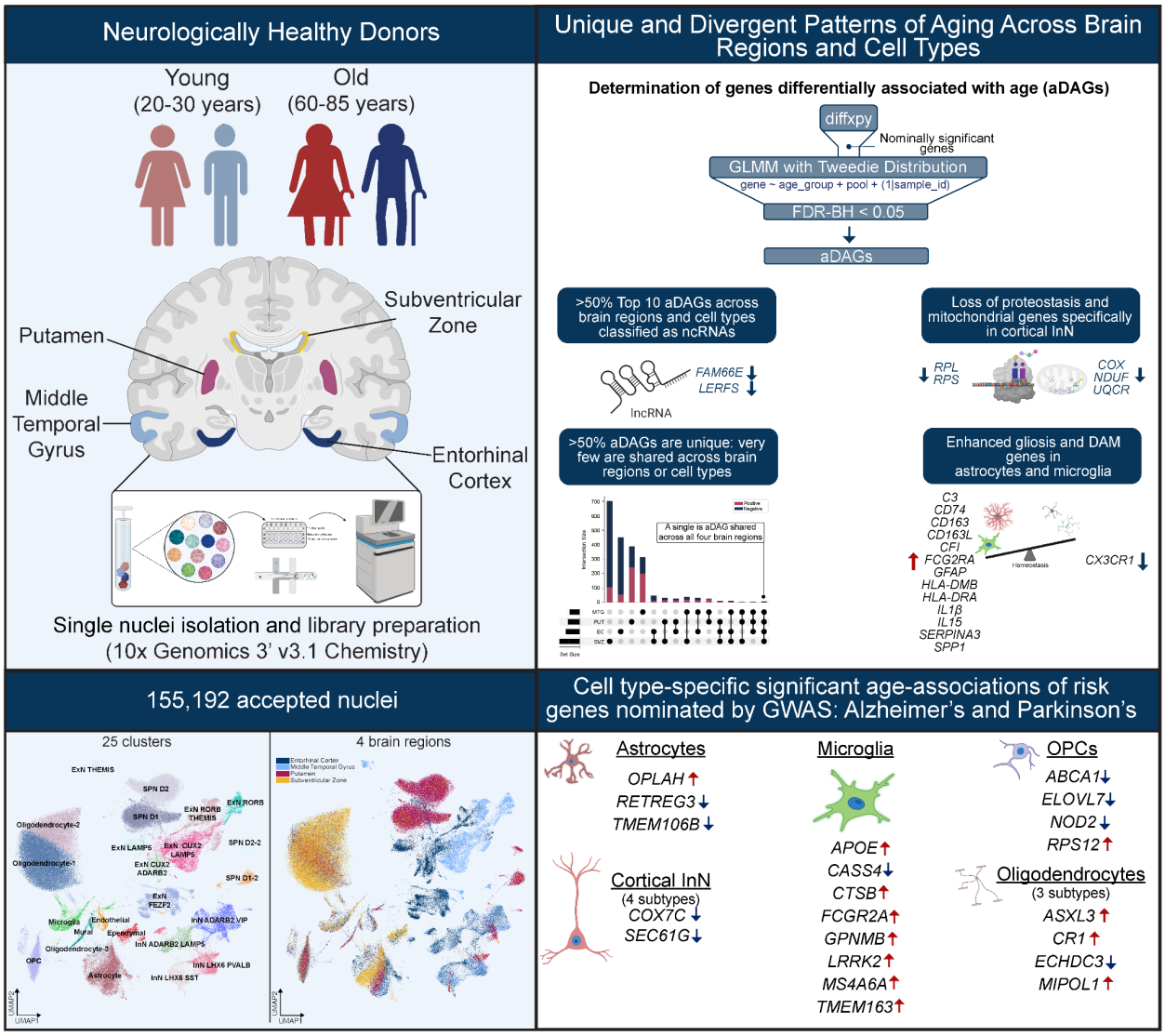

*Created using Biorender.com

Highlights

- Establishment of a single nuclei atlas of human aging in four brain regions
- Each region and cell type exhibits a unique aging-associated transcriptome signature
- Gene expression changes occur in absence of overt cell loss and are categorically unique across cell types
- Neurological disease-associated genes have age-associated expression patterns in specific cell types in the context of healthy aging

Abstract

Age is a major common risk factor underlying neurodegenerative diseases, including Alzheimer's disease, Parkinson's disease, and amyotrophic lateral sclerosis. Previous studies reported that chronological age correlates with differential gene expression across different brain regions. However, prior datasets have not disambiguated whether expression associations with age are due to changes in cell numbers and/or gene expression per cell. In this study, we leveraged single nucleus RNA-sequencing (snRNAseq) to examine changes in cell proportions and transcriptomes in four different brain regions, each from 12 donors aged 20-30 years (young) or 60-85 years (old). We sampled 155,192 nuclei from two cortical regions (entorhinal cortex and middle temporal gyrus) and two subcortical regions (putamen and subventricular zone) relevant to neurodegenerative diseases or the proliferative niche. We found no changes in cellular composition of different brain regions with healthy aging. Surprisingly, we did find that each brain region has a distinct aging signature, with only minor overlap in differentially associated genes across regions. Moreover, each cell type shows distinct age-associated expression changes, including loss of protein synthesis genes in cortical inhibitory neurons, axonogenesis genes in excitatory neurons and oligodendrocyte precursor cells, enhanced gliosis markers in astrocytes and disease-associated markers in microglia, and genes critical for neuron-glia communication. Importantly, we find cell type-specific enrichments of age associations with genes nominated by Alzheimer's disease and Parkinson's disease genome-wide association studies (GWAS), such as apolipoprotein E (*APOE*), and leucine-rich repeat kinase 2 (*LRRK2*) in microglia that are independent of overall expression levels across cell types. We present this data as a new resource which highlights, first, region- and cell type-specific transcriptomic changes in healthy aging that may contribute to selective vulnerability and, second, provide context for testing GWAS-nominated disease risk genes in relevant subtypes and developing more targeted therapeutic strategies. The data is readily

accessible without requirement for extensive computational support in a public website, https://brainexp-hykyffa56a-uc.a.run.app/

Keywords

Aging, putamen, entorhinal cortex, middle temporal gyrus, subventricular zone, snRNAseq, neurodegeneration, Alzheimer's, Parkinson's, dementia

Introduction

Age is a common primary risk factor for multiple neurodegenerative diseases (NDDs), including Alzheimer's disease and related dementias (ADRD), Parkinson's (PD), and amyotrophic lateral sclerosis (ALS)[1]. For example, the incidence of AD approximately doubles in five-year increments between 60 and 90 years of age, and the prevalence of ADRD is expected to triple by 2050[2–4]. In this context, identifying the molecular events associated with healthy human brain aging becomes imperative in understanding predisposing conditions for neurodegeneration.

Prior studies used bulk transcriptomic and epigenomic analyses to understand the effects of aging on the human brain. The major themes emerging from these investigations include loss of synaptic gene expression and acquisition of inflammatory signaling networks[5]. Our previous RNA-sequencing (RNA-seq) analysis of the human dorsolateral prefrontal cortex identified networks of gene expression changes with age, including loss of neuronal genes[6]. For example, there was a strong decrease in *SST,* encoding the peptide neurotransmitter somatostatin, in a subset of GABAergic interneurons in the cortex.

Although this literature suggests robust changes in gene expression correlating with age, several aspects of the data remain difficult to interpret. For example, loss of neuronal markers could reflect a loss of neurons and/or changes in gene expression per neuron. Recent development of single-cell methods allows for the identification of cell types and the interrogation of gene expression in each cell type. Here, we applied snRNA-seq to disambiguate cell proportions and gene expression per cell in the context of healthy human brain aging across multiple brain regions. We compared the entorhinal cortex (EC), susceptible to AD pathology[7,8], with another cortical region, the middle temporal gyrus (MTG)[9,10]. We also included the putamen (PUT), affected in Huntington's disease (HD)[11,12] and PD[13–15], and the subventricular zone (SVZ) region permissive for neurogenesis during development, although whether this remains true in

the adult human brain is still contested[16]. We find substantial numbers of brain region- and cell type-specific aging associations in gene expression during healthy aging. However, we also identify novel cell type- and brain region-specific differences in age-associated gene expression relevant to neurodegenerative diseases.

Results

Cell type composition of four brain regions

Our final dataset contained 155,192 nuclei from post-mortem EC (47,566 nuclei), MTG (25,394 nuclei), PUT (46,489 nuclei), and SVZ (35,753 nuclei) from six younger (20-30 years old) and six older (60-85 years old) adults following QC and preprocessing (see **Methods**; **Fig. 1a-c; Supplemental Table 1**). We projected nuclei from all donors and regions into a single UMAP and confirmed each cluster contained nuclei from all donors and both sexes (**Supplemental Fig. 1a-e**).First, we assigned Leiden clusters to general cellular categories (referred to as *broad type*) based on the expression of markers for neurons (*RBFOX3*, *SYP*, *GRIN1*, *GRIA2;* 51.32% of all nuclei), microglia (*CSF1R*, *AIF1*, *P2RY12;* 2.1%), astrocytes (*AQP4;* 7.27%), oligodendrocyte precursors (*PDGFRα*; 4.31%), ependymal cells (*FOXJ1*; 1.83%), and oligodendrocytes (*MBP*; **Fig. 1d-f; Supplemental Fig. 1f-h**). Following *broad type* classification, we examined the diversity of neuronal subtypes using a combination of canonical markers, differential expression, brain region origin, and previously published snRNAseq datasets[17,18]. We assigned each cell subtype according to its 1) broad type marker, 2) subtype marker, and 3) secondary cluster-specific marker (**Fig. 1d**).

Inhibitory neurons (InN) were broadly identified by expression of genes encoding glutamate decarboxylase 1 and 2 (*GAD1*, *GAD2)* and represented ~31.2% of recovered nuclei (**Fig. 1d-f; Supplemental Fig. 1h**). Cortical InNs were split by expression of either *ADARB2* or

LIM Homeobox 6 (*LHX6*). *ADARB2*$^{+}$ InNs were subdivided by expression of either *LAMP5* (2.07%) or vasoactive intestinal peptide (*VIP*, 4.92%). *LHX6*$^{+}$ InN subtypes were further determined by expression of either somatostatin (*SST*, 1.89%) or parvalbumin (*PVALB*, 2.94%). Subcortical *GAD1*$^{+}$ and *GAD2*$^{+}$ InN (21.59%) consisted of putaminal spiny projection neurons (SPN), which were further divided by expression of dopamine receptor D1 (*DRD1*, 9.91%) or D2 (*DRD2*, 9.85%). We also identified subsets of each SPN subtype. SPN D1-2 neurons (1.54%) coexpressed *ADARB2*, while SPN D2-2 neurons (0.3%) coexpressed adenosine A2a receptor (*ADORA2A;* **Fig. 1d**).

Excitatory neurons (ExN), identified by expression of genes encoding vesicular glutamate transporters 1 and 2 (*SLC17A6* and *SLC17A7;* **Fig. 1d, Supplemental Fig. 1h**), represented 18.4% of recovered nuclei. Iterative clustering subdivided these into seven distinct clusters, which were primarily restricted to the EC and MTG (**Supplemental Fig. 1c,h**). ExN clusters were distinguished by differential expression of marker genes related to cortical layers as previously published[17] **(Fig. 1d-f**).

Non-neuronal cells represented nearly half of all recovered nuclei (48.6%) and were found across all brain regions (**Fig. 1f; Supplemental Fig. 1c-d**). Oligodendrocytes separated into 3 clusters, all expressing myelin basic protein (*MBP*) and proteolipid protein 1 (*PLP1*). Although Oligodendrocyte-1 (23.51%) and Oligodendrocyte-2 (8.28%) clusters are directly adjacent in the UMAP space, Oligodendrocyte-1 nuclei displayed higher expression of oligodendrocytic myelin paranodal and inner loop protein (*OPALIN*), which is involved in oligodendrocyte differentiation. Therefore, Oligodendrocyte-1 may represent a less mature subtype than Oligodendrocyte-2. Oligodendrocyte-3 (0.5%) expressed canonical oligodendrocyte markers *MBP* and *PLP1* but were also positive for *GFAP* and *AQP4* and likely represent O2A progenitors (**Fig. 1d-f**).

Diverging patterns of gene expression by brain region in absence of cell type proportion shifts

Due to limitations imposed by bulk RNAseq on interpreting if age-related expression patterns are due to cell type or gene expression changes, we examined whether cell proportions, particularly neuronal and oligodendrocyte subtypes, differed with age. The total number of nuclei recovered from young (78,690) and old (76,502) individuals was similar (**Fig. 2a**). There were no significant differences in cell type proportions with age for most cell types (**Fig. 2b-d**). The one exception was *LAMP5*$^{+}$ ExN, which were poorly recovered in the older age group and represented the most superficial layer of excitatory neurons[17]. However, even this difference was not statistically significant and is likely due to variability across individual donors (**Fig. 2d**). Additionally, the proportion of young versus old nuclei recovered by brain region did not significantly differ with age (**Supplemental Fig. 2a-b**). These results suggest that most aging-associated gene expression differences are not due to cellular proportions changes during aging

We next examined gene-aging associations at the level of brain region. For this analysis, we considered all nuclei within each of the four regions, irrespective of cell type. Using a two-step approach (see **Methods**), we found 2,071 genes exhibiting a significant differential association with age across the SVZ (767), EC (508), PUT (433), and MTG (363; **Supplemental Fig. 2c; Supplemental Table 2**). Most aging differentially associated genes (aDAGs) were unique to each brain region, with a single gene negatively associated with age (*AC240274.1*) intersecting all four regions. The SVZ and EC harbored more aDAGs with negative age associations than the PUT and MTG (641, 435, 157, 17 negative aDAGs, respectively), where >50% of significant genes were positively associated with aging. Of note, many aDAGs in each brain region were pseudogenes or long noncoding RNAs (lncRNAs). Of the top protein-coding

genes most strongly associated with age at the brain region level, *HLA-DQA2*, *LILRA6*, *CD209*, *TNFSF14*, *TNFRSF10C*, *CCL3L1*, and *MUCL3* were notable in that they have established roles in the immune response (**Supplemental Fig. 2d**).

We next documented all gene-age associations at the level of *broad types* **(Supplemental Table 2)**. Of 2,071 brain region aDAGs, 923 were also significant at the broad cell type level (**Supplemental Table 3**). At this resolution, cortical InN exhibited the most significant number of aDAGs, totaling 2,684 genes **(Supplemental Table 2; Supplemental Fig. 2e**). Many of the top aDAGs are lncRNAs or pseudogenes (**Supplemental Fig. 2f**). For example, the lncRNAs *FAM66E* and *LERFS* were decreased with age in all cell types except endothelial, ependymal, and mural cells. While a small subset of aDAGs was shared between ≥ 2 broad types, more than half of aDAGs were unique to each broad cell type.

Negative association of protein translation and mitochondrial genes in cortical inhibitory neurons with age

We next examined all gene-age associations by cluster-specific cell types beginning with cortical InN and subcortical SPN broad classes, each composed of 4 cluster-specific cell types (**Fig. 3a**). We observed diverging directions of gene-aging associations between cortical InNs and subcortical inhibitory SPNs (**Fig. 3b**). Surprisingly, only 33 aDAGs were shared between the four cortical InN subtypes (**Fig. 3b**).

We next examined the top five aDAGs in each direction for cortical and subcortical InN subtypes. Similar to observations at the brain region and broad cell type levels, we noted an abundance of differentially associated lncRNAs, including *FAM66E* in all cortical InN subtypes and SPN D1-2 and D2 subtypes (**Supplemental Fig. 3a**). We next performed gene set enrichment analysis (GSEA) on both broad type and cluster-specific significant aDAG sets (**Supplementary Information**). Using the broad type cortical InN list of 2,864 aDAGs, we

identified a large number of ontogeny enrichments clustered in themes of protein targeting and translation, gene expression, ncRNA processing, and mitochondrial electron transport (**Fig. 3c; Supplementary Information**). We then examined which genes within these GO term sets were differentially associated with age by plotting the coefficient estimate of enriched genes in different cell types (**Fig. 3d, h, k**). In cortical InNs, there was a striking negative association for ribosomal protein-coding genes in the GO term 'protein targeting to ER (GO:0045047),' particularly in the *LHX6*$^{+}$*PVALB*$^{+}$ InN cluster, but not in subcortical inhibitory SPNs (**Fig. 3d**). Several genes in this category were similarly negatively associated with age across multiple cortical InN subtypes, such as ribosomal protein S7 (*RPS7*) and SEC61 translocon subunit gamma (*SEC61G*; **Fig. 3d,f**). In contrast, many other genes in this category were negatively associated with age in a specific cell subtype, such as ubiquitin A-52 residue ribosomal protein fusion product 1 (*UBA52*) in *LHX6*$^{+}$*PVALB*$^{+}$ InNs only (**Fig. 3d-e,g**).

Given the strong negative association of these genes with age in cortical InNs, we next asked if these cells exhibited differential expression of these genes compared to other neuronal cell types in younger individuals. Surprisingly, young cortical InNs have lower expression of ribosomal protein-coding genes than excitatory neurons and subcortical inhibitory SPNs (**Fig. 3e**), showing that the decrease in protein synthesis genes with age in cortical InNs is not due to higher expression than other cell types.

In contrast to the abundance of ontology enrichments observed in cortical InNs at the level of broad cell type, only cluster-specific SPN D1-2 neurons exhibited enrichments (**Supplementary Information**). Notably, enrichment categories differed, and the enrichments' strength was substantially lower than those observed in cortical InNs. Specifically, aDAGs in SPN D1-2 neurons fell under molecular function enrichment categories of voltage-gated sodium channel activity, calcium channel genes, and TAP1 binding activity (**Fig. 3k–m**). Notably, all SPN D1-2 aDAGs falling under enrichment categories were negatively associated with age, except for *HLA-F* (**Fig. 3l-m**).

Additionally, we examined the broad type- and cell-subtype gene enrichments for terms in the “Aging” and “Disease Perturbations” from GEO gene sets, subset by genes increased or decreased in expression with age or disease. Both cortical and subcortical InN-specific negative aDAGs significantly overlapped with genes previously shown in animals and humans to have decreased expression in aged cortical and hippocampal tissue. InN-specific negative aDAGs additionally overlapped with “Disease Perturbations (Down)” from both animal and human datasets including senescence, dystonia, ALS, and HD (**Supplemental Fig. 3b-c; Supplementary Information**).

Excitatory neurons have categorically different and fewer aDAGs compared to inhibitory neurons

We next examined ExNs, which had substantially fewer aDAGs (1,060) compared to InNs at the broad type level (**Supplemental Table 2**). ExN were clustered into seven subtypes (**Fig. 4a**). We observe the most aDAGs in *FEZF2*$^+$ ExN representing layers 4-6 of the cortex (1250 total, 806 unique; **Supplemental Table 2**; **Fig. 4b**)[17]. Many top aDAGs were shared between ExN subtypes, including Rhomboid Like 3 which was previously documented to increase with aging in human frontal cortex[6,19] (*RHBDL3;* **Supplemental Fig. 4a-b**). Interestingly, in the case of some related genes like calcium channel regulators *STAC* and *STAC2*, we observed association in opposing directions, sometimes within the same cell type cluster (**Supplemental Fig. 4a, c-d**).

Two striking differences between broad cortical ExNs and InNs were apparent. First, ExNs had many more positive aDAGs with age (**Fig. 4b**). Second, we did not observe any significant ExN broad type enrichments (**Supplementary Information**). Thus, we next examined each of the seven subtypes of ExN and found significant enrichments in *LAMP5*$^+$ (layers 1-2), *THEMIS*$^+$ (layer 5-6) and *RORB*$^+$ ExNs (layers 3-6; **Fig. 4c**; **Supplementary**

Information)[17]. Surprisingly, although *FEZF2*+ ExN had the highest abundance of aDAGs, we did not observe any gene set enrichments, suggesting broad, non-specific effects of aging on ExN. Notably, ExN and InN enrichment categories differed (**Fig. 3c, 4c**). ExN subtype enrichment pathways included 'axonogenesis (GO:0007409)' and 'neuron projection (GO:0043005)' as well as cell-cell adhesion pathways (**Fig. 4c-e**). Specifically, we observe differential association of semaphorins, SLIT guidance ligands and SLIT and NTRK-like family members, cadherins, and ephrins (**Fig. 4d-e; Supplemental Table 4**). Interestingly, while some enrichment pathways are shared between ExN subtypes, many aDAGs within these pathways differ between ExN subtypes (**Fig. 4d**). In contrast to the negative aDAGs observed in cortical InN, the directionality of age-related aDAGs in ExN subtypes was mixed, which may be due to less robust and more heterogeneous expression of marker genes than InN. Given the general decrease in protein translation-related genes observed in cortical InNs, we wanted to see if cortical ExNs also displayed any decrease in those same genes, despite the absence of enrichment for this category. With the exception of *RPS5* in *FEZF2*$^{+}$ ExN, we did not observe any 'protein targeting to ER (GO:0045047)' genes differentially associated with age in ExN (**Fig. 4f**).

ExN subtype aDAGs significantly overlapped with "Aging and Disease Perturbations" from GEO gene sets. Of particular relevance: young vs. aged human frontal cortex, AD, HD, and Lewy Body Dementia (**Supplemental Fig. 4e, Supplemental Fig 7f; Supplementary Information)**. Collectively, these results suggest that aging differentially affects ExN and InN in the number and strength of aDAGs and in the functional categories to which those aDAGs belong.

OPC-specific negative association of myelination transcription factors with aging in absence of changes in oligodendrocyte lineage cell proportions

Many studies have documented aging-associated decreases in white matter volume and myelin integrity with age[20,21]. Therefore, we investigated cell-type proportions and aDAGs in oligodendrocyte lineage cell types (**Fig. 5a**). Unexpectedly, we did not observe a significant shift in oligodendrocyte lineage cell proportions with age overall or within brain regions (**Fig. 5b, Supplemental Table 5**). Therefore, we next examined the top aDAGs and associated enrichments across these cell types. Similar to previous observations, >50% of top aDAGs in either direction are noncoding (**Supplemental Fig. 5a**). Only five aDAGs shared between mature oligodendrocytes and three aDAGs shared across all four cell types (**Fig. 5c**).

We next examined the effect of age on CNS myelination genes derived from the GO term “central nervous system myelination (GO:0022010)” and several of the most abundantly expressed myelination genes (*MBP*, *PLP1*, *MOBP* and 2',3'-cyclic nucleotide 3' phosphodiesterase *CNP*). In OPCs, we observed a strong negative association of Hes family bHLH transcription factor 5 (*HES5*), a transcription factor regulating myelination, and weaker negative associations of SRY-box transcription factor 10 (*SOX10*) and teneurin transmembrane protein 4 (*TENM4*, **Supplemental Fig. 5b**). Surprisingly, we observed very weak negative associations of *MBP* in oligodendrocytes as a broad type (coefficient est.= -0.04, FDR-BH p=9.26x10^{-4}, SE= 0.009) and in cluster-specific Oligodendrocyte-1 coefficient est.= -0.04, FDR-BH p=4.03x10^{-4}, SE=0.009) and Oligodendrocyte-2 (coefficient est. = -0.02, FDR-BH p=7.61x10^{-5}, SE=0.005). PLP1 also had a weak association with age in only Oligodendrocyte-2 (coefficient est = -0.06, FDR-BH p= 2.02x10^{-3}, SE=0.01; **Supplemental Fig. 5b**). MOBP and CNP did not have a significant association with age in any cell subtype (**Supplemental Table**

4). We next investigated gene set enrichment for oligodendrocytes as a broad type followed by each oligodendrocyte subtype. Mature oligodendrocyte aDAGs were only enriched for the “GO cellular component: cell-cell junction (GO:0005911)” category (**Supplementary Information)**. However, when we analyzed oligodendrocyte subtype-specific aDAGs, we observed enrichments for all subtypes **(Supplementary Information**; **Fig. 5d**). We examined aDAGs falling under the GO cellular component category “cell-cell junction (GO:0005911)” since this gene set was significant for both OPCs and Oligodendrocyte-1 (**Fig. 5d**). Among significant aDAGs in this category are cadherins and catenins (**Fig. 5e,i**). Interestingly, most aDAGs in this shared enrichment category differ between the two cell types, with more OPC aDAGs showing a negative association with age (**Fig. 5e**).

OPC aDAGs were also enriched for genes in GO: biological process “axonogenesis (GO:0007499)” and “KEGG: Glutamatergic synapse,” the majority of which had negative associations with age (**Fig. 5f-g**). We observed a negative association of axonogenesis gene families, including semaphorins, contactins, and ephrins (**Fig. 5f-j**). Notably, these gene families were also differentially associated with age in subsets of ExNs (**Fig. 4d**). Under “KEGG: Glutamatergic synapse”, we observed negative associations with guanine nucleotide-binding protein subunit genes, G protein-activated inward rectifier potassium channel 1, and glutamate receptors (**Fig. 5g,k**). Oligodendrocyte-2 enrichments consisted of one-carbon metabolism genes with mixed directionality (**Fig. 5h,l**). Additionally, we observed aDAGs in OPCs and oligodendrocyte subtypes populated numerous enrichments associated with Aging and Disease Perturbations from GEO gene sets. The majority of these enrichments overlapped with human cancer gene sets, such as astrocytoma, glioblastoma, and oligodendroglioma. We additionally observed overlap with gene sets from aging mouse and human brain, and human-specific AD, MS, PD, and bipolar disorder (**Supplemental Fig. 5c**).

Inflammation-associated genes and disrupted fractalkine genes in microglia and astrocytes

Converging evidence from human genetics and animal models has demonstrated that inflammation can act as a risk factor for aging-related neurodegenerative diseases[22–25]. Therefore, we next investigated top aging aDAGs and GO enrichments in microglia and astrocytes. Of the 797 total microglial aDAGs and 902 astrocyte aDAGs (**Supplemental Table 2**), <10% are similarly differentially associated with age between the two cell types (**Supplemental Fig. 6a-b**). However, we noted aDAGs in both cell types share similar ontogeny enrichments for aging gene sets from human frontal cortex and disease gene sets from related human neurodegenerative disorders, including AD, dystonia, multiple sclerosis (MS), Lewy body dementia (LBD) and HD (**Fig. 6a,f**).

Several complement pathway genes were positively associated with age in astrocytes; specifically *C1S*, *C1RL*, *C1R*, *CFI*, and *C3*[26] (**Fig. 6a-e**). C3 is particularly interesting given that it is most abundantly expressed in microglia but only has a differential association with age in astrocytes. Other notable reactive astrocyte genes with significant, age-related positive associations include *CIITA*, *GFAP*, *HLA-E*, and *IL1R1*[27] (**Fig 6b**). While we failed to observe enrichments for biological process categories related to immune response in microglia, we did note significant overlap with gene sets from aged human frontal cortex, dendritic cells, and CD4+ T lymphocytes (**Fig. 6f**). Immune response genes previously documented as increased in aging and/or neurodegeneration were also positively associated with age in microglia in this dataset, notably *IL-15*[28,29], *HLA-DMB*[26], *IL-1β*[22,26,30,31], and *TLR2*[26,32–34] (**Fig. 6g,k-l**).
We also observed positive associations for several disease-associated microglia (DAM) genes[35], specifically *CD74*, *SPP1*, and *APOE* (**Fig. 6h-j**). Finally, we observed a negative association of fractalkine receptor gene *CX3CR1* in microglia and its ligand (*CX3CL1*) in

excitatory, inhibitory, and SPN-D1 neurons (**Fig. 6g, Supplemental Table 4**). This ligand-receptor interaction has been studied extensively in animal models of neurodegeneration and suggested to suppress the production of proinflammatory cytokines[36]. Our results also suggest that neuron-glia signaling may be disrupted with age, which may contribute to immune dysregulation.

Senescence

Accumulation of senescent cells has been suggested to contribute to age-related neurological decline, which is particularly problematic for the CNS given the long-lived, post-mitotic state of neurons and limited regenerative capacity of the adult brain. We next asked whether there is an increase in the proportions of senescent cells in healthy aged donors. As there is no consensus on a CNS-specific senescence signature, we assessed how multiple senescence-associated gene sets[35,37–39] change with age across brain regions and broad cell types. We also included the DAM gene set, given it is tuned to a specific brain cell type and that we have demonstrated that several of these genes have positive associations with age in microglia (**Fig. 6h**).

At the level of brain region, 11-14% of 3 senescence gene sets exhibit significantly changed expression with age in the PUT, followed by the MTG (1-14% across 3/6 gene sets; **Fig 7a-c**). Of the broad cell types examined, OPCs exhibited expression changes in 5-15% of genes across all 6 senescence gene sets, followed by oligodendrocytes (3-29% across 5/6 gene sets), inhibitory neurons (9-17% across 5/6 gene sets), and microglia (10-43% across 4/6 gene sets; **Fig. 7a-b,d**). Senescence-associated genes, which were also significantly differentially associated with age, were then examined, with the number of significant aging aDAGs increasing in parallel with level of cell type resolution (**Fig 7c-e**).

Additionally, we examined aDAGs from cell types which exhibited significant enrichment

from previous human aging datasets. Interestingly, microglia and astrocytes were significantly enriched for positive aDAGs previously shown to be increased in the aged frontal cortex, including *SERPINA3*, *IFITM2*, *CD163*, and *CD14* (**Supplemental Fig. 7a-e**). In contrast, cell types enriched for genes decreased in aged human frontal cortex, including *KCNF1*, *LY6H*, and *PFN1*, were limited to neurons (**Supplemental Fig. 7f-i**).

Cell type-specific differential associations of genes nearest to GWAS-identified risk loci: Alzheimer's disease and Parkinson's disease

Given that aging is a risk factor for many NDDs, we next examined genes nearest to genome-wide association study (GWAS) risk loci for Alzheimer's disease (AD) and Parkinson's disease (PD). We first examined the baseline mean expression of AD- and PD-associated genes across brain regions and cell types (**Supplemental Fig. 8a-d**). While many genes are broadly expressed across multiple cell types, several exhibit cell type-specificity[40]. Therefore we next examined if these genes exhibited significant associations with age in a brain region- and/or cell type-specific manner.

We detected expression of 110/112 AD GWAS-nominated genes[41] in this dataset (**Supplemental Fig. 8a-b**), of which 52 were significantly differentially associated with age (**Fig. 8a-b**). Of particular interest is apolipoprotein E (*APOE*), variants of which can increase risk for developing late-onset AD (LOAD) and Lewy body dementia. We noted a microglia-specific increase in the percentage of cells expressing *APOE* and concomitant increase in level of expression, as well as a significant positive association with age (coefficient est.=0.41, BH-FDR $p=3.45\times10^{-3}$, SE=0.10; **Fig. 8a-c**). Interestingly, we did not observe a significant age association of *APOE* in astrocytes, where it is abundantly expressed (**Fig. 8b-c; Supplemental Fig. 8b**).

We additionally observed a strong positive association of membrane spanning 4-domains A6A (*MS4A6A*) with age in all brain regions except the putamen (**Fig. 8a**)**.** We note that the positive association of *MS4A6A* at the brain region level is driven by an increase in the number of microglia expressing *MS4A6A*, the strength of its expression in microglia, and a strong positive association with age exclusively in microglia (coefficient est.= 0.96, FDR-BH p=1.36x10^{-8}, SE=0.13; **Figure 8a-b, d**).

Other notable aDAGs include negative age associations of endoplasmic reticulum protein translocation complex gene *SEC61G* and mitochondrial electron transport chain enzyme component cytochrome c oxidase subunit 7C (*COX7C)* in multiple cortical inhibitory neuron subtypes, fatty acid biosynthesis gene *ECHDC3* in oligodendrocytes, and a positive association of complement C3b/C4b receptor 1 (*CR1*) in oligodendrocyte-1 and oligodendrocyte-2 (**Fig. 8b**).

Next, we examined aging associations of 82/87 detected genes nearest to PD GWAS-identified risk loci[42] and observed that 56/82 genes had a significant association with age, most strikingly in OPCs and microglia (**Supplemental Fig. 8c-d; Fig. 8e-f**). Notable genes which exhibited microglia-specific differential associations include cathepsin B (*CTSB*; coefficient est.= 0.20, FDR-BH p=3.14x10^{-3}, SE=0.05) glycoprotein Nmb (*GPNMB;* coefficient est.= 1.40, FDR-BH p=5.57x10^{-4}, SE=0.30), and leucine-rich repeat kinase 2 (*LRRK2*; coefficient estimate: 0.33, FDR-BH p=5.78x10^{-5}, SE=0.06; **Fig. 8f-i**). Of microglia-specific aDAGs, *GPNMB* had a strong positive association with age, despite being more highly expressed in OPCs and mural cells (**Fig. 8e,h**). Similarly, *LRRK2* exhibited a significant positive association in microglia, despite being most highly expressed in OPCs (**Fig. 8e,i**). Other notable aDAGs shared across multiple cell types include signal induced proliferation associated 1 like 2 (*SIPA1L2)*, potassium voltage-gated channel interacting protein 3 (*KCNIP3*), and peptidyl-glycine alpha-amidating monooxygenase (*PAM*; **Fig. 8f**).

These results collectively suggest that a large subset of genes nominated by AD (52/112 genes) and PD (56/87 genes) GWAS are differentially expressed with aging, independently of

disease. Many of these differential associations occur in microglia and OPCs. Additionally, we demonstrate the utility of snRNAseq in detecting moderate, cell type-specific associations with age that otherwise would be masked using bulk strategies.

Discussion

Here, we performed snRNAseq on nuclei from 12 individuals without a clinical or pathological history of neurodegenerative disease to examine changes in cell type populations and transcriptomes during healthy aging across multiple brain regions. We isolated nuclei from the entorhinal cortex, middle temporal gyrus, putamen, and subventricular zone, which are each differentially affected in neurodegenerative diseases. In total, we annotated 155,192 nuclei comprising all expected neuronal and non-neuronal cell types and subtypes (**Fig. 1**).

While we failed to observe any significant changes in cell type proportions (**Fig. 2**), we noted striking diverging transcriptome patterns across brain regions and cell types (**Supplemental Fig. 2**)**.** We observed that >50% of aging differentially associated genes (aDAGs) in each brain region, broad cell type, and cell subtype are unique with very few aDAGs shared across brain regions or cell types. At the level of brain regions, we observed predominantly more positive aDAGs in the MTG and PUT, and more negative aDAGs in the SVZ and EC, with only one aDAG shared across all regions. At the level of broad cell types, we observed predominantly negative aDAGs in InNs and OPCs, with all other broad type aDAGs exhibiting mixed directionality.

While these results suggest the absence of a global, shared aging gene signature, we noted that over 50% of the top aDAGS were annotated as lncRNAs or pseudogenes. Two of the most commonly differentially associated lnRNAs across cell types in the present dataset are *FAM66E* and *LERFS,* whose downregulation has been documented in human lung adenocarcinoma[43] and rheumatoid arthritis[44], respectively. However, their function in the brain is

unknown. Studies have suggested a regulatory role for lncRNAs in the contexts of alternative splicing, telomere stability, cell proliferation, intercellular communication, proteostasis, and epigenetic regulation; processes which are known to be altered during the course of aging and in neurodegeneration[45–48]. Given the abundance and diversity of lncRNAs in the CNS, further investigation into their role in aging and disease is warranted.

We next investigated aDAGs in InN and ExN subtypes and similarly observed that >50% of aDAGs for a given cell subtype were unique. We found striking differences between cortical and subcortical InNs, with cortical InNs exhibiting decreased associations of genes involved in protein synthesis and targeting, gene expression, and lncRNA processing, with *LHX6*$^{+}$*PVALB*$^{+}$ being most strongly affected (**Fig. 3**). aDAGs in ExNs, in contrast, were far fewer in number with more mixed directionality and categorically different GO enrichments, including axonogenesis, cell adhesion, and cell communication by electrical coupling (**Fig. 4**). The difference in strength and number of aDAGs in InNs vs. ExNs is consistent with previous studies demonstrating selective vulnerability of *LHX6*$^{+}$*PVALB*$^{+}$ and *LHX6*$^{+}$*SST*$^{+}$ cortical neurons in the EC and MTG, respectively, in AD. Given that disrupted proteostasis is a major feature of AD, our data suggest decreases of protein synthesis and targeting genes in these cell types *en masse* during normal, healthy aging may set the stage for selective vulnerability of these InNs and subsequent imbalance of inhibitory-excitatory signaling observed in AD[49,50].

Changes in white matter integrity[20,21] and expression of myelination genes[51] have been documented in previous studies of aging and neurodegeneration in animal models and humans. Surprisingly, we did not observe a change in OPC or oligodendrocyte numbers between young and old individuals in any brain region (**Supplemental Table 5**). However, we demonstrate OPC-specific negative associations of development and myelin gene-associated transcription factors *HES5*, *SOX10*, and *NKX2-2*[52–54] as well as teneurin transmembrane protein 4 (*TENM4*), with only negligible negative associations of *MBP* and *PLP1* in oligodendrocyte-1 and

oligodendrocyte-2, respectively (**Supplemental Fig. 5; Supplemental Table 4**). While our data suggest that terminal differentiation of OPCs to oligodendrocytes, upstream transcription factors regulating myelination, and support of axonogenesis may be disrupted with age in absence of cell loss, we are unable to rule out post-transcriptional and post-translational contributions to white matter integrity disruption.

Previous studies examining brain aging using bulk RNAseq have consistently demonstrated altered inflammatory signaling with age. While we failed to observe GO enrichments related to inflammation in any brain region, broad type, or cell subtype, we did observe that the majority of the top protein-coding aDAGs across brain regions were associated with inflammation (**Supplemental Fig. 2c**). In astrocytes, we observed positive associations of reactive gliosis genes and multiple complement pathway genes, the latter of which is particularly interesting given the complement system's role in synaptic pruning during development and its potential involvement in elimination of aberrant synapses in neurodegenerative diseases[43–48]. In microglia, we observed positive associations of proinflammatory cytokine, major histocompatibility complex, and disease-associated microglia genes. Moreover, we noted a decreased association of fractalkine ligand and receptor (CX3CL1-CX3CR1) genes in neurons and microglia, respectively (**Fig. 6; Supplemental Table 4**). Our results suggest that inflammatory genes are increased with age and that homeostatic neuron-glia signaling may be disrupted, thus contributing to chronic immune dysregulation and synapse elimination seen in both aging and neurodegenerative diseases.

Importantly, we found significant overlap with previous mouse, non-human primate, and human brain aging and neurodegeneration datasets. Examples include a strong positive association of protease *RHBDL3* in ExN subtypes, previously shown to be strongly increased with age in the human frontal cortex[6,19], and negative associations of *NPY* and its receptor *NPYR1* in the MTG, SVZ, subsets of ExN, and OPCs. We additionally replicated an aging-associated decrease in neuropeptide *SST*[6,19] in both the EC and MTG, and in

ADARB2^{+}*LAMP5*$^{+}$ cortical InNs, noting negative associations of related receptors *SSTR1* and *SSTR2* across cortical InNs, ExNs, and mural cells. When comparing aDAGs from this study to human aging datasets, we note that cell types with significant enrichments for genes increased with age included astrocytes and microglia, while cell types with significant enrichments for genes decreased with age were restricted to neuron subtypes (**Supplemental Fig. 7**).

Notably, these differential associations occur in absence of any widespread overt loss or gain of cell types with age (**Fig. 2**, **Supplemental Fig. 2**). These findings demonstrate the utility and robustness of snRNAseq in 1) replicating previous findings from bulk RNAseq; 2) providing increased resolution to disambiguate changes in gene expression from cell loss; and 3) determining which particular cell types significant transcriptional changes are occurring.

Our analysis of senescence gene sets is consistent with previous senescence studies in postmortem brain tissue. The percentage of senescent cells is dependent on which gene set is used. While OPCs appear to have differential expression of senescence markers across all gene sets, consistent with results from mouse models of amyloid-beta accumulation and post-mortem human AD brain[61], further investigation is needed to define cell type-specific senescence signatures in the CNS, particularly in post-mitotic neurons (**Fig. 7**).

Finally, we examined the relationship between aging and the expression of genes nearest to GWAS-identified risk loci for AD and PD. Many of these disease-associated genes had a significant age-association specific to a single cell type, despite being more abundantly expressed in other cell types at baseline. For example, AD-associated *APOE* and PD-associated *LRRK2*[62,63] and *GPNMB*[64,65] are positively associated with age in microglia, despite being more highly expressed in astrocytes and OPCs, respectively (**Fig. 8**). Our data provide context for and highlight the necessity of testing GWAS-nominated disease risk genes in relevant subtypes for preclinical mechanistic studies *in vitro* and *in vivo*, and subsequently, for developing more cell type-specific, targeted therapeutic strategies.

We note several limitations of our study. First, we examined aging as a categorical rather than continuous variable, in part due to the multiregion/donor design of the study. Given that the prodromal period for age-related neurodegenerative diseases is estimated to be >10 years, examining individuals aged 40-60 could be particularly insightful. While we cannot rule out the possibility that donors would eventually go on to develop dementia or other NDDs given a long prodrome, tissue was selected based on lack of clinical and postmortem neuropathological criteria consistent with NDDs. Second, while we balanced each age group by sex, we were not sufficiently powered to examine a gene expression*sex*age interaction. This analysis could be particularly informative in the context of neurodegenerative diseases like PD and AD, which differentially affect males and females, respectively.

In summary, the current dataset provides a novel resolution of the effects of chronological aging across brain regions and cell types. Surprisingly, using unbiased approaches, we show that multiple aDAGS are also genes that modulate risk of NDDs. These data support that future studies should be directed to larger sample series and incorporate additional single cell measures of the effects of aging in the healthy brain.

Data and Code Availability

Code: https://github.com/neurogenetics/ADRD_Brain_Aging

Summary level results: https://zenodo.org/record/7847472

Individual level data: https://nda.nih.gov/edit_collection.html?id=3151

Streamlit App: https://brainexp-hykyffa56a-uc.a.run.app/

Acknowledgements

We would like to thank members of the National Institute of Mental Health's Human Brain Collection Core, particularly Drs. Stephano Marenco and Pavan Auluck for their time and efforts in providing post-mortem brain dissections for this study as well as the NIH Intramural Sequencing Core (NISC). This research was supported by the Intramural Research Program of the National Institutes of Health, National Institute on Aging project 1ZIAAG000539-01 (to M.R.C), and in part by project ZO1 AG000535 (to M.A.N.); as well as the National Institute of Neurological Disorders and Stroke (1ZIANS003154, S.W.S.). This work utilized the computational resources of the NIH HPC Biowulf cluster (http://hpc.nih.gov).

Author contributions

Conceptualization: M.D., R.L., S.W.S., J.R.G., M.R.C.

Supervision: M.R.C.

Investigation: M.D., J.R.G., J.D., M.R.C.

Formal Analysis: M.D., J.R.G., J.D., M.R.C.

Funding Acquisition: M.R.C., M.A.N.

Writing: Original Draft: M.D., J.R.G., M.R.C.

Writing: Review & Editing: M.D., R.L., J.D., S.W.S., S.J.S., M.A.N., S.M., P.A., D.T.W., J.R.G., M.R.C.

Visualization: M.D., J.R.G., M.R.C.

Streamlit App: S.W.S., M.A.N.

Declaration of interests

M.A.N. and S.W.S.'s participation in this project was part of a competitive contract awarded to Data Tecnica International LLC by the National Institutes of Health to support open science research. M.A.N. also currently serves on the scientific advisory board for Character Bio Inc. and Neuron23 Inc. S.W.S. serves on the scientific advisory board of the Lewy Body Dementia Association and the Multiple System Atrophy Coalition. S.W.S. is an editorial board member for the *Journal of Parkinson's Disease* and *JAMA Neurology.* S.W.S. receives research support from Cerevel Therapeutics.

Methods

Isolation of nuclei from human brain

Nuclei were isolated using the Nuclei PURE Prep Nuclei Isolation Kit (Sigma #NUC201) per the manufacturer's instructions with slight modifications. To streamline workflow and decrease potential batch effects, we used a pooling approach prior to library preparation followed by post-sequencing demultiplexing, resulting in 6 pools of 8 samples each. Each pool was balanced for age group and sex. Of note, no single pool contained tissue from 2 regions from the same donor.

A 100mg piece of tissue was placed on a fresh, pre-chilled petri dish, trimmed, and weighed. Approximately 25 mg tissue/sample for a total of 8 samples per pool was combined and homogenized in a single cold douncer containing 2 ml ice-cold lysis buffer (Nuclei PURE Lysis Buffer (Sigma #L9286), 0.1M DTT from freshly thawed aliquot (Sigma #GE17-1318-01), and 0.1% Triton X-100 (Thermofisher Scientific #T1565) Tissue was homogenized with 25 strokes of a loose pestle, and 25 strokes of a tight pestle before being transferred to a tube containing 8ml cold lysis buffer, vortexed 2-3s, and left on ice for 10 minutes. Following lysis, cold 1.8M sucrose cushion solution (Nuclei PURE 2M Sucrose Cushion Solution (Sigma #S9308), Nuclei PURE Sucrose Cushion Buffer (Sigma #S9058) and 0.1M DTT) was added to the bottom of an ultracentrifuge tube (Beckman Coulter #344058) on ice. To each lysate, cold 1.8M sucrose cushion solution was added and mixed using a serological pipette. The lysate solution was slowly layered on top of the sucrose cushion, placed in a precooled ultracentrifuge, and centrifuged for 45 min. at 30,000 x *g* at 4℃.

Sample tubes were removed from the ultracentrifuge and placed on ice. The supernatant was aspirated completely, and the nuclei pellet was resuspended in Nuclei Suspension Buffer

on ice (NSB; 1ml cold PBS (Thermofisher Scientific #10010-023), 0.01% BSA (New England Biolabs #B9000S), 0.1% SUPERase RNase inhibitor (Thermofisher Scientific #AM2696), transferred to a 15ml tube containing an additional 4ml NSB buffer, mixed, and washed by centrifugation at 500 x *g* for 5 min. at 4℃. The pellet was resuspended in 1 ml NSB, filtered through a 70μM Cell Strainer (STEMCELL Technologies #27216) to remove debris, and washed again by centrifugation. The supernatant was aspirated, and nuclei were resuspended in a final volume of 110μl.

To determine nuclei concentration, Acridine Orange/Propidium Iodide (Logos Biosystems #F23001) was added to nuclei suspension in a separate tube and counted using a LUNA-FL Dual Fluorescence Cell Counter (Logos Biosystems). An appropriate volume of nuclei was diluted with NSB to achieve a final single suspension of 80,000 nuclei to achieve maximum nuclei recovery while minimizing the multiplet rate. Approximately 10,000 nuclei from this single suspension were loaded into each of 8 lanes of a 10x Genomics NextGEM Chip G (10x Genomics #1000127) and inserted into a 10xGenomics Chromium Controller (10xGenomics #1000204) according to the manufacturer's instructions. We loaded 10k nuclei per lane, targeting ~6k nuclei recovered per lane with a multiplet rate of ≤5%. The remainder of library preparation was conducted according to the Chromium Single Cell 3' Reagent Kits User Guide (v3.1 Chemistry; Rev.D). Final libraries were sequenced at the NIH Intramural Sequencing Center (NISC) at a read depth of 25,000 paired-end reads per nucleus on an Illumina NovaSeq 6000. Data was processed with CellRanger count v5.0.1 with refdata-gex-GRCh38-2020-A as the reference, with introns included.

Genotype preparation

Genotypes were assayed from three array-based genotyping platforms: Human1M-Duov3_B, HumanHap650Yv3.0, and HumanOmni5-Quad. Genotypes were merged and filtered to variants

common to all three platforms and called in 95% of the samples, and that are single-nucleotide variants (SNVs). Genotype files were lifted over from hg19 to hg38. The Plink2[66], bcftools[67], and Picard (https://broadinstitute.github.io/picard/) tool sets were used to filter, format, and liftover the genotype files.

Demultiplexing of Pooled Samples

Pooled samples were demultiplexed using the demuxlet tool[68]. The prepared subject genotypes and the aligned single-nuclei bam files were used to deconvolute the cells' sample identities. Data were processed on the Google Cloud Platform (GCP) using the Cumulus/Demuxlet workflow (WDL, https://cumulus-doc.readthedocs.io/en/0.12.0/demuxlet.html), which executes the demuxlet tool contained in the Statgen Popcle suite (https://github.com/statgen/popscle). Job submission to GCP for execution was done via the Broad WDL runner (https://github.com/broadinstitute/wdl-runner) and GCP Life Sciences interface (https://cloud.google.com/life-sciences/docs). SCANPY[69] was used to read in the 10X filtered matrix files into an AnnData object and integrate sample identity for the deconvoluted cells, along with sample information into the 'obs' information and then combine all data into a single AnnData object.

Clustering and cell-type identification

The single-cell analysis tool Pegaus[70] (https://pegasus.readthedocs.io/en/stable/index.html) was used to combine, filter, normalize, cluster, and perform the initial cell-type identities of the demultiplexed single-nuclei count data. Basic filtering was done with Pegasus excluding cells that did not include at least 200 genes, genes that were not present in at least three cells, and cells that had more than 10% mitochondrial content[71]. Counts were transformed to a total-count normalization of 10,000 reads per cell and log transformation. Highly variable features were

used for clustering, 2000 genes. Principal components analysis was used to reduce the dimensionality of the data from 2000 high variable genes to 50 principal components (PC). Batch effects were corrected with Harmony[72] applied to the 50 PCs. The k-nearest neighbors were computed from the Harmony corrected components based on 100 nearest neighbors for each cell the L2 distance and the hnswlib search algorithm[73]. The Leiden[74] algorithm was used to identify clusters on the neighborhood graph; multiple resolutions were used after inspection. Differential expression for each cluster against all others along with known marker genes for broad central nervous system cell-types was used to make the initial inferences for each cluster's putative cell-type. For the differential expression analysis performed with Pegasus the default Mann-Whitney U test was used. Uniform Manifold Approximation and Projection (UMAP)[75] was used to visualize, inspect, and evaluate the clustering and initial cell-type assignments. Inspection and evaluation of the clusters and their cell-type assignments were performed using dendrograms, dot plots, violin plots, volcano plots, and UMAP scatter plots over combinations of gene makers and sample information entities. After evaluation, a final Leiden resolution of 0.85 was used. During inspection more refined cell-type markers were included and where needed cell-type assignments were corrected. As part of the evaluation and inspection a sub-clustering approach was also used where subsets of cells based on specific clusters were subset and re-clustered. Cell trajectory and diffusion was evaluated using the Force-directed Layout[76] algorithm available in the Pegasus tool. Three clusters (12,753 nuclei), where a determination of the cell-type assignment could not be made via algorithm or manual inspection and evaluation were excluded for further analysis.

Age-related differential expression and association

Three sets of differential expression analysis were performed with age group as the independent variable. The three sets were brain region, cell-type, cluster specific. Where the

difference between cell-type and cluster specific is in instances where multiple clusters had the same cell-type assignment each of these clusters were analyzed separately as well as together as a cell-type. For example, multiple clusters of oligodendrocytes were identified, and each of these were analyzed separately as well as a single cell-type oligodendrocyte. Age was treated as a binary variable representing young or old, where young subjects were 20 to 30 years of age at death while old subjects were 60 to 85 years of age at death. Only genes with non-zero values in at least 3 cells within the individual analysis set and with non-zero cells from at least 50% of the subjects were included in differential expression analysis between the age groups. For computational efficiency, the differential expression analysis was performed in two steps. First, a simple t-test between age groups was performed using the diffxpy package (https://diffxpy.readthedocs.io/en/latest/index.html). Any result where a nominally significant difference was detected was considered for follow-up in a second step. For the second step of the differential expression analysis, in order to address pseudoreplication and zero-inflation that impact analyses in single-cell experiments, we utilized a generalized linear mixed model (GLMM) with a Tweedie distribution[77]. To account for pseudoreplication a fixed-effect term is included to account for the sample, while a Tweedie distribution was specified to account for zero-inflation. Additionally, the pool number was included as a term to account for residual batch effects from pooling that were not corrected by the Harmony batch effects correction step. The glmmTMB[78] R package was used to run this model; gene ~ age_group + pool + (1|sample_id). To correct for multiple testing within each analysis set the resulting p-values were adjusted using Benjamini and Hochberg false discovery rate (fdr_bh), as implemented in the statsmodel multitest Python package (https://www.statsmodels.org).

Gene Set Enrichment

To determine biological pathways with significant age associations, we used the GSEApy package[79] with Enrichr (gseapy.enrichr) to perform overrepresentation analysis on aDAGs determined by glmmTMB (*FDR BH p*< 0.05) for each brain region, broad type, and cell subtype. We queried significant aDAGs against libraries within the 'Human' enrichr database: 'GO_Biological_Process_2021', 'GO_Cellular_Component_2021', 'GO_Molecular_Function_2021', 'KEGG_2021_Human', 'WIKIPATHWAYS_2021_Human'. We additionally queried 'Aging_Perturbations_from_GEO_up, 'Disease_Perturbations_from_GEO_up,' 'Aging_Perturbations_from_GEO_down,' and 'Disease_Perturbations_from_GEO_down' gene sets using positive *or* negative aDAGs only, respectively. A cutoff of FDR < 0.05 was used to display significant terms. All gseapy.enrichr results are available in the supplementary information.

Senescence Scoring

The score_genes function from SCANPY[69] was used to score sets of marker genes for both senescence and DAM. The score_genes function generates a score based on the average expression of the provided gene markers against the average expression of a reference set; here all genes were used as the reference set. In these analyses any cell with a score of more than two standard deviations from the mean of a broad cell-type's scored cells was considered positive. The senescence marker genes included six separate sets and the DAM signature was based on a single set of marker genes. These marker sets are from previously published studies. The DAM signature consisted of six genes[35]. The senescence sets include: custom senescence signature (CSS) comprised of 7 genes[35], Canonical Senescence Pathway (CSP) using 11 genes, Senescence Response Pathway (SRP) using 18 genes, Senescence Initiating

Pathway (SIP) using 30 genes[38], Cell Age using 73 genes[80]. Cells for each broad cell-type were scored for each senescence marker set and the DAM set was only scored for microglia.

References

1. Hou, Y. *et al.* Ageing as a risk factor for neurodegenerative disease. *Nat Rev Neurol* **15**, 565–581 (2019).
2. Kawas, C., Gray, S., Brookmeyer, R., Fozard, J. & Zonderman, A. Age-specific incidence rates of Alzheimer's disease: the Baltimore Longitudinal Study of Aging. *Neurology* **54**, 2072–2077 (2000).
3. Hebert, L. E. *et al.* Age-specific incidence of Alzheimer's disease in a community population. *JAMA* **273**, 1354–1359 (1995).
4. Hebert, L. E., Weuve, J., Scherr, P. A. & Evans, D. A. Alzheimer disease in the United States (2010–2050) estimated using the 2010 census. *Neurology* **80**, 1778–1783 (2013).
5. Ham, S. & Lee, S.-J. V. Advances in transcriptome analysis of human brain aging. *Exp Mol Med* **52**, 1787–1797 (2020).
6. Dillman, A. A. *et al.* Transcriptomic profiling of the human brain reveals that altered synaptic gene expression is associated with chronological aging. *Sci Rep* **7**, 16890 (2017).
7. Gómez-Isla, T. *et al.* Profound loss of layer II entorhinal cortex neurons occurs in very mild Alzheimer's disease. *J Neurosci* **16**, 4491–4500 (1996).
8. Van Hoesen, G. W., Hyman, B. T. & Damasio, A. R. Entorhinal cortex pathology in Alzheimer's disease. *Hippocampus* **1**, 1–8 (1991).
9. Piras, I. S. *et al.* Transcriptome Changes in the Alzheimer's Disease Middle Temporal Gyrus: Importance of RNA Metabolism and Mitochondria-Associated Membrane Genes. *Journal of Alzheimer's Disease* **70**, 691–713 (2019).
10. Flores, R. de *et al.* Medial Temporal Lobe Networks in Alzheimer's Disease: Structural and Molecular Vulnerabilities. *J. Neurosci.* **42**, 2131–2141 (2022).
11. Coppen, E. M., van der Grond, J. & Roos, R. A. C. Atrophy of the putamen at time of clinical motor onset in Huntington's disease: a 6-year follow-up study. *Journal of Clinical Movement*

Disorders **5**, 2 (2018).

12. Matsushima, A. *et al.* Transcriptional vulnerabilities of striatal neurons in human and rodent models of Huntington's disease. *Nat Commun* **14**, 282 (2023).
13. Shen, B. *et al.* Altered putamen and cerebellum connectivity among different subtypes of Parkinson's disease. *CNS Neurosci Ther* **26**, 207–214 (2020).
14. Jackson, H. *et al.* Hoehn and Yahr Stage and Striatal Dat-SPECT Uptake Are Predictors of Parkinson's Disease Motor Progression. *Front Neurosci* **15**, 765765 (2021).
15. Ye, R. *et al.* Serum NFL levels predict progression of motor impairment and reduction in putamen dopamine transporter binding ratios in de novo Parkinson's disease: An 8-year longitudinal study. *Parkinsonism Relat Disord* **85**, 11–16 (2021).
16. Winner, B., Kohl, Z. & Gage, F. H. Neurodegenerative disease and adult neurogenesis. *European Journal of Neuroscience* **33**, 1139–1151 (2011).
17. Hodge, R. D. *et al.* Conserved cell types with divergent features in human versus mouse cortex. *Nature* **573**, 61–68 (2019).
18. Pande, R. *et al.* Single Cell Atlas of Human Putamen Reveals Disease Specific Changes in Synucleinopathies: Parkinson's Disease and Multiple System Atrophy. 2021.05.06.442950 Preprint at https://doi.org/10.1101/2021.05.06.442950 (2021).
19. Kumar, A. *et al.* Age associated changes in gene expression in human brain and isolated neurons. *Neurobiol Aging* **34**, 1199–1209 (2013).
20. Coelho, A. *et al.* Signatures of white-matter microstructure degradation during aging and its association with cognitive status. *Sci Rep* **11**, 4517 (2021).
21. Wang, F. *et al.* Myelin degeneration and diminished myelin renewal contribute to age-related deficits in memory. *Nat Neurosci* **23**, 481–486 (2020).
22. Pan, J., Ma, N., Yu, B., Zhang, W. & Wan, J. Transcriptomic profiling of microglia and astrocytes throughout aging. *J Neuroinflammation* **17**, 97 (2020).
23. Boyd, R. J., Avramopoulos, D., Jantzie, L. L. & McCallion, A. S. Neuroinflammation

represents a common theme amongst genetic and environmental risk factors for Alzheimer and Parkinson diseases. *Journal of Neuroinflammation* **19**, 223 (2022).

24. Harms, A. S., Ferreira, S. A. & Romero-Ramos, M. Periphery and brain, innate and adaptive immunity in Parkinson's disease. *Acta Neuropathol* **141**, 527–545 (2021).
25. Yu, E. *et al.* Fine mapping of the HLA locus in Parkinson's disease in Europeans. *npj Parkinsons Dis.* **7**, 1–7 (2021).
26. Cribbs, D. H. *et al.* Extensive innate immune gene activation accompanies brain aging, increasing vulnerability to cognitive decline and neurodegeneration: a microarray study. *J Neuroinflammation* **9**, 179 (2012).
27. Liddelow, S. A. *et al.* Neurotoxic reactive astrocytes are induced by activated microglia. *Nature* **541**, 481–487 (2017).
28. Asby, D., Boche, D., Allan, S., Love, S. & Miners, J. S. Systemic infection exacerbates cerebrovascular dysfunction in Alzheimer's disease. *Brain* **144**, 1869–1883 (2021).
29. Rentzos, M. *et al.* IL-15 is elevated in cerebrospinal fluid of patients with Alzheimer's disease and frontotemporal dementia. *J Geriatr Psychiatry Neurol* **19**, 114–117 (2006).
30. Cacabelos, R., Barquero, M., García, P., Alvarez, X. A. & Varela de Seijas, E. Cerebrospinal fluid interleukin-1 beta (IL-1 beta) in Alzheimer's disease and neurological disorders. *Methods Find Exp Clin Pharmacol* **13**, 455–458 (1991).
31. Rossi, S. *et al.* Interleukin-1β causes excitotoxic neurodegeneration and multiple sclerosis disease progression by activating the apoptotic protein p53. *Mol Neurodegener* **9**, 56 (2014).
32. Doorn, K. J. *et al.* Microglial phenotypes and toll-like receptor 2 in the substantia nigra and hippocampus of incidental Lewy body disease cases and Parkinson's disease patients. *Acta Neuropathol Commun* **2**, 90 (2014).
33. Dzamko, N. *et al.* Toll-like receptor 2 is increased in neurons in Parkinson's disease brain and may contribute to alpha-synuclein pathology. *Acta Neuropathol* **133**, 303–319 (2017).

34. Kim, C. *et al.* Neuron-released oligomeric α-synuclein is an endogenous agonist of TLR2 for paracrine activation of microglia. *Nat Commun* **4**, 1562 (2013).
35. Hu, Y. *et al.* Replicative senescence dictates the emergence of disease-associated microglia and contributes to Aβ pathology. *Cell Reports* **35**, 109228 (2021).
36. Finneran, D. J. & Nash, K. R. Neuroinflammation and fractalkine signaling in Alzheimer's disease. *J Neuroinflammation* **16**, 30 (2019).
37. Casella, G. *et al.* Transcriptome signature of cellular senescence. *Nucleic Acids Research* **47**, 7294–7305 (2019).
38. Dehkordi, S. K. *et al.* Profiling senescent cells in human brains reveals neurons with CDKN2D/p19 and tau neuropathology. *Nat Aging* **1**, 1107–1116 (2021).
39. Wechter, N. *et al.* Single-cell transcriptomic analysis uncovers diverse and dynamic senescent cell populations. *Aging (Albany NY)* **15**, 2824–2851 (2023).
40. Alvarado, C. X. *et al.* Human brain single nucleus cell type enrichments in neurodegenerative diseases. 2023.06.30.23292084 Preprint at https://doi.org/10.1101/2023.06.30.23292084 (2023).
41. Andrews, S. J. *et al.* The complex genetic architecture of Alzheimer's disease: novel insights and future directions. *eBioMedicine* **90**, (2023).
42. Nalls, M. A. *et al.* Identification of novel risk loci, causal insights, and heritable risk for Parkinson's disease: a meta-analysis of genome-wide association studies. *The Lancet Neurology* **18**, 1091–1102 (2019).
43. Yang, Z. *et al.* Microarray expression profile of long non-coding RNAs in human lung adenocarcinoma. *Thorac Cancer* **9**, 1312–1322 (2018).
44. Zou, Y. *et al.* Long noncoding RNA LERFS negatively regulates rheumatoid synovial aggression and proliferation. *J Clin Invest* **128**, 4510–4524 (2018).
45. Marttila, S., Chatsirisupachai, K., Palmer, D. & de Magalhães, J. P. Ageing-associated changes in the expression of lncRNAs in human tissues reflect a transcriptional modulation

in ageing pathways. *Mech Ageing Dev* **185**, 111177 (2020).

46. Huaying, C. *et al.* A Signature of Five Long Non-Coding RNAs for Predicting the Prognosis of Alzheimer's Disease Based on Competing Endogenous RNA Networks. *Front Aging Neurosci* **12**, 598606 (2021).
47. Srinivas, T., Mathias, C., Oliveira-Mateos, C. & Guil, S. Roles of lncRNAs in brain development and pathogenesis: Emerging therapeutic opportunities. *Molecular Therapy* **31**, 1550–1561 (2023).
48. Ouyang, J. *et al.* Long non-coding RNAs are involved in alternative splicing and promote cancer progression. *Br J Cancer* **126**, 1113–1124 (2022).
49. Lauterborn, J. C. *et al.* Increased excitatory to inhibitory synaptic ratio in parietal cortex samples from individuals with Alzheimer's disease. *Nat Commun* **12**, 2603 (2021).
50. Ranasinghe, K. G. *et al.* Altered excitatory and inhibitory neuronal subpopulation parameters are distinctly associated with tau and amyloid in Alzheimer's disease. *eLife* **11**, e77850.
51. Hentrich, T. *et al.* Increased expression of myelin-associated genes in frontal cortex of SNCA overexpressing rats and Parkinson's disease patients. *Aging (Albany NY)* **12**, 18889–18906 (2020).
52. Chiou, K. L. *et al.* Multiregion transcriptomic profiling of the primate brain reveals signatures of aging and the social environment. *Nat Neurosci* **25**, 1714–1723 (2022).
53. Dimovasili, C. *et al.* Aging compromises oligodendrocyte precursor cell maturation and efficient remyelination in the monkey brain. *GeroScience* **45**, 249–264 (2022).
54. Qi, Y. *et al.* Control of oligodendrocyte differentiation by the Nkx2.2 homeodomain transcription factor. *Development* **128**, 2723–2733 (2001).
55. Lian, H. *et al.* NFκB-activated astroglial release of complement C3 compromises neuronal morphology and function associated with Alzheimer's disease. *Neuron* **85**, 101–115 (2015).
56. Shi, Q. *et al.* Complement C3-Deficient Mice Fail to Display Age-Related Hippocampal

Decline. *J. Neurosci.* **35**, 13029–13042 (2015).

57. Wu, T. *et al.* Complement C3 Is Activated in Human AD Brain and Is Required for Neurodegeneration in Mouse Models of Amyloidosis and Tauopathy. *Cell Rep* **28**, 2111-2123.e6 (2019).
58. Dejanovic, B. *et al.* Complement C1q-dependent excitatory and inhibitory synapse elimination by astrocytes and microglia in Alzheimer's disease mouse models. *Nat Aging* **2**, 837–850 (2022).
59. Stevens, B. *et al.* The Classical Complement Cascade Mediates CNS Synapse Elimination. *Cell* **131**, 1164–1178 (2007).
60. Hong, S. *et al.* Complement and Microglia Mediate Early Synapse Loss in Alzheimer Mouse Models. *Science* **352**, 712–716 (2016).
61. Zhang, P. *et al.* Senolytic therapy alleviates Aβ-associated oligodendrocyte progenitor cell senescence and cognitive deficits in an Alzheimer's disease model. *Nat Neurosci* **22**, 719–728 (2019).
62. Langston, R. G. *et al.* Association of a common genetic variant with Parkinson's disease is mediated by microglia. *Sci. Transl. Med.* **14**, eabp8869 (2022).
63. Kluss, J. H., Mamais, A. & Cookson, M. R. LRRK2 links genetic and sporadic Parkinson's disease. *Biochemical Society Transactions* **47**, 651–661 (2019).
64. Smajić, S. *et al.* Single-cell sequencing of human midbrain reveals glial activation and a Parkinson-specific neuronal state. *Brain* **145**, 964–978 (2022).
65. Diaz-Ortiz, M. E. *et al.* GPNMB confers risk for Parkinson's disease through interaction with α-synuclein. *Science* **377**, (2022).
66. Chang, C. C. *et al.* Second-generation PLINK: rising to the challenge of larger and richer datasets. *Gigascience* **4**, 7 (2015).
67. Li, H. A statistical framework for SNP calling, mutation discovery, association mapping and population genetical parameter estimation from sequencing data. *Bioinformatics* **27**,

2987–2993 (2011).

68. Kang, H. M. *et al.* Multiplexed droplet single-cell RNA-sequencing using natural genetic variation. *Nat Biotechnol* **36**, 89–94 (2018).
69. Wolf, F. A., Angerer, P. & Theis, F. J. SCANPY: large-scale single-cell gene expression data analysis. *Genome Biology* **19**, 15 (2018).
70. Li, B. *et al.* Cumulus provides cloud-based data analysis for large-scale single-cell and single-nucleus RNA-seq. *Nat Methods* **17**, 793–798 (2020).
71. McCarthy, D. J., Campbell, K. R., Lun, A. T. L. & Wills, Q. F. Scater: pre-processing, quality control, normalization and visualization of single-cell RNA-seq data in R. *Bioinformatics* **33**, 1179–1186 (2017).
72. Korsunsky, I. *et al.* Fast, sensitive and accurate integration of single-cell data with Harmony. *Nat Methods* **16**, 1289–1296 (2019).
73. Malkov, Y. A. & Yashunin, D. A. Efficient and Robust Approximate Nearest Neighbor Search Using Hierarchical Navigable Small World Graphs. *IEEE Trans Pattern Anal Mach Intell* **42**, 824–836 (2020).
74. Traag, V. A., Waltman, L. & van Eck, N. J. From Louvain to Leiden: guaranteeing well-connected communities. *Sci Rep* **9**, 5233 (2019).
75. McInnes, L., Healy, J., Saul, N. & Großberger, L. UMAP: Uniform Manifold Approximation and Projection. *Journal of Open Source Software* **3**, 861 (2018).
76. Jacomy, M., Venturini, T., Heymann, S. & Bastian, M. ForceAtlas2, a continuous graph layout algorithm for handy network visualization designed for the Gephi software. *PLoS One* **9**, e98679 (2014).
77. Zimmerman, K. D., Espeland, M. A. & Langefeld, C. D. A practical solution to pseudoreplication bias in single-cell studies. *Nat Commun* **12**, 738 (2021).
78. Brooks, M. E. *et al.* glmmTMB Balances Speed and Flexibility Among Packages for Zero-inflated Generalized Linear Mixed Modeling. *The R Journal* **9**, 378–400 (2017).

79. Fang, Z., Liu, X. & Peltz, G. GSEApy: a comprehensive package for performing gene set enrichment analysis in Python. *Bioinformatics* **39**, btac757 (2023).

80. Avelar, R. A. *et al.* A multidimensional systems biology analysis of cellular senescence in aging and disease. *Genome Biol* **21**, 91 (2020).

Figure legends

Figure 1: Experimental design and cell type composition of human entorhinal cortex, middle temporal gyrus, putamen, and subventricular zone

(a) Schematic depicting experimental workflow for 10x Genomics snRNAseq library preparation and subsequent analysis of 4 brain regions from 12 individuals aged 20-30 (n=5-6) and 60-85 (n=7) balanced for sex (red, female; blue, male). See also: Methods. Created with BioRender.com.

(**b**) Proportion of total accepted nuclei (155,192) split by sex and age

(c) Proportion of total accepted nuclei (155,192) split by brain region

(d) Dot plot of mean expression of multiple marker genes used to define each cell subtype. Size of circle denotes percentage of cells in a cluster expressing a gene and color represents strength of expression (purple, high expression; light blue, low expression).

(e) UMAP of 155,192 annotated nuclei from all brain regions

(f) Cell type proportions expressed as a percentage of total recovered nuclei

Abbreviations: aDAG, aging-differentially associated gene; EC, entorhinal cortex; ExN, excitatory neuron; InN, inhibitory neuron; MTG, middle temporal gyrus; OPC, oligodendrocyte precursor cell; PUT, putamen; SPN, spiny projection neuron; SVZ, subventricular zone; UMAP, uniform manifold approximation and projection.

Figure 2: Cell type proportions are similar between young and old individuals

(a) Total number of nuclei recovered by age group

(b) UMAP of 24 cell type clusters colored by age group (young, light blue; old,dark blue)

(c) Percentage of nuclei recovered for each cell type, split by age group (young, light blue; old, dark blue); proportion of recovered nuclei by cell type and age group raw numbers displayed as "young | old"

(d) Cell type proportions split by age group, with each data point representing a single donor. Data expressed as percentage of total nuclei (young + old) recovered per cell type; n.s. = not significant; $p>0.05$, Welch's t-test.

Abbreviations: ExN, excitatory neuron; InN, inhibitory neuron; OPC, oligodendrocyte precursor cell; SPN, spiny projection neuron; UMAP, uniform manifold approximation and projection.

Figure 3: Diverging aging-associated changes in gene expression in cortical and subcortical spiny projection inhibitory neurons

(a) UMAP of cortical and subcortical InN subtypes (left) and marker genes (right).

(b) UpSet plot showing number of unique vs. shared aDAGs across cortical and subcortical InN subtypes, where rows on the x-axis correspond to [cell type] aDAG sets, columns correspond to intersection size between sets, and bar color corresponds to direction of association (dark blue, negative association with age; magenta, positive association with age). Lines between sets indicate shared aDAGs. Only intersection sizes of ≥50 are displayed. Cell type sets ordered by cardinality.

(c) Significant GSE of cortical neuron aDAGs as a *broad type*.

(d) Clustermap of significant aDAGs in “GO BP: protein targeting to ER (GO:0045047)” with strength of association enumerated as coefficient estimate (blue, negative association; magenta, positive association; grey, no significant association). Cell types ordered alphabetically.

(d) Dot plot showing percentage of cells expressing (indicated by dot size) and mean expression (indicated by color) of a subset of “GO BP: protein targeting to ER (GO:0045047)” aDAGs, split by age group. Red asterisk indicates genes chosen to display in feature scatter plots.

(f) Feature scatter showing expression *RPS7* and **(g)** *UBA52* across all clusters (left) and cluster[s] where the gene is significantly differentially associated with age (demarcated by red box and magnified on right).

(h) Clustermap of significant aDAGs in “GO MF: oxidoreduction-driven active transmembrane transporter activity (GO:0015453).” Cell types ordered alphabetically.

(i) Feature scatter showing expression of *NDUFB2 and* **(j)** *COX8A*.

(k) GSEA of significant aDAGs in SPN D1-2 neurons.

(l) Clustermap of significant aDAGs in: “GO MF: voltage-gated sodium channel activity (GO:0005248)” and “TAP1 binding (GO:0046978).” Cell types ordered alphabetically.

(m) Feature scatter showing expression of *HLA-F* and **(n)** *SCN5A*.

Abbreviations: aDAG, aging-differentially associated gene; BP, biological process; CC, cellular component; *COX8A*, cytochrome C oxidase subunit 8A; GO, gene ontology; GSE, gene set enrichment; *HLA-F,* major histocompatibility complex, Class I, F; InN, inhibitory neuron; KEGG, Kyoto Encyclopedia of Genes and Genomes; MF, molecular function; *NDUFB2*, NADH:ubiquinone oxidoreductase subunit B2; *RPS7*, ribosomal protein S7; *SCN5A*, sodium voltage-gated channel alpha subunit 5; SPN, spiny projection neuron; *TAP1*, transporter 1, ATP binding cassette subfamily B member; UMAP, uniform manifold approximation and projection.

Figure 4: Aging-associated changes in gene expression between excitatory neuron subtypes differ in strength and GO categories from cortical inhibitory neurons

(a) UMAP of cell type annotations (left) and feature plots depicting marker genes used to classify ExN subtypes (right).

(b) UpSet plot depicting unique vs. shared aDAGs across ExN subtypes Only intersection sizes of ≥50 are displayed. Cell type sets ordered by cardinality.

(c) Significant GSE in 3/7 ExN subtypes.

(d) Clustermap of significant aDAGs in ExN under the term “GO BP: axonogenesis (GO:0007409).” Strength of association enumerated as coefficient estimate. Cell types ordered alphabetically.

(e) Clustermap of significant aDAGs in ExN under the term “GO BP: cell-cell adhesion via plasma-membrane adhesion molecules (GO:0098742).” Cell types ordered alphabetically.

(f) Clustermap comparing significant aDAGs under the category of “GO BP: protein targeting to ER (GO:0045047)” between cortical InN, cortical ExN, and subcortical InN. Cell types ordered alphabetically.

Abbreviations: aDAG, aging-differentially associated gene; BP, biological process; CC, cellular component; ExN, excitatory neuron; GO, gene ontology; InN, inhibitory neuron; KEGG, Kyoto Encyclopedia of Genes and Genomes; MF, molecular function; SPN, spiny projection neuron; UMAP, uniform manifold approximation and projection.

Figure 5: Aging-associated changes in gene expression in oligodendrocyte precursors and oligodendrocytes suggest dysregulation of axon guidance

(a) UMAP of cell type annotations (left) and feature plots depicting marker genes used to classify OPCs and oligodendrocyte subtypes (right).

(b) Cell type proportions of OPCs and oligodendrocytes between age groups (see **Supplemental Table 5**). Oligodendrocyte lineage cells comprise ~35% of total recovered nuclei from both young and old individuals.

(c) UpSet plot depicting unique vs. shared aDAGs across OPCs and oligodendrocyte subtypes. Cell type sets ordered by cardinality.

(d) Aging-associated GSE in OPCs and oligodendrocyte subtypes, colored by GO term sets.

(e) Clustermap of significant aDAGs in OPCs and Oligodendrocytes under the term "GO CC: cell-cell junction (GO:0005911)."

(f) Clustermap comparing significant aDAGs in OPCs and Oligodendrocytes under the category of "GO BP: axonogenesis (GO:0007409)."

(g) Clustermap comparing significant aDAGs in OPCs and Oligodendrocytes under the category of "KEGG: Glutamatergic synapse."

(h) Clustermap comparing significant aDAGs in OPCs and Oligodendrocytes under the category of "KEGG: one carbon pool by folate."

(i) Feature scatters demonstrating decreased expression and association of *FAT2*, **(j)** *SEMA6D*, **(k)** *KCNJ3* in aged OPCs.

(l) Feature scatter demonstrating increased expression and association of *FTCD* in Oligodendrocyte-2.

Abbreviations: aDAG, aging-differentially associated gene; BP, biological process; CC, cellular component; *FAT2*, FAT atypical cadherin 2; *FTCD*, formimidoyltransferase cyclodeaminase; GO, gene ontology; *KCNJ3*, potassium inwardly rectifying channel subfamily J member 3; KEGG, Kyoto Encyclopedia of Genes and Genomes; MF, molecular function; OPC, oligodendrocyte precursor cell; *SEMA6D*, semaphorin 6D, UMAP, uniform manifold approximation and projection.

Figure 6: Differentially associated genes with age in astrocytes and microglia overlap with immune response, aging and disease gene sets

(a) GSE of aDAGs in astrocytes for Aging and Disease Perturbations from GEO gene sets. Top 10 most significant GO terms are shown. For a full list, see Supplementary Information.

(b) Dotplot of increased expression and/or percentage of astrocytes expressing complement, immune, and gliosis genes.

(c) Feature scatter showing increased expression and association of complement pathway genes *C1S*, **(d)** *C3*, and **(e)** *CFI* in aged astrocytes.

(f) GSE of aDAGs in microglia for “GO: Biological Process” and “Aging and Disease Perturbations from GEO” gene sets. Top 10 most significant GO terms are shown. For a full list, see Supplementary Information.

(g) Dotplot showing significant changes in expression and/or percentage of microglia expressing immune response or **(h)** DAM genes

(i) Feature plots showing significant increases and associations of *CD74*, **(j)** *SPP1*, **(k)** *IL15*, and **(l)** *HLA-DMB* in aged microglia.

Abbreviations: aDAG, aging-differentially associated gene; BP, biological process; *C1S*, complement component 1, S subcomponent; *C3*, complement C3; *CD74*, CD74 Antigen (invariant polypeptide of major histocompatibility complex, class II antigen-associated); *CFI*, complement factor I; GEO, Gene Expression Omnibus; GSE, gene set enrichment; *HLA-DMB*, major histocompatibility complex, class II, DM beta; *IL15*, interleukin 15; *SPP1*, secreted phosphoprotein 1

Figure 7: Scoring of senescence-associated gene sets at the level of brain region and broad cell types

(a) Fraction of senescence associated gene sets changed with age across brain region and broad cell types

(b) Genes comprising senescence-associated gene sets used for scoring in (a). Genes in bold italics denote significant aDAGs

(c) Clustermap of significant aDAGs at the level of brain region with strength of association enumerated as coefficient estimate (magenta, significant positive association with age; blue, significant negative association with age). Brain regions ordered by hierarchical clustering.

(d) Clustermap of significant senescence-related aDAGs at the level of broad type. Broad types ordered by hierarchical clustering.

(e) Clustermap of significant senescence-related aDAGs at the level of cell subtypes. Cell types ordered by hierarchical clustering.

Abbreviations: CSP, canonical senescence pathway; CSS, custom senescence signature; DAM, disease-associated microglia; SIP, senescence initiating pathway; SRP, senescence response pathway

Figure 8: Aging-associated changes in genes nearest to GWAS-identified risk loci for Alzheimer's disease and Parkinson's disease

(a) Clustermap of significant aDAGs which overlap with genes nearest to AD GWAS-nominated risk loci at the level of brain region. Strength of association enumerated as coefficient estimate (magenta, significant positive association with age; blue, significant negative association with age). Brain regions ordered by hierarchical clustering.

(b) Clustermap of significant aDAGs which overlap with genes nearest to AD GWAS-nominated risk loci across cell types. Cell types ordered by hierarchical clustering.

(c) Feature scatter and dot plot showing increased expression and association of *APOE* and **(d)** *MS4A6A* with age in microglia

(e) Clustermap of significant aDAGs which overlap with genes nearest to PD GWAS-nominated risk loci across brain regions. Brain regions ordered by hierarchical clustering.

(f) Clustermap of significant aDAGs which overlap with genes nearest to PD GWAS-nominated risk loci across cell types. Cell types ordered by hierarchical clustering.

(g) Feature scatter and dot plot showing increased expression and association of *CTSB*, **(h)** *GPNMB*, and **(i)** *LRRK2* with age in microglia

Abbreviations: aDAG, aging-differentially associated gene; AD, Alzheimer's disease; *APOE*, apolipoprotein E; *CTSB*, cathepsin B; *GPNMB*, glycoprotein nmb; GWAS, genome-wide association study; *LRRK2*, leucine-rich repeat kinase 2; *MS4A6A*, membrane spanning 4-domains A6A; PD, Parkinson's disease

Supplemental Figure 1: Cell type composition by sex, brain region, donor and classification by broad cell type markers

(a) UMAP of 155,192 nuclei by sex (female, pink; dark blue, male)

(b) Proportion of cell types recovered by sex

(**c)** UMAP of 155,192 nuclei colored by brain region (EC, dark blue; MTG, light blue; PUT, magenta; SVZ, gold) demonstrating the region-specific origin of some cell types.

(d) Proportion of cell types recovered by region.

(e) UMAP projection of nuclei split by brain region and sample ID demonstrating no single cluster is derived from a single donor.

(f) Leiden clustering at resolution 0.85 identified 23 distinct clusters after removal of low quality or poorly distinguished clusters.

(g) Dot plot of genes used to assign broad cell type categories to Leiden clusters, where dot size indicates percentage of cells expressing a gene and color indicates level of mean expression within that cluster.

(h) Feature plots of broad cell type markers to identify clusters as broadly as neurons, excitatory neurons, cortical inhibitory neurons, spiny projection neurons, astrocytes, endothelial cells, mural cells, ependymal cells, microglia, oligodendrocyte precursor cells, and oligodendrocytes.

(i) Force-directed graph of developmental relationships between cell types.

Abbreviations: *ANPEP*, alanyl aminopeptidase, membrane; *AQP4*, aquaporin 4; *CSF1R*, colony stimulating factor 1 receptor; *DRD1*, dopamine receptor D1; *DRD2*, dopamine receptor D2; EC, entorhinal cortex; ExN, excitatory neuron; FLE, force-directed; *FLT1*, fms related receptor tyrosine kinase 1; *FOXJ1*, forkhead box J1; *GAD2*, glutamate decarboxylase 2; InN, inhibitory neuron; *MBP*, myelin basic protein; MTG, middle temporal gyrus; *OPALIN*, oligodendrocytic myelin paranodal and inner loop protein; OPC, oligodendrocyte precursor cell;

PDGFRA, platelet derived growth factor receptor alpha; *PLP1*, proteolipid protein 1; PUT, putamen; *RBFOX3*, RNA binding fox-1 homolog 3; *SLC17A6*, solute carrier family 17 member 6; *SLC17A7*, solute carrier family 17 member 7

Supplemental Figure 2: Unique and diverging patterns of aging across brain regions and broad cell types in absence of cell loss

(a) Percentage of nuclei recovered per brain region by age group (light blue, young; dark blue, old) with raw numbers expressed as 'young | old'.

(b) Proportion of nuclei recovered by age group and donor showed no significant differences between age groups. n.s. = not significant; $p>0.05$, Welch's t-test.

(c) UpSet plot of unique vs. shared aDAGs across brain regions where rows on the x-axis correspond to [brain region] aDAG sets, columns correspond to intersection size between sets, and bar color corresponds to direction of association (blue, negative association with age; magenta, positive association with age). Lines between sets indicate shared aDAGs. Cell type sets ordered by cardinality.

(d) Clustermap of the top 5 aDAGs across brain regions (blue, negative association; magenta, positive association). Non-coding and pseudogenes distinguished by gray italics. Cell types ordered by hierarchical clustering.

(e) UpSet plot of unique and shared aDAGs across broad cell types. Only intersection sizes of ≥50 are displayed. Cell type sets ordered by cardinality.

(f) Clustermap of the top 5 positive and negative aDAGs across broad cell types. Cell types ordered by hierarchical clustering.

Abbreviations: aDAG, aging-differentially associated gene; EC, entorhinal cortex; ExN, excitatory neuron; InN, inhibitory neuron; MTG, middle temporal gyrus; OPC, oligodendrocyte precursor cell; PUT, putamen; SPN, spiny projection neuron; SVZ, subventricular zone

Supplemental Figure 3: Top aDAGs across cortical and subcortical InN subtypes and overlap with aging and disease gene sets

(a) Clustermap of the top 5 positive and negative aDAGs across cortical and subcortical InN subtypes (blue, negative association with age; magenta, positive association with age). Non-coding and pseudogenes distinguished by gray italics. Cell types ordered by hierarchical clustering.

(b) Enrichment of cortical and **(c)** subcortical InN subtype aDAGS from previous aging and disease perturbation gene sets from GEO.

Abbreviations: aDAG, aging-differentially associated gene; GEO, Gene Expression Omnibus; InN, inhibitory neuron; SPN, spiny projection neuron

Supplemental Figure 4: Top aDAGs across ExN subtypes and overlap with aging and disease gene sets

(a) Clustermap of the top 5 positive and negative aDAGs across ExN subtypes (blue, negative association with age; magenta, positive association with age). Non-coding and pseudogenes are distinguished by gray italics. Cell types ordered by hierarchical clustering.

(b) Feature scatter increased expression and association of *RHBDL3*; **(c)** decreased expression and association of *STAC*; and **(d)** increased expression and association of *STAC2* with age in ExN.

(e) Enrichment of ExN subtype aDAGS from previous aging and disease perturbation gene sets from GEO.

Abbreviations: aDAG, aging-differentially associated gene; ExN, excitatory neuron; GEO, Gene Expression Omnibus; *RHBDL3*, rhomboid like 3; *STAC*, SH3 and cysteine rich domain; *STAC2,* SH3 and cysteine rich domain 2

Supplemental Figure 5: Top aDAGs across oligodendrocyte subtypes, myelination-related genes, and overlap with aging and disease gene sets

(a) Clustermap of the top 5 positive and negative aDAGs across OPCs and oligodendrocyte subtypes (blue, negative association with age; magenta, positive association with age). Non-coding and pseudogenes are distinguished by gray italics. Cell types ordered by hierarchical clustering.

(b) Clustermap of aDAGs related to CNS myelination across cell types (blue, negative association with age; magenta, positive association with age). OPCs and oligodendrocytes are demarcated by black boxes.

(c) Enrichment of OPC and oligodendrocyte subtype aDAGS from previous aging and disease perturbation gene sets from GEO.

Abbreviations: CNS, central nervous system; ExN, excitatory neuron; GEO, Gene Expression Omnibus; OPC, oligodendrocyte precursor cell.

Supplemental Figure 6: Top aDAGs across non-neuronal, non-oligodendrocyte cells and overlap with aging and disease gene sets

(a) Clustermap of the top 5 positive and negative aDAGs across astrocytes, endothelial cells, mural cells, ependymal cells, and microglia (blue, negative association with age; magenta, positive association with age). Non-coding and pseudogenes are distinguished by gray italics. Cell types ordered by hierarchical clustering.

(b) UpSet plot of unique vs. shared aDAGs across astrocytes, endothelial cells, mural cells, ependymal cells, and microglia, where rows on the x-axis correspond to [cell type] aDAG sets, columns correspond to intersection size between sets, and bar color corresponds to the direction of association (blue, negative association with age; magenta, positive association with age)

(c) GSE of aDAGs in endothelial, ependymal, and mural cells.

Abbreviations: aDAG, aging-differentially associated gene; GSE, gene set enrichment

Supplemental Figure 7: Overlap of aDAGs across cell types with genes differentially expressed in aging human frontal cortex from GEO

(a) Astrocytes, microglia, and oligodendrocyte-3 aDAGs were significantly enriched for genes previously demonstrated to be increased in aged (28 years vs. 100 years) human frontal cortex (magenta, positive association; dark blue, negative association). Non-coding and pseudogenes are demarcated by gray italics. Cell types ordered by hierarchical clustering.

Asterisks mark cell types with significant enrichment.

(b) Feature scatter showing increased expression and association of *SERPINA3* and **(c)** *IFITM2* in with age in astrocytes

(d) Feature scatter showing increased expression and association of *CD163* and **(e)** *CD14* in with age in microglia

(f) Only neuronal subtypes were significantly enriched for genes previously demonstrated to be decreased in aged (28 years vs. 100 years) human frontal cortex (magenta, positive association; dark blue, negative association). Non-coding and pseudogenes are demarcated by gray italics. Asterisks mark cell types with significant enrichment. Cell types ordered by hierarchical clustering.

(g) Feature scatter showing decreased expression and association with age of *KCNF1* in *LHX*$^{+}$*PVALB*$^{+}$ cortical InN, **(h)** *LY6H* in cortical InN and *RORB*$^{+}$ ExN, and **(i)** *PFN1* in *LHX6*$^{+}$*PVALB*$^{+}$ cortical InN

Abbreviations: aDAG, aging-differentially associated gene; EC, entorhinal cortex; ExN, excitatory neuron; *IFITM2*, interferon-induced transmembrane protein 2; InN, inhibitory neuron; *KCNF1*, potassium voltage-gated channel modifier subfamily F member 1; *LY6H*, lymphocyte antigen 6 family member H; MTG, middle temporal gyrus; OPC, oligodendrocyte precursor cell; *PFN1*, profilin 1; PUT, putamen; *SERPINA3*, serpin family A member 3; SPN, spiny projection neuron; SVZ, subventricular zone; UMAP, uniform manifold approximation and projection.

Supplemental Figure 8: Mean expression of genes nearest to AD and PD GWAS-identified risk loci across brain regions and cell types

(a) Dot plot of mean expression of genes nearest to AD GWAS-nominated risk loci across brain regions. Size of circle denotes percentage of cells in a brain region expressing a gene and color represents strength of expression (purple, high expression; light blue, low expression)

(b) Dot plot of mean expression of genes nearest to AD GWAS-nominated risk loci across cell types

(c) Dot plot of mean expression of genes nearest to PD GWAS-nominated risk loci across brain regions and **(d)** cell types

Supplemental Table 1: Donor Demographics

Supplemental Table 2: Number of Significant Differentially Associated Genes with Age by Brain Region, Broad Type, and Cell Subtype

Supplemental Table 3: Coefficient estimates for significant brain region aDAGs that are also significant at the broad type level

Supplemental Table 4: glmmTMB All Significant aDAGs (FDR BH < 0.05)

Supplemental Table 5: Oligodendrocyte Proportions by Brain Region and Age

Supplemental Information: Age-Associated Gene Set Enrichment Outputs for Brain Region, Broad Type, and Cell Type

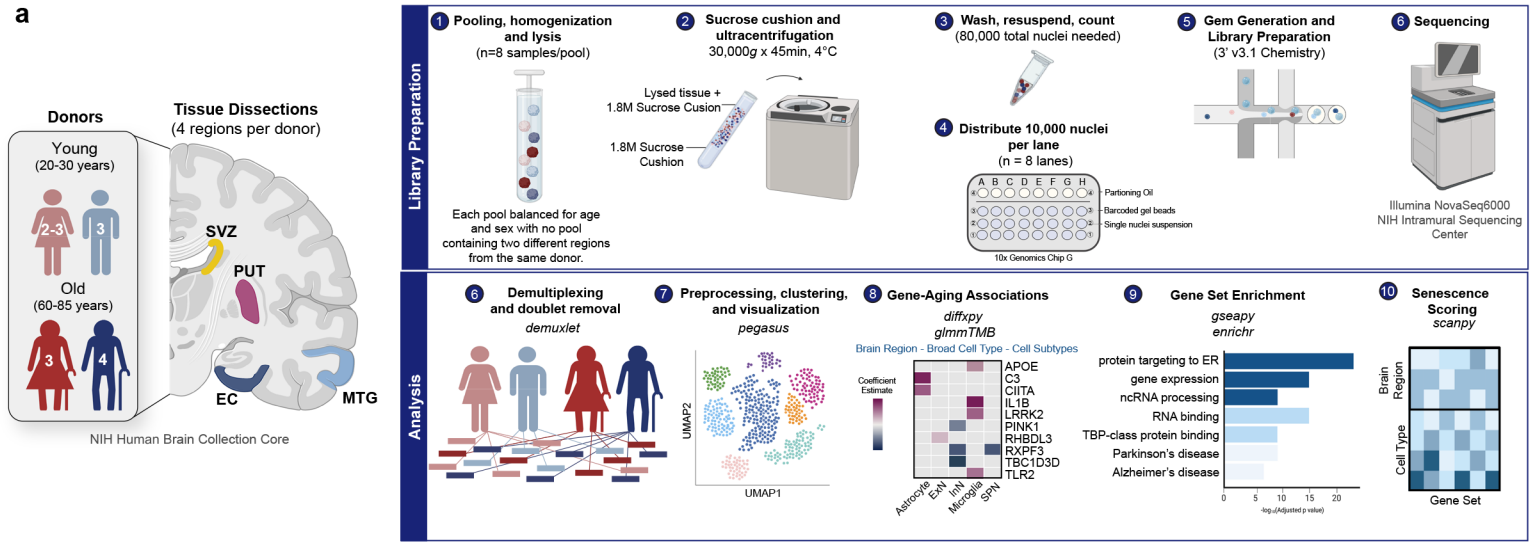
a
Donors
Young
(20-30 years)
2-3
3
Old
(60-85 years)
3
4
Tissue Dissections
(4 regions per donor)
SVZ
PUT
EC
MTG
NIH Human Brain Collection Core
Library Preparation
1 Pooling, homogenization and lysis
(n=8 samples/pool)
Each pool balanced for age and sex with no pool containing two different regions from the same donor.
2 Sucrose cushion and ultracentrifugation
30,000g x 45min, 4°C
Lysed tissue + 1.8M Sucrose Cusion
1.8M Sucrose Cushion
3 Wash, resuspend, count
(80,000 total nuclei needed)
4 Distribute 10,000 nuclei per lane
(n = 8 lanes)
A B C D E F G H
Partioning Oil
Barcoded gel beads
Single nuclei suspension
10x Genomics Chip G
5 Gem Generation and Library Preparation
(3' v3.1 Chemistry)
6 Sequencing
Illumina NovaSeq6000
NIH Intramural Sequencing Center
Analysis
6 Demultiplexing and doublet removal
demuxlet
7 Preprocessing, clustering, and visualization
pegasus
UMAP2
UMAP1
8 Gene-Aging Associations
diffxpy
glmmTMB
Brain Region - Broad Cell Type - Cell Subtypes
Coefficient Estimate
APOE
C3
CIITA
IL1B
LRRK2
PINK1
RHBDL3
RXPF3
TBC1D3D
TLR2
Astrocyte
ExN
InN
Microglia
SPN
9 Gene Set Enrichment
gseapy
enrichr
protein targeting to ER
gene expression
ncRNA processing
RNA binding
TBP-class protein binding
Parkinson's disease
Alzheimer's disease
0
5
10
15
20
-log10(Adjusted p value)
10 Senescence Scoring
scanpy
Brain Region
Cell Type
Gene Set

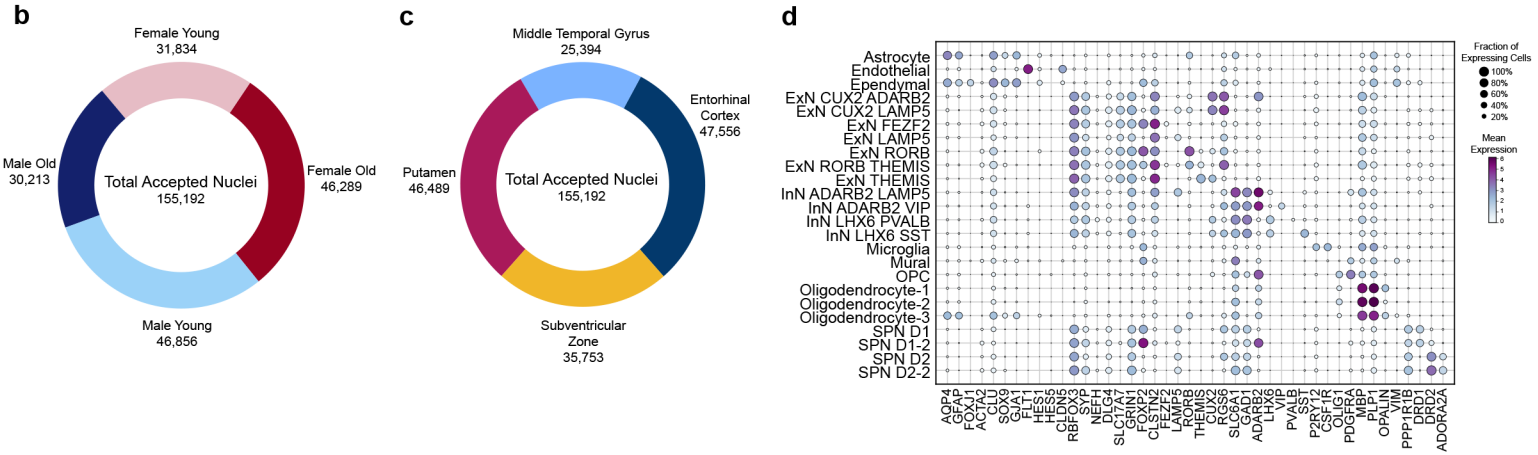
b
Female Young
31,834
Male Old
30,213
Total Accepted Nuclei
155,192
Female Old
46,289
Male Young
46,856
c
Middle Temporal Gyrus
25,394
Entorhinal Cortex
47,556
Putamen
46,489
Total Accepted Nuclei
155,192
Subventricular Zone
35,753
d
Astrocyte
Endothelial
Ependymal
ExN CUX2 ADARB2
ExN CUX2 LAMP5
ExN FEZF2
ExN LAMP5
ExN RORB
ExN RORB THEMIS
ExN THEMIS
InN ADARB2 LAMP5
InN ADARB2 VIP
InN LHX6 PVALB
InN LHX6 SST
Microglia
Mural
OPC
Oligodendrocyte-1
Oligodendrocyte-2
Oligodendrocyte-3
SPN D1
SPN D1-2
SPN D2
SPN D2-2
AQP4
GFAP
FOXJ1
ACTA2
CLDN5
SOX9
GJA1
FLT1
HES1
HES5
CLDN5
RBFOX3
SYP
NEFH
DLG4
SLC17A7
GRIN1
FOXP2
CLSTN2
FEZF2
LAMP5
LAMP5
THEMIS
CUX2
RGS6
SLC6A1
GAD1
ADARB2
LHX6
VIP
PVALB
SST
P2RY1
CSF1R
OLIG1
PDGFRA
MBP
PLP1
PLIN
OPALIN
VIM
PPP1R1B
DRD1
DRD2
ADORA2A
Fraction of Expressing Cells
100%
80%
60%
40%
20%
Mean Expression
5
4
3
2
1
0

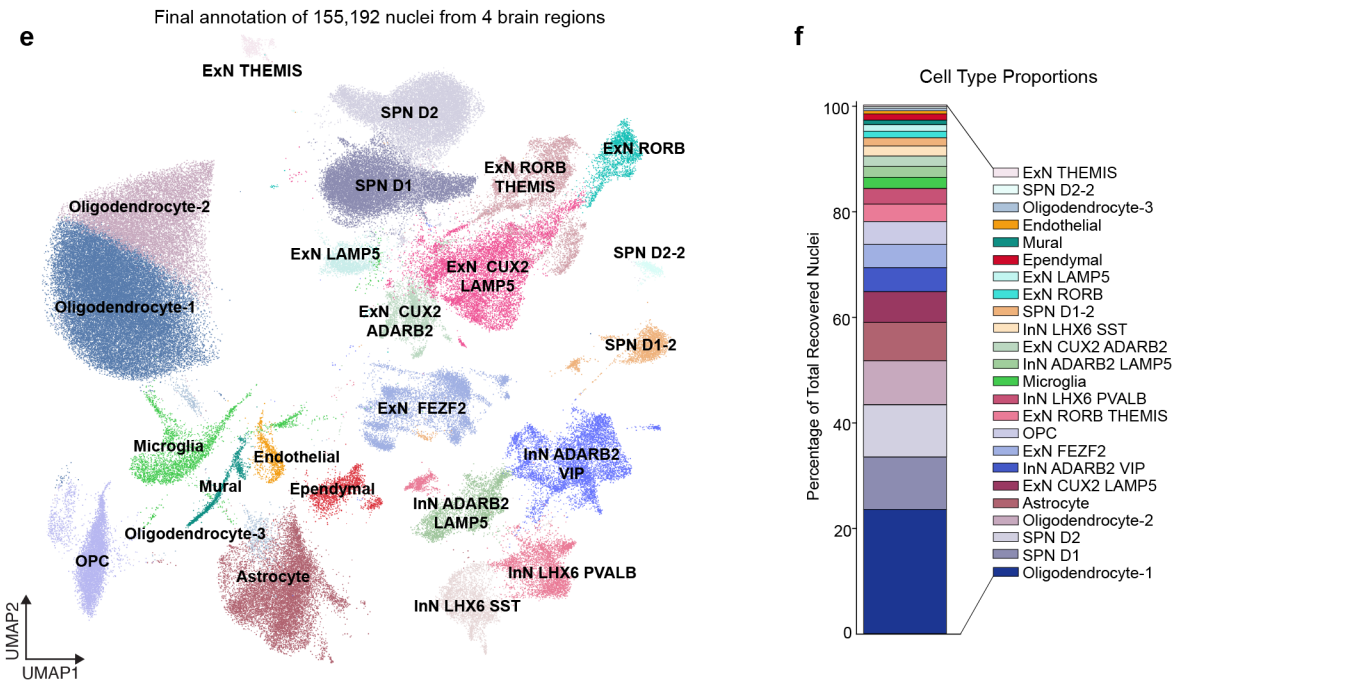
Final annotation of 155,192 nuclei from 4 brain regions
e
ExN THEMIS
SPN D2
ExN RORB
SPN D1
ExN RORB THEMIS
Oligodendrocyte-2
ExN LAMP5
ExN CUX2 LAMP5
SPN D2-2
Oligodendrocyte-1
ExN CUX2 ADARB2
SPN D1-2
ExN FEZF2
Microglia
Endothelial
InN ADARB2 VIP
Mural
Ependymal
InN ADARB2 LAMP5
Oligodendrocyte-3
OPC
Astrocyte
InN LHX6 PVALB
InN LHX6 SST
UMAP2
UMAP1
f
Cell Type Proportions
Percentage of Total Recovered Nuclei
0
20
40
60
80
100
ExN THEMIS
SPN D2-2
Oligodendrocyte-3
Endothelial
Mural
Ependymal
ExN LAMP5
ExN RORB
SPN D1-2
InN LHX6 SST
ExN CUX2 ADARB2
InN ADARB2 LAMP5
Microglia
InN LHX6 PVALB
ExN RORB THEMIS
OPC
ExN FEZF2
InN ADARB2 VIP
ExN CUX2 LAMP5
Astrocyte
Oligodendrocyte-2
SPN D2
SPN D1
Oligodendrocyte-1

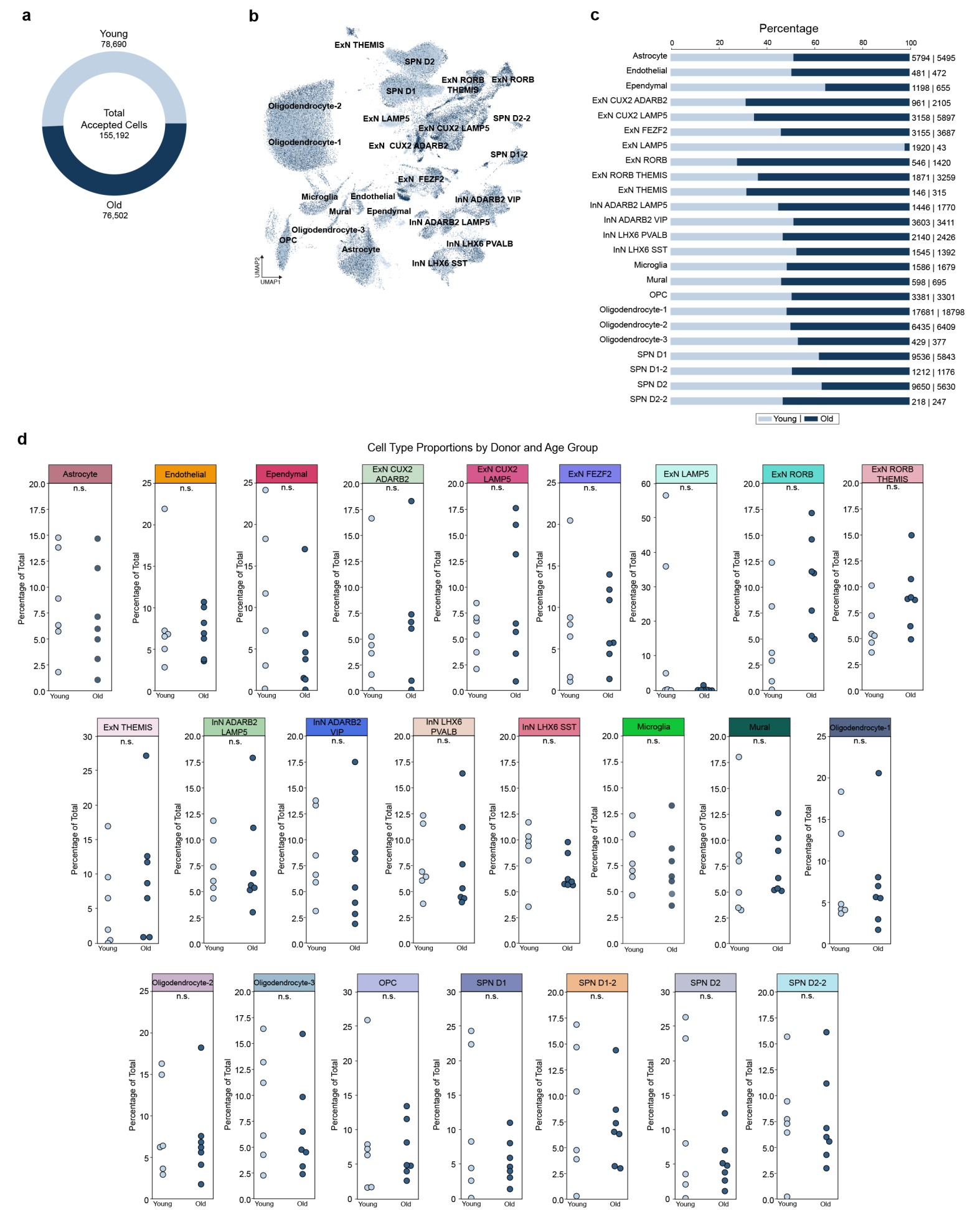
a
Young
78,690
Total
Accepted Cells
155,192
Old
76,502
b
ExN THEMIS
SPN D2
ExN RORB THEMIS
ExN RORB
SPN D1
Oligodendrocyte-2
ExN LAMP5
SPN D2-2
ExN CUX2 LAMP5
Oligodendrocyte-1
ExN CUX2 ADARB2
SPN D1-2
ExN FEZF2
Microglia
Endothelial
InN ADARB2 VIP
Mural
Ependymal
InN ADARB2 LAMP5
Oligodendrocyte-3
OPC
Astrocyte
InN LHX6 PVALB
InN LHX6 SST
UMAP2
UMAP1
c
Percentage
0
20
40
60
80
100
Astrocyte 5794 | 5495
Endothelial 481 | 472
Ependymal 1198 | 655
ExN CUX2 ADARB2 961 | 2105
ExN CUX2 LAMP5 3158 | 5897
ExN FEZF2 3155 | 3687
ExN LAMP5 1920 | 43
ExN RORB 546 | 1420
ExN RORB THEMIS 1871 | 3259
ExN THEMIS 146 | 315
InN ADARB2 LAMP5 1446 | 1770
InN ADARB2 VIP 3603 | 3411
InN LHX6 PVALB 2140 | 2426
InN LHX6 SST 1545 | 1392
Microglia 1586 | 1679
Mural 598 | 695
OPC 3381 | 3301
Oligodendrocyte-1 17681 | 18798
Oligodendrocyte-2 6435 | 6409
Oligodendrocyte-3 429 | 377
SPN D1 9536 | 5843
SPN D1-2 1212 | 1176
SPN D2 9650 | 5630
SPN D2-2 218 | 247
Young | Old
d
Cell Type Proportions by Donor and Age Group
Astrocyte
Endothelial
Ependymal
ExN CUX2 ADARB2
ExN CUX2 LAMP5
ExN FEZF2
ExN LAMP5
ExN RORB
ExN RORB THEMIS
ExN THEMIS
InN ADARB2 LAMP5
InN ADARB2 VIP
InN LHX6 PVALB
InN LHX6 SST
Microglia
Mural
Oligodendrocyte-1
Oligodendrocyte-2
Oligodendrocyte-3
OPC
SPN D1
SPN D1-2
SPN D2
SPN D2-2
n.s.
Percentage of Total
Young
Old

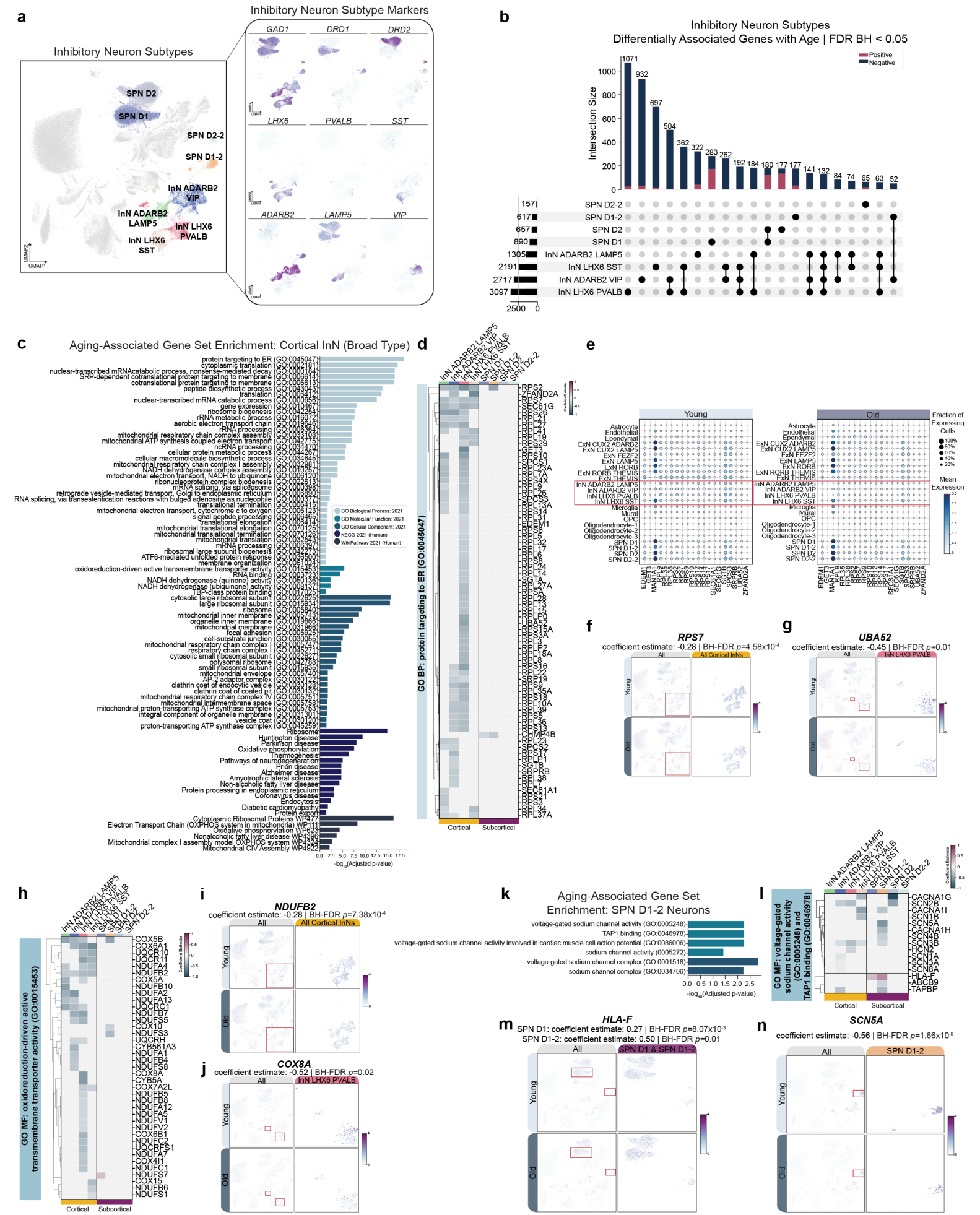
a
Inhibitory Neuron Subtypes
SPN D2
SPN D1
SPN D2-2
SPN D1-2
InN ADARB2 VIP
InN ADARB2 LAMP5
InN LHX6 PVALB
InN LHX6 SST
UMAP1
UMAP2
Inhibitory Neuron Subtype Markers
GAD1
DRD1
DRD2
LHX6
PVALB
SST
ADARB2
LAMP5
VIP
b
Inhibitory Neuron Subtypes
Differentially Associated Genes with Age | FDR BH < 0.05
Positive
Negative
Intersection Size
1071
932
697
504
362
322
283
262
192
184
180
177
177
141
132
84
74
65
63
52
157
617
657
890
1305
2191
2717
3097
2500
0
c
Aging-Associated Gene Set Enrichment: Cortical InN (Broad Type)
GO Biological Process: 2021
GO Molecular Function: 2021
GO Cellular Component: 2021
KEGG 2021 (Human)
WikiPathway 2021 (Human)
-log10(Adjusted p-value)
d
GO BP: protein targeting to ER (GO:0045047)
Cortical
Subcortical
e
Young
Old
Fraction of Expressing Cells
Mean Expression
f
RPS7
coefficient estimate: -0.28 | BH-FDR p=4.58x10-4
All
All Cortical InNs
g
UBA52
coefficient estimate: -0.45 | BH-FDR p=0.01
All
InN LHX6 PVALB
h
GO MF: oxidoreduction-driven active transmembrane transporter activity (GO:0015453)
Cortical
Subcortical
i
NDUFB2
coefficient estimate: -0.28 | BH-FDR p=7.38x10-4
All
All Cortical InNs
j
COX8A
coefficient estimate: -0.52 | BH-FDR p=0.02
All
InN LHX6 PVALB
k
Aging-Associated Gene Set Enrichment: SPN D1-2 Neurons
voltage-gated sodium channel activity (GO:0005248)
TAP1 binding (GO:0046978)
voltage-gated sodium channel activity involved in cardiac muscle cell action potential (GO:0086006)
sodium channel activity (0005272)
voltage-gated sodium channel complex (GO:0001518)
sodium channel complex (GO:0034706)
-log10(Adjusted p-value)
l
GO MF: voltage-gated sodium channel activity (GO:0005248) and TAP1 binding (GO:0046978)
Cortical
Subcortical
m
HLA-F
SPN D1: coefficient estimate: 0.27 | BH-FDR p=8.07x10-3
SPN D1-2: coefficient estimate: 0.50 | BH-FDR p=0.01
All
SPN D1 & SPN D1-2
n
SCN5A
coefficient estimate: -0.56 | BH-FDR p=1.66x10-8
All
SPN D1-2

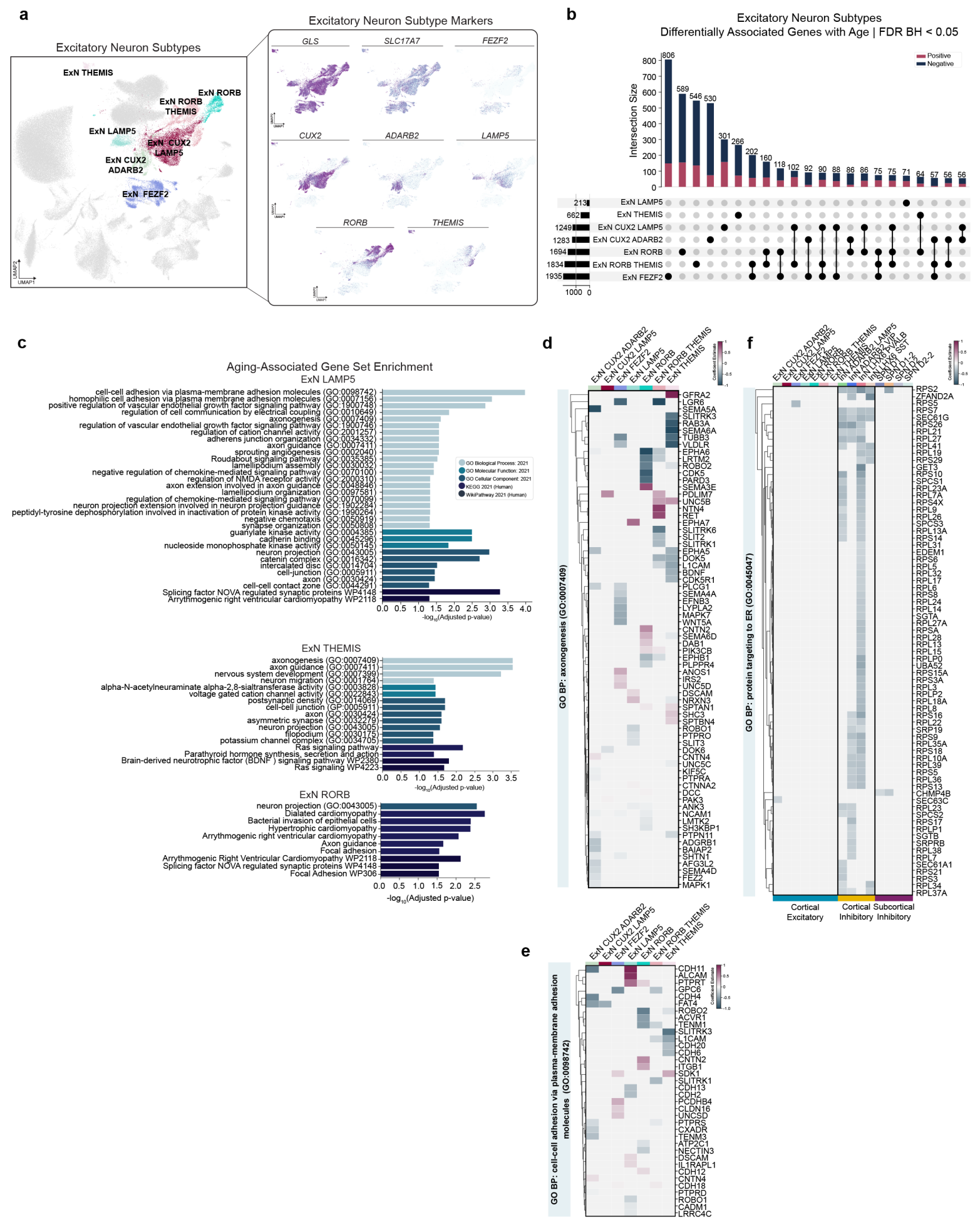
a
Excitatory Neuron Subtypes
ExN THEMIS
ExN RORB
ExN RORB THEMIS
ExN LAMP5
ExN CUX2 LAMP5
ExN CUX2 ADARB2
ExN FEZF2
UMAP1
UMAP2
Excitatory Neuron Subtype Markers
GLS
SLC17A7
FEZF2
CUX2
ADARB2
LAMP5
RORB
THEMIS
b
Excitatory Neuron Subtypes
Differentially Associated Genes with Age | FDR BH < 0.05
Positive
Negative
Intersection Size
806
589
546
530
301
266
202
160
118
102
92
90
88
86
86
75
75
71
64
57
56
56
213 ExN LAMP5
662 ExN THEMIS
1249 ExN CUX2 LAMP5
1283 ExN CUX2 ADARB2
1694 ExN RORB
1834 ExN RORB THEMIS
1935 ExN FEZF2
c
Aging-Associated Gene Set Enrichment
ExN LAMP5
cell-cell adhesion via plasma-membrane adhesion molecules (GO:0098742)
homophilic cell adhesion via plasma membrane adhesion molecules (GO:0007156)
positive regulation of vascular endothelial growth factor signaling pathway (GO:1900748)
regulation of cell communication by electrical coupling (GO:0010649)
axonogenesis (GO:0007409)
regulation of vascular endothelial growth factor signaling pathway (GO:1900746)
regulation of cation channel activity (GO:2001257)
adherens junction organization (GO:0034332)
axon guidance (GO:0007411)
sprouting angiogenesis (GO:0002040)
Roudabout signaling pathway (GO:0035385)
lamellipodium assembly (GO:0030032)
negative regulation of chemokine-mediated signaling pathway (GO:0070100)
regulation of NMDA receptor activity (GO:2000310)
axon extension involved in axon guidance (GO:0048846)
lamellipodium organization (GO:0097581)
regulation of chemokine-mediated signaling pathway (GO:0070099)
neuron projection extension involved in neuron projection guidance (GO:1902284)
peptidyl-tyrosine dephosphorylation involved in inactivation of protein kinase activity (GO:1990264)
negative chemotaxis (GO:0050919)
synapse organization (GO:0050808)
guanylate kinase activity (GO:0004385)
cadherin binding (GO:0045296)
nucleoside monophosphate kinase activity (GO:0050145)
neuron projection (GO:0043005)
catenin complex (GO:0016342)
intercalated disc (GO:0014704)
cell-junction (GO:0005911)
axon (GO:0030424)
cell-cell contact zone (GO:0044291)
Splicing factor NOVA regulated synaptic proteins WP4148
Arrythmogenic right ventricular cardiomyopathy WP2118
GO Biological Process: 2021
GO Molecular Function: 2021
GO Cellular Component: 2021
KEGG 2021 (Human)
WikiPathway 2021 (Human)
0.0 0.5 1.0 1.5 2.0 2.5 3.0 3.5 4.0
-log10(Adjusted p-value)
ExN THEMIS
axonogenesis (GO:0007409)
axon guidance (GO:0007411)
nervous system development (GO:0007399)
neuron migration (GO:0001764)
alpha-N-acetylneuraminate alpha-2,8-sialtransferase activity (GO:0003828)
voltage gated cation channel activity (GO:0022843)
postsynaptic density (GO:0014069)
cell-cell junction (GP:0005911)
axon (GO:0030424)
asymmetric synapse (GO:0032279)
neuron projection (GO:0043005)
filopodium (GO:0030175)
potassium channel complex (GO:0034705)
Ras signaling pathway
Parathyroid hormone synthesis, secretion and action
Brain-derived neurotrophic factor (BDNF) signaling pathway WP2380
Ras signaling WP4223
0.0 0.5 1.0 1.5 2.0 2.5 3.0 3.5
-log10(Adjusted p-value)
ExN RORB
neuron projection (GO:0043005)
Dialated cardiomyopathy
Bacterial invasion of epithelial cells
Hypertrophic cardiomyopathy
Arrythmogenic right ventricular cardiomyopathy
Axon guidance
Focal adhesion
Arrythmogenic Right Ventricular Cardiomyopathy WP2118
Splicing factor NOVA regulated synaptic proteins WP4148
Focal Adhesion WP306
0.0 0.5 1.0 1.5 2.0 2.5
-log10(Adjusted p-value)
d
ExN CUX2 ADARB2
ExN CUX2 LAMP5
ExN FEZF2
ExN LAMP5
ExN RORB
ExN RORB THEMIS
ExN THEMIS
Coefficient Estimate
GO BP: axonogenesis (GO:0007409)
GFRA2
LGR6
SEMA5A
SLITRK3
RAB3A
SEMA6A
TUBB3
VLDLR
EPHA6
LRTM2
ROBO2
CDK5
PARD3
SEMA3E
PDLIM7
UNC5B
NTN4
RET
EPHA7
SLITRK6
SLIT2
SLITRK1
EPHA5
DOK5
L1CAM
BDNF
CDK5R1
PLCG1
SEMA4A
EFNB3
LYPLA2
MAPK7
WNT5A
CNTN2
SEMA6D
DAB1
PIK3CB
EPHB1
PLPPR4
ANOS1
IRS2
UNC5D
DSCAM
NRXN3
SPTAN1
SHC3
SPTBN4
ROBO1
PTPRO
SLIT3
DOK6
CNTN4
UNC5C
KIF5C
PTPRA
CTNNA2
DCC
PAK3
ANK3
NCAM1
LMTK2
SH3KBP1
PTPN11
ADGRB1
BAIAP2
SHTN1
AFG3L2
SEMA4D
FEZ2
MAPK1
f
ExN CUX2 ADARB2
ExN CUX2 LAMP5
ExN FEZF2
ExN LAMP5
ExN RORB
ExN RORB THEMIS
ExN THEMIS
InhN ADARB2 LAMP5
InhN ADARB2 PVALB
InhN LAMP5 VIP
InhN LAMP5 SST
SPN D1-1
SPN D1-2
SPN D2-1
SPN D2-2
Coefficient Estimate
GO BP: protein targeting to ER (GO:0045047)
RPS2
ZFAND2A
RPS5
RPS7
SEC61G
RPS26
RPL21
RPL27
RPL41
RPL19
RPS29
GET3
RPS10
SPCS1
RPL23A
RPL7A
RPS4X
RPL9
RPL26
SPCS3
RPL13A
RPS14
RPL31
EDEM1
RPS6
RPL5
RPL32
RPL17
RPL6
RPS8
RPL24
RPL14
SGTA
RPL27A
RPSA
RPL28
RPL13
RPL15
RPLP0
UBA52
RPS15A
RPS3A
RPL3
RPLP2
RPL18A
RPL8
RPS16
RPL22
SRP19
RPS9
RPL35A
RPS18
RPL10A
RPL39
RPS5
RPL36
RPS13
CHMP4B
SEC63C
RPL23
SPCS2
RPS17
RPLP1
SGTB
SRPRB
RPL38
RPL7
SEC61A1
RPS21
RPS3
RPL34
RPL37A
Cortical Excitatory
Cortical Inhibitory
Subcortical Inhibitory
e
ExN CUX2 ADARB2
ExN CUX2 LAMP5
ExN FEZF2
ExN LAMP5
ExN RORB
ExN RORB THEMIS
ExN THEMIS
Coefficient Estimate
GO BP: cell-cell adhesion via plasma-membrane adhesion molecules (GO:0098742)
CDH11
ALCAM
PTPRT
GPC6
CDH4
FAT4
ROBO2
ACVR1
TENM1
SLITRK3
L1CAM
CDH20
CDH6
CNTN2
ITGB1
SDK1
SLITRK1
CDH13
CDH2
PCDHB4
CLDN16
UNCSD
PTPRS
CXADR
TENM3
ATP2C1
NECTIN3
DSCAM
IL1RAPL1
CDH12
CNTN4
CDH18
PTPRD
ROBO1
CADM1
LRRC4C

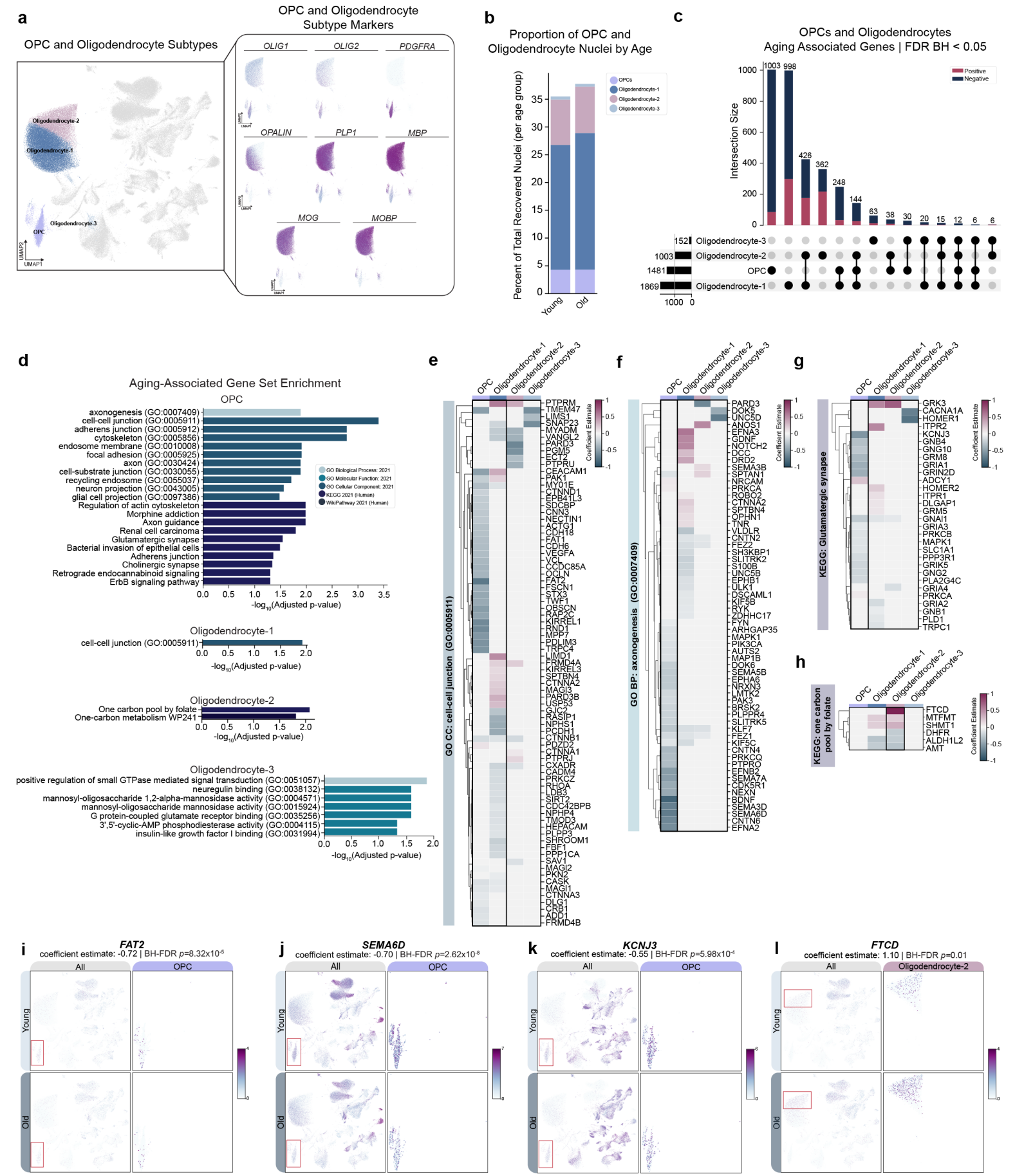
a
OPC and Oligodendrocyte Subtypes
Oligodendrocyte-2
Oligodendrocyte-1
Oligodendrocyte-3
OPC
UMAP2
UMAP1
OPC and Oligodendrocyte Subtype Markers
OLIG1
OLIG2
PDGFRA
OPALIN
PLP1
MBP
MOG
MOBP
b
Proportion of OPC and Oligodendrocyte Nuclei by Age
Percent of Total Recovered Nuclei (per age group)
OPCs
Oligodendrocyte-1
Oligodendrocyte-2
Oligodendrocyte-3
Young
Old
c
OPCs and Oligodendrocytes
Aging Associated Genes | FDR BH < 0.05
Intersection Size
Positive
Negative
1003
998
426
362
248
144
63
38
30
20
15
12
6
6
152
1481
1869
Oligodendrocyte-3
Oligodendrocyte-2
OPC
Oligodendrocyte-1
d
Aging-Associated Gene Set Enrichment
OPC
axonogenesis (GO:0007409)
cell-cell junction (GO:0005911)
adherens junction (GO:0005912)
cytoskeleton (GO:0005856)
endosome membrane (GO:0010008)
focal adhesion (GO:0005925)
axon (GO:0030424)
cell-substrate junction (GO:0030055)
recycling endosome (GO:0055037)
neuron projection (GO:0043005)
glial cell projection (GO:0097386)
Regulation of actin cytoskeleton
Morphine addiction
Axon guidance
Renal cell carcinoma
Glutamatergic synapse
Bacterial invasion of epithelial cells
Adherens junction
Cholinergic synapse
Retrograde endocannabinoid signaling
ErbB signaling pathway
GO Biological Process: 2021
GO Molecular Function: 2021
GO Cellular Component: 2021
KEGG 2021 (Human)
WikiPathway 2021 (Human)
-log10(Adjusted p-value)
Oligodendrocyte-1
cell-cell junction (GO:0005911)
Oligodendrocyte-2
One carbon pool by folate
One-carbon metabolism WP241
Oligodendrocyte-3
positive regulation of small GTPase mediated signal transduction (GO:0051057)
neuregulin binding (GO:0038132)
mannosyl-oligosaccharide 1,2-alpha-mannosidase activity (GO:0004571)
mannosyl-oligosaccharide mannosidase activity (GO:0015924)
G protein-coupled glutamate receptor binding (GO:0035256)
3',5'-cyclic-AMP phosphodiesterase activity (GO:0004115)
insulin-like growth factor I binding (GO:0031994)
e
GO CC: cell-cell junction (GO:0005911)
Coefficient Estimate
f
GO BP: axonogenesis (GO:0007409)
g
KEGG: Glutamatergic synapse
h
KEGG: one carbon pool by folate
FTCD
MTFMT
SHMT1
DHFR
ALDH1L2
AMT
i
FAT2
coefficient estimate: -0.72 | BH-FDR p=8.32x10-5
All
OPC
Young
Old
j
SEMA6D
coefficient estimate: -0.70 | BH-FDR p=2.62x10-8
k
KCNJ3
coefficient estimate: -0.55 | BH-FDR p=5.98x10-4
l
FTCD
coefficient estimate: 1.10 | BH-FDR p=0.01
Oligodendrocyte-2

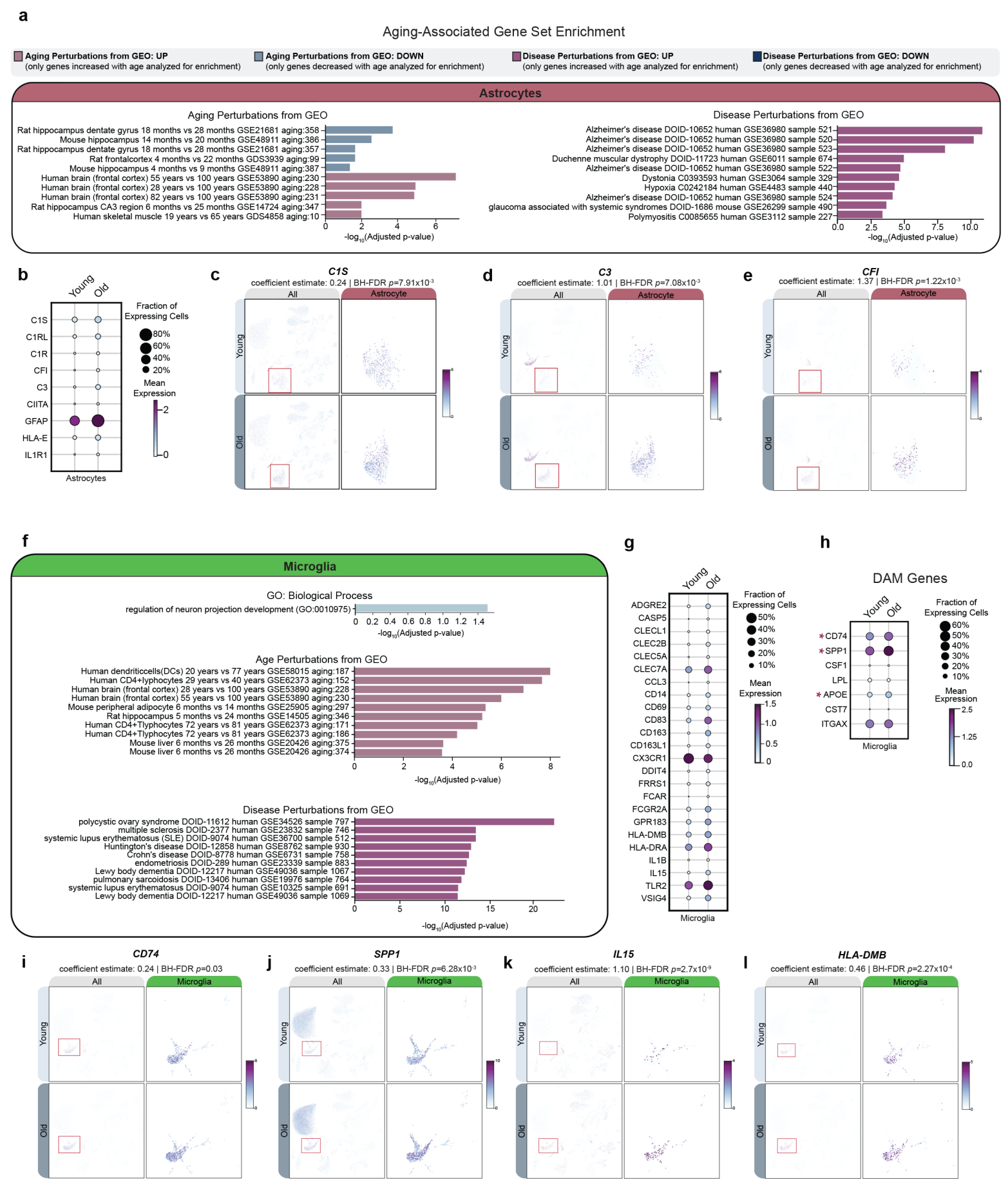
a
Aging-Associated Gene Set Enrichment
Aging Perturbations from GEO: UP (only genes increased with age analyzed for enrichment)
Aging Perturbations from GEO: DOWN (only genes decreased with age analyzed for enrichment)
Disease Perturbations from GEO: UP (only genes increased with age analyzed for enrichment)
Disease Perturbations from GEO: DOWN (only genes decreased with age analyzed for enrichment)
Astrocytes
Aging Perturbations from GEO
Rat hippocampus dentate gyrus 18 months vs 28 months GSE21681 aging:358
Mouse hippocampus 14 months vs 20 months GSE48911 aging:386
Rat hippocampus dentate gyrus 18 months vs 28 months GSE21681 aging:357
Rat frontalcortex 4 months vs 22 months GDS3939 aging:99
Mouse hippocampus 4 months vs 9 months GSE48911 aging:387
Human brain (frontal cortex) 55 years vs 100 years GSE53890 aging:230
Human brain (frontal cortex) 28 years vs 100 years GSE53890 aging:228
Human brain (frontal cortex) 82 years vs 100 years GSE53890 aging:231
Rat hippocampus CA3 region 6 months vs 25 months GSE14724 aging:347
Human skeletal muscle 19 years vs 65 years GDS4858 aging:10
-log10(Adjusted p-value)
Disease Perturbations from GEO
Alzheimer's disease DOID-10652 human GSE36980 sample 521
Alzheimer's disease DOID-10652 human GSE36980 sample 520
Alzheimer's disease DOID-10652 human GSE36980 sample 523
Duchenne muscular dystrophy DOID-11723 human GSE6011 sample 674
Alzheimer's disease DOID-10652 human GSE36980 sample 522
Dystonia C0393593 human GSE3064 sample 329
Hypoxia C0242184 human GSE4483 sample 440
Alzheimer's disease DOID-10652 human GSE36980 sample 524
glaucoma associated with systemic syndromes DOID-1686 mouse GSE26299 sample 490
Polymyositis C0085655 human GSE3112 sample 227
-log10(Adjusted p-value)
b
Young
Old
C1S
C1RL
C1R
CFI
C3
CIITA
GFAP
HLA-E
IL1R1
Astrocytes
Fraction of Expressing Cells
80%
60%
40%
20%
Mean Expression
c
C1S
coefficient estimate: 0.24 | BH-FDR p=7.91x10-3
All
Astrocyte
d
C3
coefficient estimate: 1.01 | BH-FDR p=7.08x10-3
e
CFI
coefficient estimate: 1.37 | BH-FDR p=1.22x10-3
f
Microglia
GO: Biological Process
regulation of neuron projection development (GO:0010975)
-log10(Adjusted p-value)
Age Perturbations from GEO
Human dendriticcells(DCs) 20 years vs 77 years GSE58015 aging:187
Human CD4+lyphocytes 29 years vs 40 years GSE62373 aging:152
Human brain (frontal cortex) 28 years vs 100 years GSE53890 aging:228
Human brain (frontal cortex) 55 years vs 100 years GSE53890 aging:230
Mouse peripheral adipocyte 6 months vs 14 months GSE25905 aging:297
Rat hippocampus 5 months vs 24 months GSE14505 aging:346
Human CD4+Tlyphocytes 72 years vs 81 years GSE62373 aging:171
Human CD4+Tlyphocytes 72 years vs 81 years GSE62373 aging:186
Mouse liver 6 months vs 26 months GSE20426 aging:375
Mouse liver 6 months vs 26 months GSE20426 aging:374
-log10(Adjusted p-value)
Disease Perturbations from GEO
polycystic ovary syndrome DOID-11612 human GSE34526 sample 797
multiple sclerosis DOID-2377 human GSE23832 sample 746
systemic lupus erythematosus (SLE) DOID-9074 human GSE36700 sample 512
Huntington's disease DOID-12858 human GSE8762 sample 930
Crohn's disease DOID-8778 human GSE6731 sample 758
endometriosis DOID-289 human GSE23339 sample 883
Lewy body dementia DOID-12217 human GSE49036 sample 1067
pulmonary sarcoidosis DOID-13406 human GSE19976 sample 764
systemic lupus erythematosus DOID-9074 human GSE10325 sample 691
Lewy body dementia DOID-12217 human GSE49036 sample 1069
-log10(Adjusted p-value)
g
Young
Old
ADGRE2
CASP5
CLECL1
CLEC2B
CLEC5A
CLEC7A
CCL3
CD14
CD69
CD83
CD163
CD163L1
CX3CR1
DDIT4
FRRS1
FCAR
FCGR2A
GPR183
HLA-DMB
HLA-DRA
IL1B
IL15
TLR2
VSIG4
Microglia
Fraction of Expressing Cells
50%
40%
30%
20%
10%
Mean Expression
h
DAM Genes
Young
Old
CD74
SPP1
CSF1
LPL
APOE
CST7
ITGAX
Microglia
Fraction of Expressing Cells
60%
50%
40%
30%
20%
10%
Mean Expression
i
CD74
coefficient estimate: 0.24 | BH-FDR p=0.03
All
Microglia
j
SPP1
coefficient estimate: 0.33 | BH-FDR p=6.28x10-3
k
IL15
coefficient estimate: 1.10 | BH-FDR p=2.7x10-9
l
HLA-DMB
coefficient estimate: 0.46 | BH-FDR p=2.27x10-4

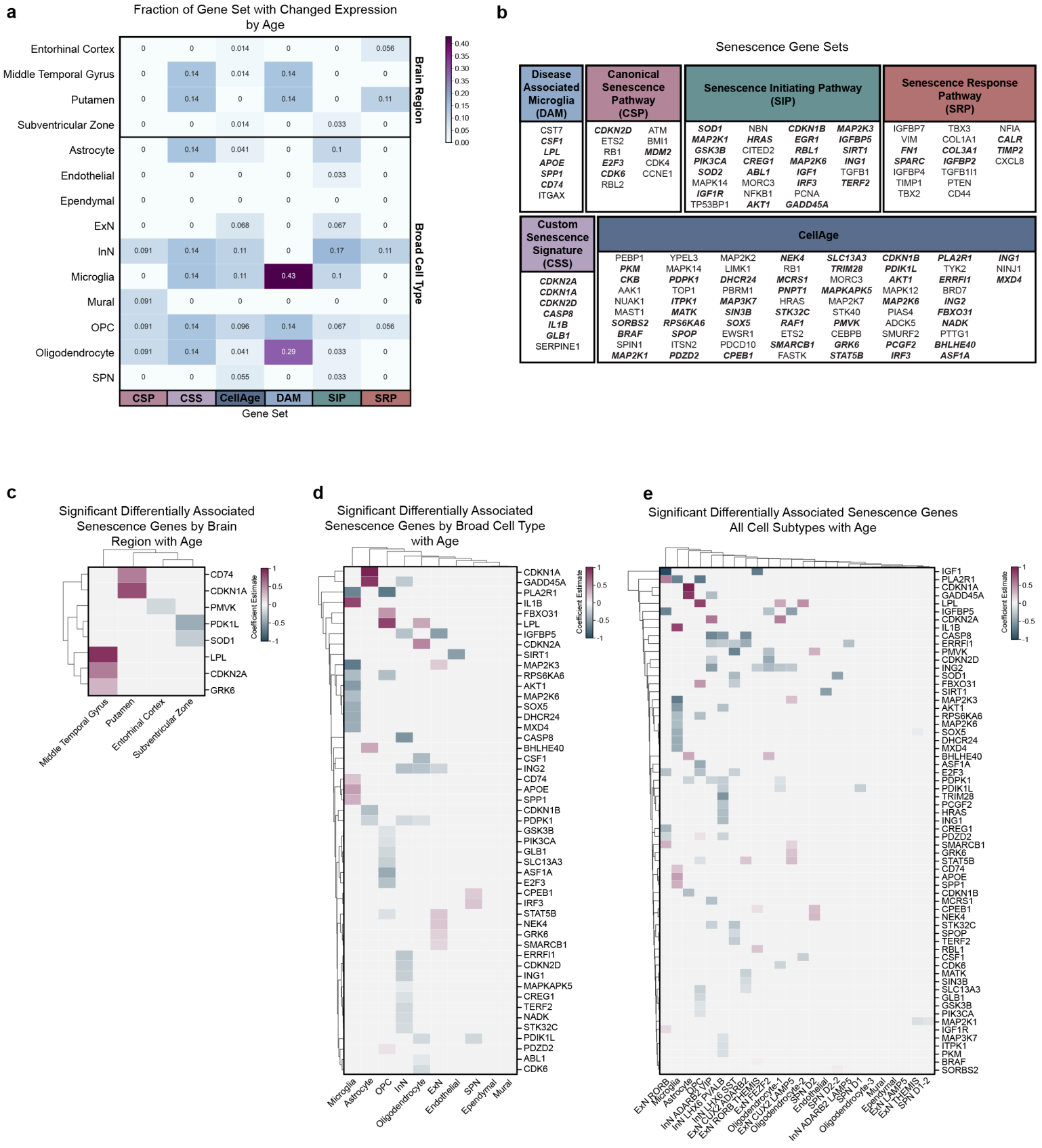
a
Fraction of Gene Set with Changed Expression by Age
Entorhinal Cortex
Middle Temporal Gyrus
Putamen
Subventricular Zone
Astrocyte
Endothelial
Ependymal
ExN
InN
Microglia
Mural
OPC
Oligodendrocyte
SPN
Brain Region
Broad Cell Type
CSP
CSS
CellAge
DAM
SIP
SRP
Gene Set
b
Senescence Gene Sets
Disease Associated Microglia (DAM)
Canonical Senescence Pathway (CSP)
Senescence Initiating Pathway (SIP)
Senescence Response Pathway (SRP)
Custom Senescence Signature (CSS)
CellAge
c
Significant Differentially Associated Senescence Genes by Brain Region with Age
Coefficient Estimate
Middle Temporal Gyrus
Putamen
Entorhinal Cortex
Subventricular Zone
d
Significant Differentially Associated Senescence Genes by Broad Cell Type with Age
Microglia
Astrocyte
OPC
InN
Oligodendrocyte
ExN
Endothelial
SPN
Ependymal
Mural
e
Significant Differentially Associated Senescence Genes All Cell Subtypes with Age

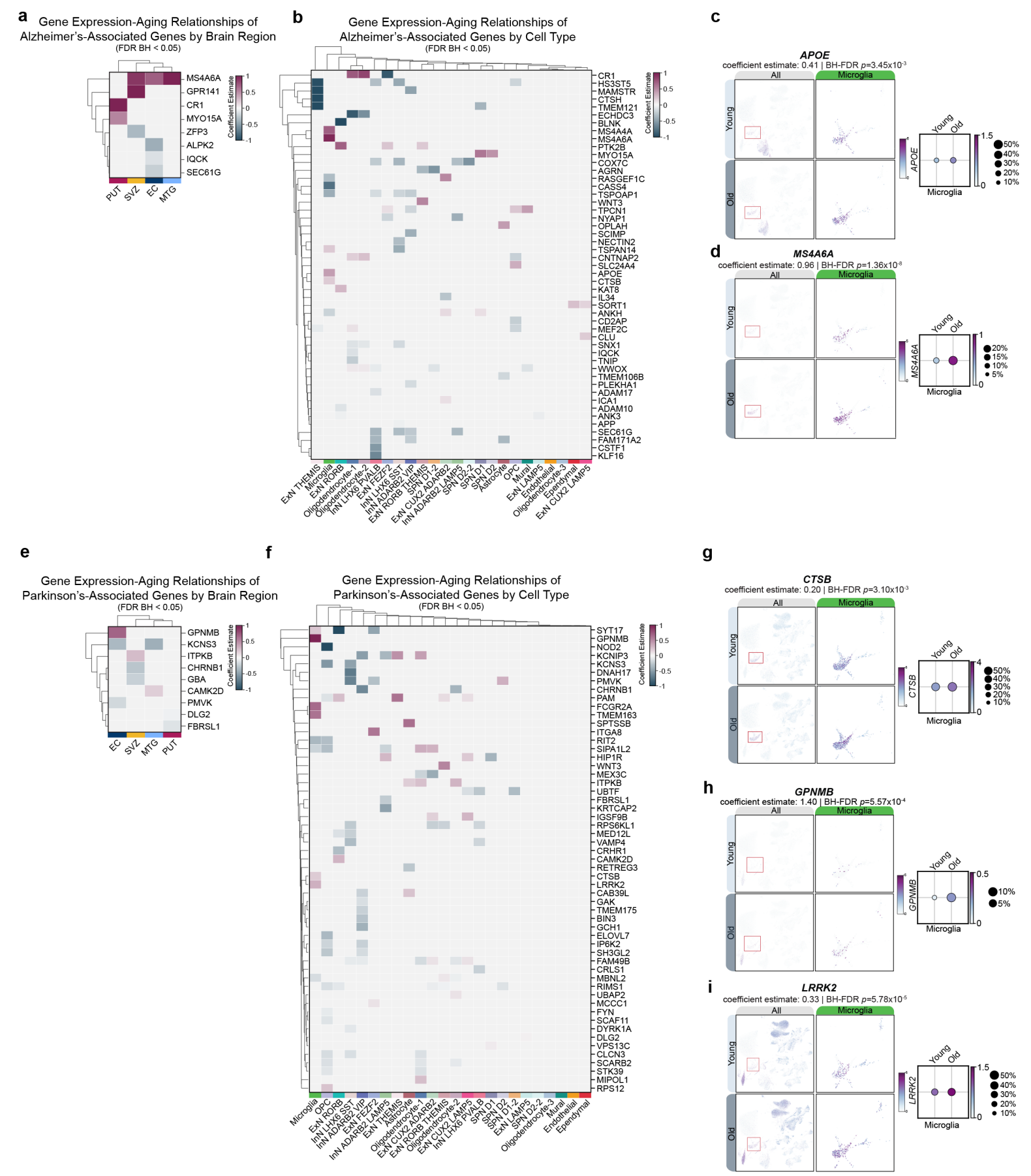
a
Gene Expression-Aging Relationships of Alzheimer's-Associated Genes by Brain Region
(FDR BH < 0.05)
MS4A6A
GPR141
CR1
MYO15A
ZFP3
ALPK2
IQCK
SEC61G
PUT
SVZ
EC
MTG
Coefficient Estimate
b
Gene Expression-Aging Relationships of Alzheimer's-Associated Genes by Cell Type
(FDR BH < 0.05)
c
APOE
coefficient estimate: 0.41 | BH-FDR p=3.45x10-3
All
Microglia
Young
Old
d
MS4A6A
coefficient estimate: 0.96 | BH-FDR p=1.36x10-8
e
Gene Expression-Aging Relationships of Parkinson's-Associated Genes by Brain Region
(FDR BH < 0.05)
GPNMB
KCNS3
ITPKB
CHRNB1
GBA
CAMK2D
PMVK
DLG2
FBRSL1
f
Gene Expression-Aging Relationships of Parkinson's-Associated Genes by Cell Type
(FDR BH < 0.05)
g
CTSB
coefficient estimate: 0.20 | BH-FDR p=3.10x10-3
h
GPNMB
coefficient estimate: 1.40 | BH-FDR p=5.57x10-4
i
LRRK2
coefficient estimate: 0.33 | BH-FDR p=5.78x10-5

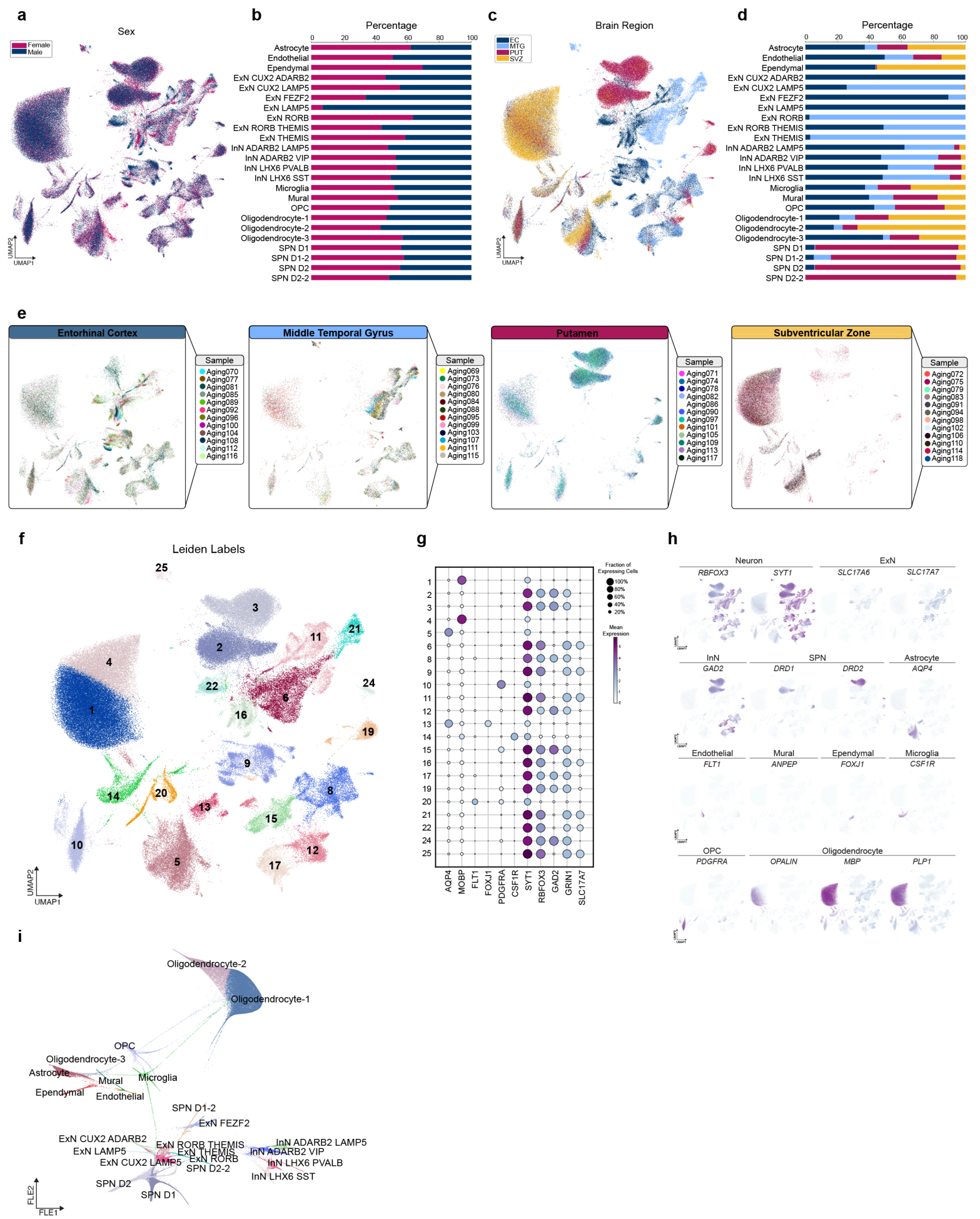
a
Sex
Female
Male
UMAP2
UMAP1
b
Percentage
0
20
40
60
80
100
Astrocyte
Endothelial
Ependymal
ExN CUX2 ADARB2
ExN CUX2 LAMP5
ExN FEZF2
ExN LAMP5
ExN RORB
ExN RORB THEMIS
ExN THEMIS
InN ADARB2 LAMP5
InN ADARB2 VIP
InN LHX6 PVALB
InN LHX6 SST
Microglia
Mural
OPC
Oligodendrocyte-1
Oligodendrocyte-2
Oligodendrocyte-3
SPN D1
SPN D1-2
SPN D2
SPN D2-2
c
Brain Region
EC
MTG
PUT
SVZ
UMAP2
UMAP1
d
Percentage
0
20
40
60
80
100
Astrocyte
Endothelial
Ependymal
ExN CUX2 ADARB2
ExN CUX2 LAMP5
ExN FEZF2
ExN LAMP5
ExN RORB
ExN RORB THEMIS
ExN THEMIS
InN ADARB2 LAMP5
InN ADARB2 VIP
InN LHX6 PVALB
InN LHX6 SST
Microglia
Mural
OPC
Oligodendrocyte-1
Oligodendrocyte-2
Oligodendrocyte-3
SPN D1
SPN D1-2
SPN D2
SPN D2-2
e
Entorhinal Cortex
Sample
Aging070
Aging077
Aging081
Aging085
Aging089
Aging092
Aging096
Aging100
Aging104
Aging108
Aging112
Aging116
Middle Temporal Gyrus
Sample
Aging069
Aging073
Aging076
Aging080
Aging084
Aging088
Aging095
Aging099
Aging103
Aging107
Aging111
Aging115
Putamen
Sample
Aging071
Aging074
Aging078
Aging082
Aging086
Aging090
Aging097
Aging101
Aging105
Aging109
Aging113
Aging117
Subventricular Zone
Sample
Aging072
Aging075
Aging079
Aging083
Aging091
Aging094
Aging098
Aging102
Aging106
Aging110
Aging114
Aging118
f
Leiden Labels
25
3
11
21
2
4
22
24
6
1
16
19
9
14
20
8
13
15
10
12
5
17
UMAP2
UMAP1
g
Fraction of Expressing Cells
100%
80%
60%
40%
20%
Mean Expression
1
2
3
4
5
6
8
9
10
11
12
13
14
15
16
17
19
20
21
22
24
25
AQP4
MOBP
FLT1
FOXJ1
PDGFRA
CSF1R
SYT1
RBFOX3
GAD2
GRIN1
SLC17A7
h
Neuron
RBFOX3
SYT1
ExN
SLC17A6
SLC17A7
InN
GAD2
SPN
DRD1
DRD2
Astrocyte
AQP4
Endothelial
FLT1
Mural
ANPEP
Ependymal
FOXJ1
Microglia
CSF1R
OPC
PDGFRA
Oligodendrocyte
OPALIN
MBP
PLP1
i
Oligodendrocyte-2
Oligodendrocyte-1
OPC
Oligodendrocyte-3
Astrocyte
Mural
Microglia
Ependymal
Endothelial
SPN D1-2
ExN FEZF2
ExN CUX2 ADARB2
ExN RORB THEMIS
InN ADARB2 LAMP5
ExN LAMP5
ExN THEMIS
InN ADARB2 VIP
ExN CUX2 LAMP5
ExN RORB
SPN D2-2
InN LHX6 PVALB
InN LHX6 SST
SPN D2
SPN D1
FLE2
FLE1

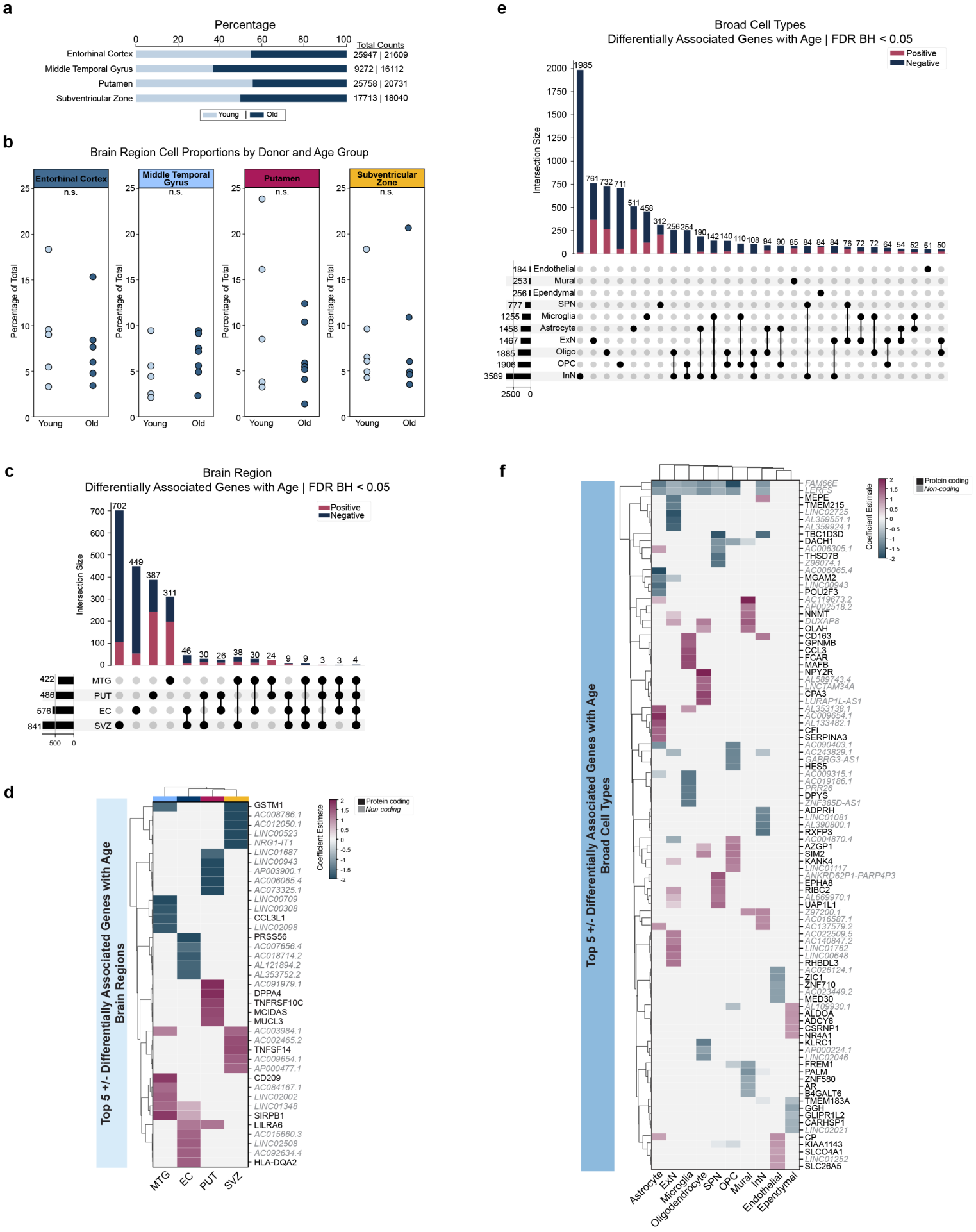
a
Percentage
Total Counts
Entorhinal Cortex 25947 | 21609
Middle Temporal Gyrus 9272 | 16112
Putamen 25758 | 20731
Subventricular Zone 17713 | 18040
Young
Old
b
Brain Region Cell Proportions by Donor and Age Group
Entorhinal Cortex
Middle Temporal Gyrus
Putamen
Subventricular Zone
n.s.
Percentage of Total
Young
Old
c
Brain Region
Differentially Associated Genes with Age | FDR BH < 0.05
Positive
Negative
Intersection Size
MTG
PUT
EC
SVZ
d
Top 5 +/- Differentially Associated Genes with Age
Brain Regions
Coefficient Estimate
Protein coding
Non-coding
MTG
EC
PUT
SVZ
e
Broad Cell Types
Differentially Associated Genes with Age | FDR BH < 0.05
Positive
Negative
Intersection Size
Endothelial
Mural
Ependymal
SPN
Microglia
Astrocyte
ExN
Oligo
OPC
InN
f
Top 5 +/- Differentially Associated Genes with Age
Broad Cell Types
Coefficient Estimate
Protein coding
Non-coding
Astrocyte
ExN
Microglia
Oligodendrocyte
SPN
OPC
Mural
InN
Endothelial
Ependymal

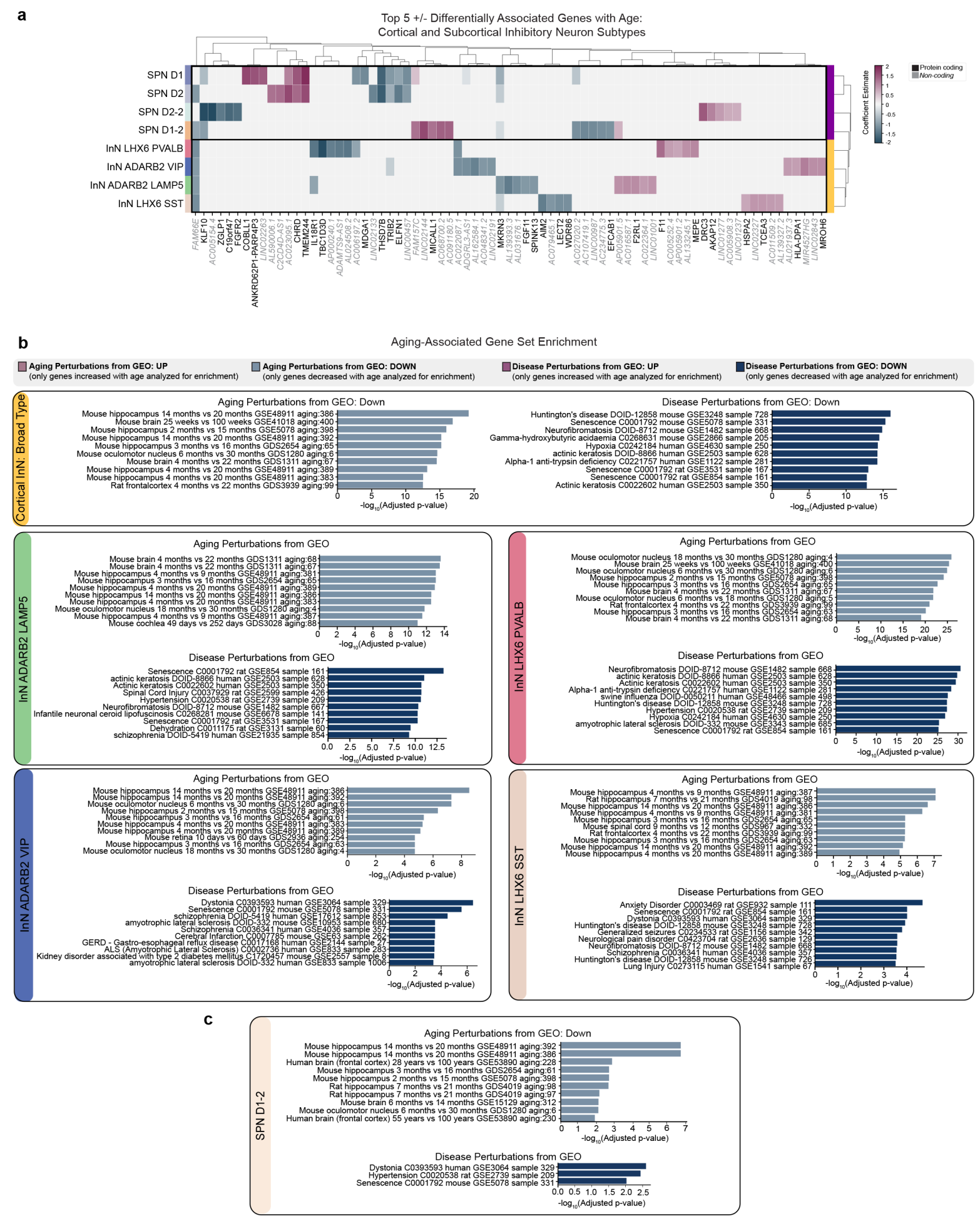
a
Top 5 +/- Differentially Associated Genes with Age:
Cortical and Subcortical Inhibitory Neuron Subtypes
SPN D1
SPN D2
SPN D2-2
SPN D1-2
InN LHX6 PVALB
InN ADARB2 VIP
InN ADARB2 LAMP5
InN LHX6 SST
Protein coding
Non-coding
Coefficient Estimate
b
Aging-Associated Gene Set Enrichment
Aging Perturbations from GEO: UP
(only genes increased with age analyzed for enrichment)
Aging Perturbations from GEO: DOWN
(only genes decreased with age analyzed for enrichment)
Disease Perturbations from GEO: UP
(only genes increased with age analyzed for enrichment)
Disease Perturbations from GEO: DOWN
(only genes decreased with age analyzed for enrichment)
Cortical InN: Broad Type
Aging Perturbations from GEO: Down
Mouse hippocampus 14 months vs 20 months GSE48911 aging:386
Mouse brain 25 weeks vs 100 weeks GSE41018 aging:400
Mouse hippocampus 2 months vs 15 months GSE5078 aging:398
Mouse hippocampus 14 months vs 20 months GSE48911 aging:392
Mouse hippocampus 3 months vs 16 months GDS2654 aging:65
Mouse oculomotor nucleus 6 months vs 30 months GDS1280 aging:6
Mouse brain 4 months vs 22 months GDS1311 aging:67
Mouse hippocampus 4 months vs 20 months GSE48911 aging:389
Mouse hippocampus 4 months vs 20 months GSE48911 aging:383
Rat frontalcortex 4 months vs 22 months GDS3939 aging:99
-log10(Adjusted p-value)
Disease Perturbations from GEO: Down
Huntington's disease DOID-12858 mouse GSE3248 sample 728
Senescence C0001792 mouse GSE5078 sample 331
Neurofibromatosis DOID-8712 mouse GSE1482 sample 668
Gamma-hydroxybutyric acidaemia C0268631 mouse GSE2866 sample 205
Hypoxia C0242184 human GSE4630 sample 250
actinic keratosis DOID-8866 human GSE2503 sample 628
Alpha-1 anti-trypsin deficiency C0221757 human GSE1122 sample 281
Senescence C0001792 rat GSE3531 sample 167
Senescence C0001792 rat GSE854 sample 161
Actinic keratosis C0022602 human GSE2503 sample 350
-log10(Adjusted p-value)
InN ADARB2 LAMP5
Aging Perturbations from GEO
Mouse brain 4 months vs 22 months GDS1311 aging:68
Mouse brain 4 months vs 22 months GDS1311 aging:67
Mouse hippocampus 4 months vs 9 months GSE48911 aging:381
Mouse hippocampus 3 months vs 16 months GDS2654 aging:65
Mouse hippocampus 4 months vs 20 months GSE48911 aging:389
Mouse hippocampus 14 months vs 20 months GSE48911 aging:386
Mouse hippocampus 4 months vs 20 months GSE48911 aging:383
Mouse oculomotor nucleus 18 months vs 30 months GDS1280 aging:4
Mouse hippocampus 4 months vs 9 months GSE48911 aging:387
Mouse cochlea 49 days vs 252 days GDS3028 aging:88
-log10(Adjusted p-value)
Disease Perturbations from GEO
Senescence C0001792 rat GSE854 sample 161
actinic keratosis DOID-8866 human GSE2503 sample 628
Actinic keratosis C0022602 human GSE2503 sample 350
Spinal Cord Injury C0037929 rat GSE2599 sample 426
Hypertension C0020538 rat GSE2739 sample 209
Neurofibromatosis DOID-8712 mouse GSE1482 sample 667
Infantile neuronal ceroid lipofuscinosis C0268281 mouse GSE6678 sample 141
Senescence C0001792 rat GSE3531 sample 167
Dehydration C0011175 rat GSE3131 sample 60
schizophrenia DOID-5419 human GSE21935 sample 854
-log10(Adjusted p-value)
InN LHX6 PVALB
Aging Perturbations from GEO
Mouse oculomotor nucleus 18 months vs 30 months GDS1280 aging:4
Mouse brain 25 weeks vs 100 weeks GSE41018 aging:400
Mouse oculomotor nucleus 6 months vs 30 months GDS1280 aging:6
Mouse hippocampus 2 months vs 15 months GSE5078 aging:398
Mouse hippocampus 3 months vs 16 months GDS2654 aging:65
Mouse brain 4 months vs 22 months GDS1311 aging:67
Mouse oculomotor nucleus 6 months vs 18 months GDS1280 aging:5
Rat frontalcortex 4 months vs 22 months GDS3939 aging:99
Mouse hippocampus 3 months vs 16 months GDS2654 aging:63
Mouse brain 4 months vs 22 months GDS1311 aging:68
-log10(Adjusted p-value)
Disease Perturbations from GEO
Neurofibromatosis DOID-8712 mouse GSE1482 sample 668
actinic keratosis DOID-8866 human GSE2503 sample 628
Actinic keratosis C0022602 human GSE2503 sample 350
Alpha-1 anti-trypsin deficiency C0221757 human GSE1122 sample 281
swine influenza DOID-0050211 human GSE48466 sample 498
Huntington's disease DOID-12858 mouse GSE3248 sample 728
Hypertension C0020538 rat GSE2739 sample 209
Hypoxia C0242184 human GSE4630 sample 250
amyotrophic lateral sclerosis DOID-332 mouse GSE3343 sample 685
Senescence C0001792 rat GSE854 sample 161
-log10(Adjusted p-value)
InN ADARB2 VIP
Aging Perturbations from GEO
Mouse hippocampus 14 months vs 20 months GSE48911 aging:386
Mouse hippocampus 14 months vs 20 months GSE48911 aging:392
Mouse oculomotor nucleus 6 months vs 30 months GDS1280 aging:6
Mouse hippocampus 2 months vs 15 months GSE5078 aging:398
Mouse hippocampus 3 months vs 16 months GDS2654 aging:61
Mouse hippocampus 4 months vs 20 months GSE48911 aging:383
Mouse hippocampus 4 months vs 20 months GSE48911 aging:389
Mouse retina 10 days vs 60 days GDS2936 aging:254
Mouse hippocampus 3 months vs 16 months GDS2654 aging:63
Mouse oculomotor nucleus 18 months vs 30 months GDS1280 aging:4
-log10(Adjusted p-value)
Disease Perturbations from GEO
Dystonia C0393593 human GSE3064 sample 329
Senescence C0001792 mouse GSE5078 sample 331
schizophrenia DOID-5419 human GSE17612 sample 853
amyotrophic lateral sclerosis DOID-332 mouse GSE10953 sample 680
Schizophrenia C0036341 human GSE4036 sample 357
Cerebral Infarction C0007785 mouse GSE63 sample 262
GERD - Gastro-esophageal reflux disease C0017168 human GSE2144 sample 27
ALS (Amyotrophic Lateral Sclerosis) C0002736 human GSE833 sample 283
Kidney disorder associated with type 2 diabetes mellitus C1720457 mouse GSE2557 sample 8
amyotrophic lateral sclerosis DOID-332 human GSE833 sample 1006
-log10(Adjusted p-value)
InN LHX6 SST
Aging Perturbations from GEO
Mouse hippocampus 4 months vs 9 months GSE48911 aging:387
Rat hippocampus 7 months vs 21 months GDS4019 aging:98
Mouse hippocampus 14 months vs 20 months GSE48911 aging:386
Mouse hippocampus 4 months vs 9 months GSE48911 aging:381
Mouse hippocampus 3 months vs 16 months GDS2654 aging:65
Mouse spinal cord 9 months vs 12 months GDS967 aging:332
Rat frontalcortex 4 months vs 22 months GDS3939 aging:99
Mouse hippocampus 3 months vs 16 months GDS2654 aging:63
Mouse hippocampus 14 months vs 20 months GSE48911 aging:392
Mouse hippocampus 4 months vs 20 months GSE48911 aging:389
-log10(Adjusted p-value)
Disease Perturbations from GEO
Anxiety Disorder C0003469 rat GSE932 sample 111
Senescence C0001792 rat GSE854 sample 161
Dystonia C0393593 human GSE3064 sample 329
Huntington's disease DOID-12858 mouse GSE3248 sample 728
Generalized seizures C0234533 rat GSE1156 sample 342
Neurological pain disorder C0423704 rat GSE2636 sample 129
Neurofibromatosis DOID-8712 mouse GSE1482 sample 668
Schizophrenia C0036341 human GSE4036 sample 357
Huntington's disease DOID-12858 mouse GSE3248 sample 726
Lung Injury C0273115 human GSE1541 sample 67
-log10(Adjusted p-value)
c
SPN D1-2
Aging Perturbations from GEO: Down
Mouse hippocampus 14 months vs 20 months GSE48911 aging:392
Mouse hippocampus 14 months vs 20 months GSE48911 aging:386
Human brain (frontal cortex) 28 years vs 100 years GSE53890 aging:228
Mouse hippocampus 3 months vs 16 months GDS2654 aging:61
Mouse hippocampus 2 months vs 15 months GSE5078 aging:398
Rat hippocampus 7 months vs 21 months GDS4019 aging:98
Rat hippocampus 7 months vs 21 months GDS4019 aging:97
Mouse brain 6 months vs 14 months GSE15129 aging:312
Mouse oculomotor nucleus 6 months vs 30 months GDS1280 aging:6
Human brain (frontal cortex) 55 years vs 100 years GSE53890 aging:230
-log10(Adjusted p-value)
Disease Perturbations from GEO
Dystonia C0393593 human GSE3064 sample 329
Hypertension C0020538 rat GSE2739 sample 209
Senescence C0001792 mouse GSE5078 sample 331
-log10(Adjusted p-value)

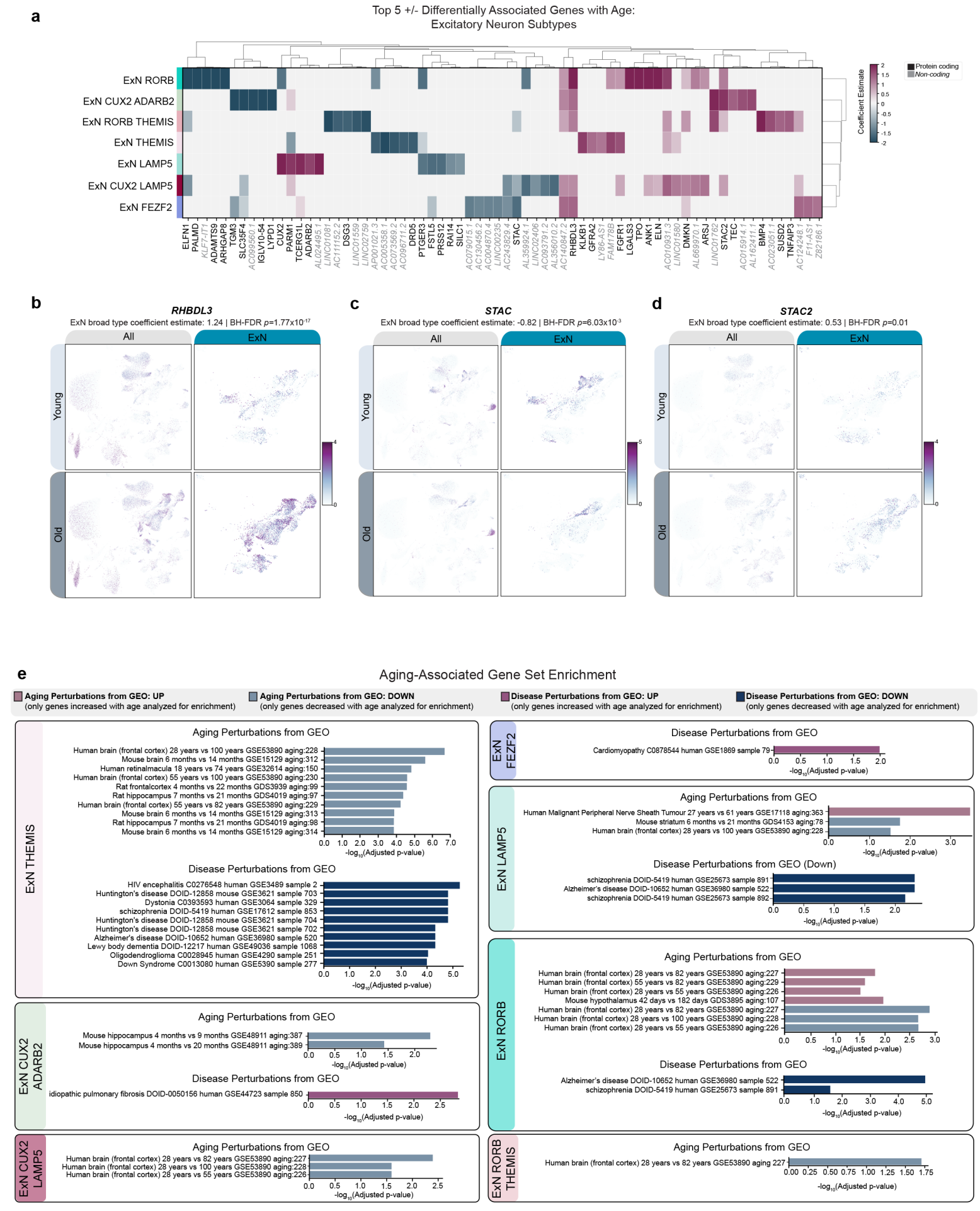
a
Top 5 +/- Differentially Associated Genes with Age:
Excitatory Neuron Subtypes
ExN RORB
ExN CUX2 ADARB2
ExN RORB THEMIS
ExN THEMIS
ExN LAMP5
ExN CUX2 LAMP5
ExN FEZF2
Coefficient Estimate
Protein coding
Non-coding
ELFN1 PALMD KLF7-IT1 ADAMTS9 ARHGAP8 TGM3 SLC35F4 AC099560.1 IGLV10-54 LYPD1 CUX2 PARM1 TCERG1L ADARB2 AL024495.1 LINC01081 AC111152.2 DSG3 LINC01559 LINC02759 AP001021.3 AC005358.1 AC073569.2 AC096711.2 DRD5 PTGER3 FSTL5 PRSS12 RAI14 SILC1 AC079015.1 AC130456.2 AC004870.4 LINC00235 AC243829.4 STAC AL359924.1 LINC02406 AC093791.2 AL356010.2 AC140847.2 RHBDL3 KLKB1 GFRA2 LY86-AS1 FAM178B FGFR1 LGALS3 TPO ANK1 ELN AC010931.3 LINC01580 DMKN AL669970.1 ARSJ LINC01762 STAC2 TEC AC015914.1 AL162411.1 BMP4 AC023051.1 SUSD2 TNFAIP3 AC124248.1 F11-AS1 Z82186.1
b
RHBDL3
ExN broad type coefficient estimate: 1.24 | BH-FDR p=1.77x10-17
All
ExN
Young
Old
c
STAC
ExN broad type coefficient estimate: -0.82 | BH-FDR p=6.03x10-3
d
STAC2
ExN broad type coefficient estimate: 0.53 | BH-FDR p=0.01
e
Aging-Associated Gene Set Enrichment
Aging Perturbations from GEO: UP (only genes increased with age analyzed for enrichment)
Aging Perturbations from GEO: DOWN (only genes decreased with age analyzed for enrichment)
Disease Perturbations from GEO: UP (only genes increased with age analyzed for enrichment)
Disease Perturbations from GEO: DOWN (only genes decreased with age analyzed for enrichment)
ExN THEMIS
Aging Perturbations from GEO
Human brain (frontal cortex) 28 years vs 100 years GSE53890 aging:228
Mouse brain 6 months vs 14 months GSE15129 aging:312
Human retinalmacula 18 years vs 74 years GSE32614 aging:150
Human brain (frontal cortex) 55 years vs 100 years GSE53890 aging:230
Rat frontalcortex 4 months vs 22 months GDS3939 aging:99
Rat hippocampus 7 months vs 21 months GDS4019 aging:97
Human brain (frontal cortex) 55 years vs 82 years GSE53890 aging:229
Mouse brain 6 months vs 14 months GSE15129 aging:313
Rat hippocampus 7 months vs 21 months GDS4019 aging:98
Mouse brain 6 months vs 14 months GSE15129 aging:314
-log10(Adjusted p-value)
Disease Perturbations from GEO
HIV encephalitis C0276548 human GSE3489 sample 2
Huntington's disease DOID-12858 mouse GSE3621 sample 703
Dystonia C0393593 human GSE3064 sample 329
schizophrenia DOID-5419 human GSE17612 sample 853
Huntington's disease DOID-12858 mouse GSE3621 sample 704
Huntington's disease DOID-12858 mouse GSE3621 sample 702
Alzheimer's disease DOID-10652 human GSE36980 sample 520
Lewy body dementia DOID-12217 human GSE49036 sample 1068
Oligodendroglioma C0028945 human GSE4290 sample 251
Down Syndrome C0013080 human GSE5390 sample 277
-log10(Adjusted p-value)
ExN CUX2 ADARB2
Aging Perturbations from GEO
Mouse hippocampus 4 months vs 9 months GSE48911 aging:387
Mouse hippocampus 4 months vs 20 months GSE48911 aging:389
-log10(Adjusted p-value)
Disease Perturbations from GEO
idiopathic pulmonary fibrosis DOID-0050156 human GSE44723 sample 850
-log10(Adjusted p-value)
ExN CUX2 LAMP5
Aging Perturbations from GEO
Human brain (frontal cortex) 28 years vs 82 years GSE53890 aging:227
Human brain (frontal cortex) 28 years vs 100 years GSE53890 aging:228
Human brain (frontal cortex) 28 years vs 55 years GSE53890 aging:226
-log10(Adjusted p-value)
ExN FEZF2
Disease Perturbations from GEO
Cardiomyopathy C0878544 human GSE1869 sample 79
-log10(Adjusted p-value)
ExN LAMP5
Aging Perturbations from GEO
Human Malignant Peripheral Nerve Sheath Tumour 27 years vs 61 years GSE17118 aging:363
Mouse striatum 6 months vs 21 months GDS4153 aging:78
Human brain (frontal cortex) 28 years vs 100 years GSE53890 aging:228
-log10(Adjusted p-value)
Disease Perturbations from GEO (Down)
schizophrenia DOID-5419 human GSE25673 sample 891
Alzheimer's disease DOID-10652 human GSE36980 sample 522
schizophrenia DOID-5419 human GSE25673 sample 892
-log10(Adjusted p-value)
ExN RORB
Aging Perturbations from GEO
Human brain (frontal cortex) 28 years vs 82 years GSE53890 aging:227
Human brain (frontal cortex) 55 years vs 82 years GSE53890 aging:229
Human brain (front cortex) 28 years vs 55 years GSE53890 aging:226
Mouse hypothalamus 42 days vs 182 days GDS3895 aging:107
Human brain (frontal cortex) 28 years vs 82 years GSE53890 aging:227
Human brain (frontal cortex) 28 years vs 100 years GSE53890 aging:228
Human brain (front cortex) 28 years vs 55 years GSE53890 aging:226
-log10(Adjusted p-value)
Disease Perturbations from GEO
Alzheimer's disease DOID-10652 human GSE36980 sample 522
schizophrenia DOID-5419 human GSE25673 sample 891
-log10(Adjusted p-value)
ExN RORB THEMIS
Aging Perturbations from GEO
Human brain (frontal cortex) 28 years vs 82 years GSE53890 aging 227
-log10(Adjusted p-value)

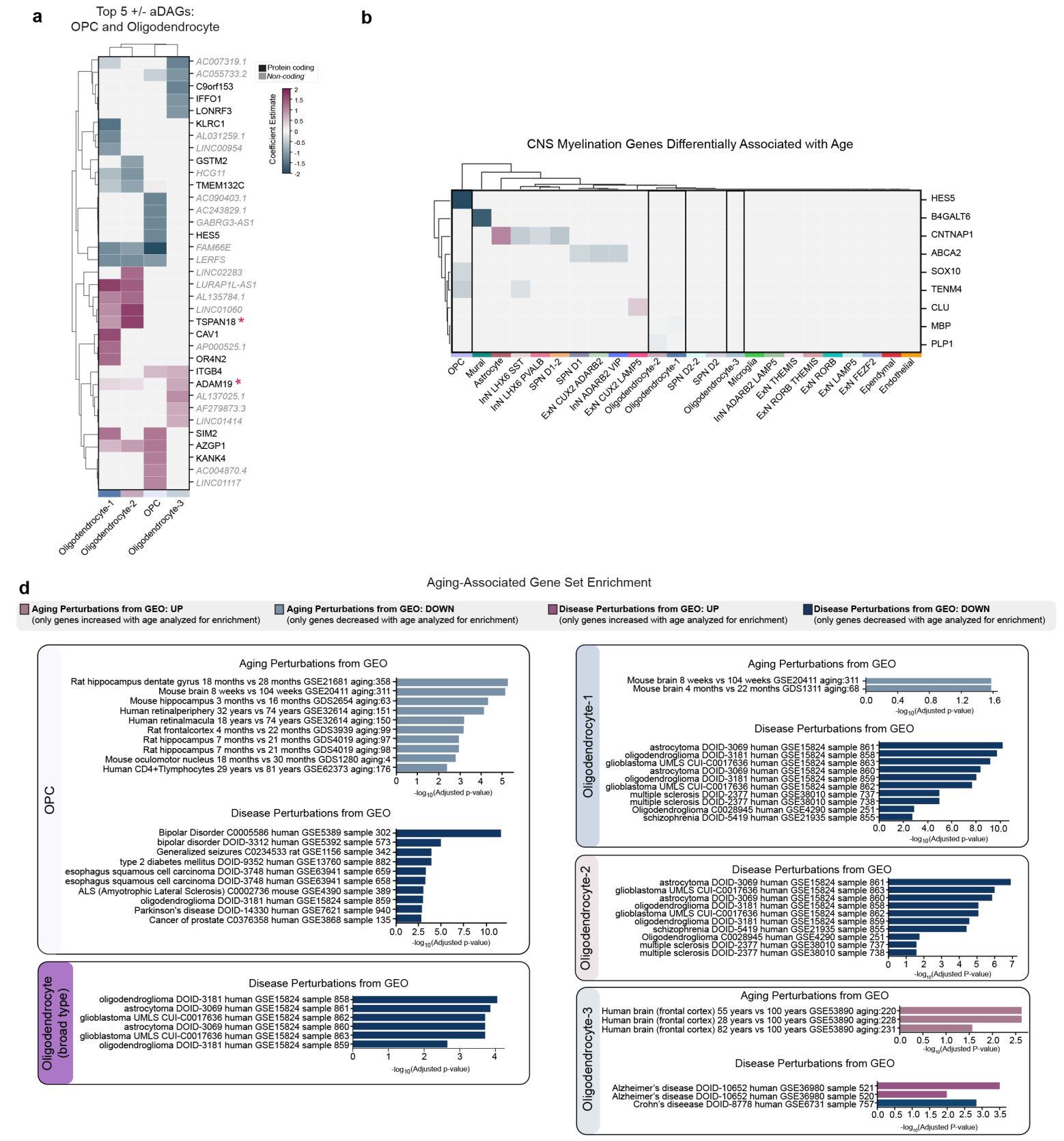
a
Top 5 +/- aDAGs:
OPC and Oligodendrocyte
Protein coding
Non-coding
Coefficient Estimate
AC007319.1
AC055733.2
C9orf153
IFFO1
LONRF3
KLRC1
AL031259.1
LINC00954
GSTM2
HCG11
TMEM132C
AC090403.1
AC243829.1
GABRG3-AS1
HES5
FAM66E
LERFS
LINC02283
LURAP1L-AS1
AL135784.1
LINC01060
TSPAN18 *
CAV1
AP000525.1
OR4N2
ITGB4
ADAM19 *
AL137025.1
AF279873.3
LINC01414
SIM2
AZGP1
KANK4
AC004870.4
LINC01117
Oligodendrocyte-1
Oligodendrocyte-2
OPC
Oligodendrocyte-3
b
CNS Myelination Genes Differentially Associated with Age
HES5
B4GALT6
CNTNAP1
ABCA2
SOX10
TENM4
CLU
MBP
PLP1
OPC
Mural
Astrocyte
InN LHX6 SST
InN LHX6 PVALB
SPN D1-2
SPN D1
ExN CUX2 ADARB2
InN ADARB2 VIP
ExN CUX2 LAMP5
Oligodendrocyte-2
Oligodendrocyte-1
SPN D2-2
SPN D2
Oligodendrocyte-3
Microglia
InN ADARB2 LAMP5
ExN THEMIS
ExN RORB THEMIS
ExN RORB
ExN LAMP5
ExN FEZF2
Ependymal
Endothelial
d
Aging-Associated Gene Set Enrichment
Aging Perturbations from GEO: UP
(only genes increased with age analyzed for enrichment)
Aging Perturbations from GEO: DOWN
(only genes decreased with age analyzed for enrichment)
Disease Perturbations from GEO: UP
(only genes increased with age analyzed for enrichment)
Disease Perturbations from GEO: DOWN
(only genes decreased with age analyzed for enrichment)
OPC
Aging Perturbations from GEO
Rat hippocampus dentate gyrus 18 months vs 28 months GSE21681 aging:358
Mouse brain 8 weeks vs 104 weeks GSE20411 aging:311
Mouse hippocampus 3 months vs 16 months GDS2654 aging:63
Human retinalperiphery 32 years vs 74 years GSE32614 aging:151
Human retinalmacula 18 years vs 74 years GSE32614 aging:150
Rat frontalcortex 4 months vs 22 months GDS3939 aging:99
Rat hippocampus 7 months vs 21 months GDS4019 aging:97
Rat hippocampus 7 months vs 21 months GDS4019 aging:98
Mouse oculomotor nucleus 18 months vs 30 months GDS1280 aging:4
Human CD4+Tlymphocytes 29 years vs 81 years GSE62373 aging:176
-log10(Adjusted p-value)
Disease Perturbations from GEO
Bipolar Disorder C0005586 human GSE5389 sample 302
bipolar disorder DOID-3312 human GSE5392 sample 573
Generalized seizures C0234533 rat GSE1156 sample 342
type 2 diabetes mellitus DOID-9352 human GSE13760 sample 882
esophagus squamous cell carcinoma DOID-3748 human GSE63941 sample 659
esophagus squamous cell carcinoma DOID-3748 human GSE63941 sample 658
ALS (Amyotrophic Lateral Sclerosis) C0002736 mouse GSE4390 sample 389
oligodendroglioma DOID-3181 human GSE15824 sample 859
Parkinson's disease DOID-14330 human GSE7621 sample 940
Cancer of prostate C0376358 human GSE3868 sample 135
-log10(Adjusted p-value)
Oligodendrocyte (broad type)
Disease Perturbations from GEO
oligodendroglioma DOID-3181 human GSE15824 sample 858
astrocytoma DOID-3069 human GSE15824 sample 861
glioblastoma UMLS CUI-C0017636 human GSE15824 sample 862
astrocytoma DOID-3069 human GSE15824 sample 860
glioblastoma UMLS CUI-C0017636 human GSE15824 sample 863
oligodendroglioma DOID-3181 human GSE15824 sample 859
-log10(Adjusted p-value)
Oligodendrocyte-1
Aging Perturbations from GEO
Mouse brain 8 weeks vs 104 weeks GSE20411 aging:311
Mouse brain 4 months vs 22 months GDS1311 aging:68
-log10(Adjusted p-value)
Disease Perturbations from GEO
astrocytoma DOID-3069 human GSE15824 sample 861
oligodendroglioma DOID-3181 human GSE15824 sample 858
glioblastoma UMLS CUI-C0017636 human GSE15824 sample 863
astrocytoma DOID-3069 human GSE15824 sample 860
oligodendroglioma DOID-3181 human GSE15824 sample 859
glioblastoma UMLS CUI-C0017636 human GSE15824 sample 862
multiple sclerosis DOID-2377 human GSE38010 sample 737
multiple sclerosis DOID-2377 human GSE38010 sample 738
Oligodendroglioma C0028945 human GSE4290 sample 251
schizophrenia DOID-5419 human GSE21935 sample 855
-log10(Adjusted p-value)
Oligodendrocyte-2
Disease Perturbations from GEO
astrocytoma DOID-3069 human GSE15824 sample 861
glioblastoma UMLS CUI-C0017636 human GSE15824 sample 863
astrocytoma DOID-3069 human GSE15824 sample 860
oligodendroglioma DOID-3181 human GSE15824 sample 858
glioblastoma UMLS CUI-C0017636 human GSE15824 sample 862
oligodendroglioma DOID-3181 human GSE15824 sample 859
schizophrenia DOID-5419 human GSE21935 sample 855
Oligodendroglioma C0028945 human GSE4290 sample 251
multiple sclerosis DOID-2377 human GSE38010 sample 737
multiple sclerosis DOID-2377 human GSE38010 sample 738
-log10(Adjusted P-value)
Oligodendrocyte-3
Aging Perturbations from GEO
Human brain (frontal cortex) 55 years vs 100 years GSE53890 aging:220
Human brain (frontal cortex) 28 years vs 100 years GSE53890 aging:228
Human brain (frontal cortex) 82 years vs 100 years GSE53890 aging:231
-log10(Adjusted P-value)
Disease Perturbations from GEO
Alzheimer's disease DOID-10652 human GSE36980 sample 521
Alzheimer's disease DOID-10652 human GSE36980 sample 520
Crohn's diseease DOID-8778 human GSE6731 sample 757
-log10(Adjusted P-value)

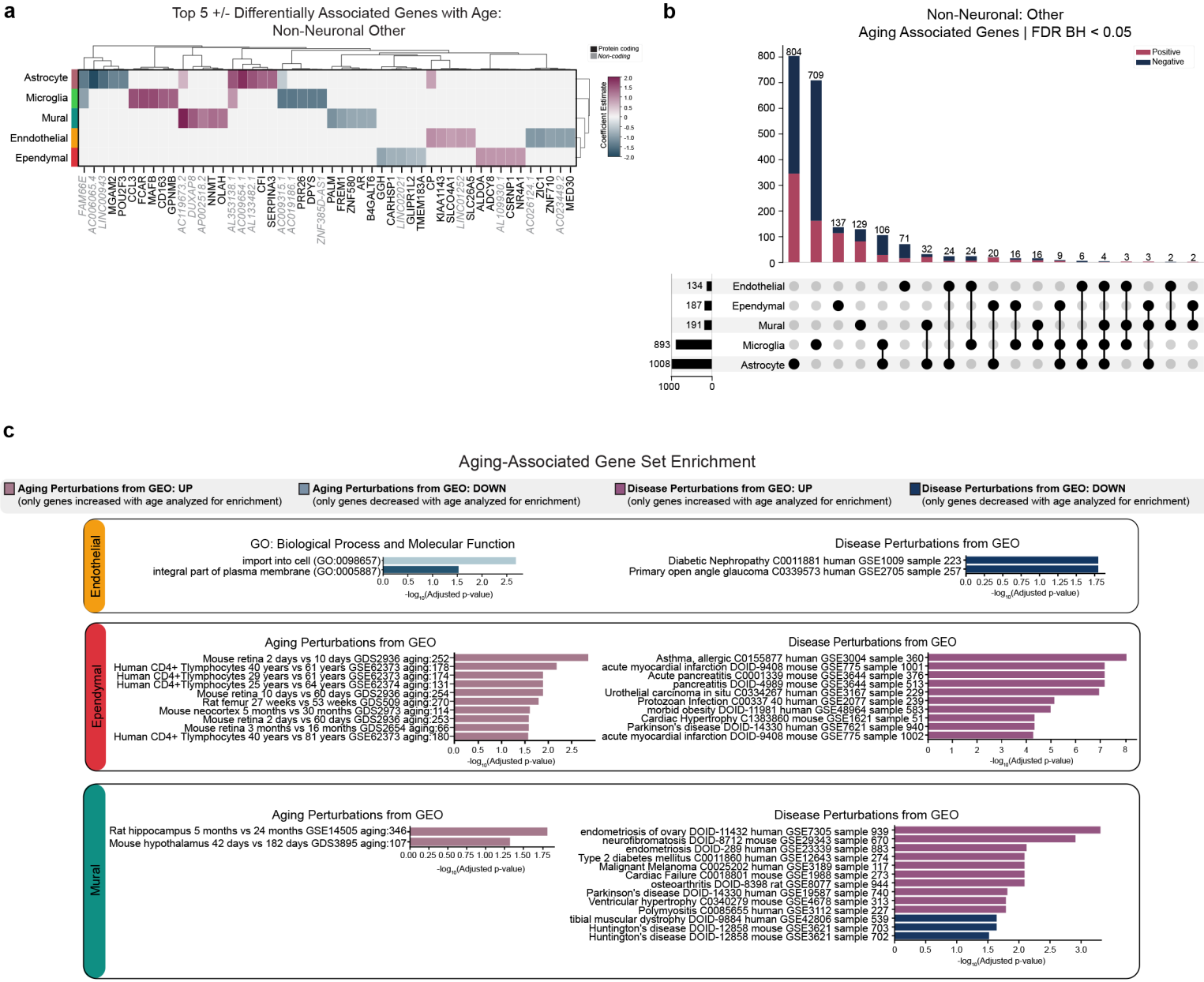
a
Top 5 +/- Differentially Associated Genes with Age:
Non-Neuronal Other
Protein coding
Non-coding
Coefficient Estimate
Astrocyte
Microglia
Mural
Enndothelial
Ependymal
FAM66E
AC006065.4
LINC00943
MGAM2
POU2F3
CCL3
FCAR
MAFB
CD163
GPNMB
AC119673.2
DUXAP8
AP002518.2
NNMT
OLAH
AL353138.1
AC009654.1
AL133482.1
CFI
SERPINA3
AC009315.1
AC019186.1
PRR26
DPYS
ZNF385D-AS1
PALM
FREM1
ZNF580
AR
B4GALT6
GGH
CARHSP1
LINC02021
GLIPR1L2
TMEM183A
CP
KIAA1143
SLCO4A1
LINC01252
SLC26A5
ALDOA
ADCY8
AL109930.1
CSRNP1
NR4A1
AC026124.1
ZIC1
ZNF710
AC023449.2
MED30
b
Non-Neuronal: Other
Aging Associated Genes | FDR BH < 0.05
Positive
Negative
804
709
137
129
106
71
32
24
24
20
16
16
9
6
4
3
3
2
2
134
187
191
893
1008
Endothelial
Ependymal
Mural
Microglia
Astrocyte
1000
0
c
Aging-Associated Gene Set Enrichment
Aging Perturbations from GEO: UP
(only genes increased with age analyzed for enrichment)
Aging Perturbations from GEO: DOWN
(only genes decreased with age analyzed for enrichment)
Disease Perturbations from GEO: UP
(only genes increased with age analyzed for enrichment)
Disease Perturbations from GEO: DOWN
(only genes decreased with age analyzed for enrichment)
Endothelial
GO: Biological Process and Molecular Function
import into cell (GO:0098657)
integral part of plasma membrane (GO:0005887)
-log10(Adjusted p-value)
Disease Perturbations from GEO
Diabetic Nephropathy C0011881 human GSE1009 sample 223
Primary open angle glaucoma C0339573 human GSE2705 sample 257
-log10(Adjusted p-value)
Ependymal
Aging Perturbations from GEO
Mouse retina 2 days vs 10 days GDS2936 aging:252
Human CD4+ Tlymphocytes 40 years vs 61 years GSE62373 aging:178
Human CD4+Tlymphocytes 29 years vs 61 years GSE62373 aging:174
Human CD4+Tlymphocytes 25 years vs 64 years GSE62374 aging:131
Mouse retina 10 days vs 60 days GDS2936 aging:254
Rat femur 27 weeks vs 53 weeks GDS509 aging:270
Mouse neocortex 5 months vs 30 months GDS2973 aging:114
Mouse retina 2 days vs 60 days GDS2936 aging:253
Mouse retina 3 months vs 16 months GDS2654 aging:66
Human CD4+ Tlymphocytes 40 years vs 81 years GSE62373 aging:180
-log10(Adjusted p-value)
Disease Perturbations from GEO
Asthma, allergic C0155877 human GSE3004 sample 360
acute myocardial infarction DOID-9408 mouse GSE775 sample 1001
Acute pancreatitis C0001339 mouse GSE3644 sample 376
pancreatitis DOID-4989 mouse GSE3644 sample 513
Urothelial carcinoma in situ C0334267 human GSE3167 sample 229
Protozoan Infection C00337 40 human GSE2077 sample 239
morbid obesity DOID-11981 human GSE48964 sample 583
Cardiac Hypertrophy C1383860 mouse GSE1621 sample 51
Parkinson's disease DOID-14330 human GSE7621 sample 940
acute myocardial infarction DOID-9408 mouse GSE775 sample 1002
-log10(Adjusted p-value)
Mural
Aging Perturbations from GEO
Rat hippocampus 5 months vs 24 months GSE14505 aging:346
Mouse hypothalamus 42 days vs 182 days GDS3895 aging:107
-log10(Adjusted p-value)
Disease Perturbations from GEO
endometriosis of ovary DOID-11432 human GSE7305 sample 939
neurofibromatosis DOID-8712 mouse GSE29343 sample 670
endometriosis DOID-289 human GSE23339 sample 883
Type 2 diabetes mellitus C0011860 human GSE12643 sample 274
Malignant Melanoma C0025202 human GSE3189 sample 117
Cardiac Failure C0018801 mouse GSE1988 sample 273
osteoarthritis DOID-8398 rat GSE8077 sample 944
Parkinson's disease DOID-14330 human GSE19587 sample 740
Ventricular hypertrophy C0340279 mouse GSE4678 sample 313
Polymyositis C0085655 human GSE3112 sample 227
tibial muscular dystrophy DOID-9884 human GSE42806 sample 539
Huntington's disease DOID-12858 mouse GSE3621 sample 703
Huntington's disease DOID-12858 mouse GSE3621 sample 702
-log10(Adjusted p-value)

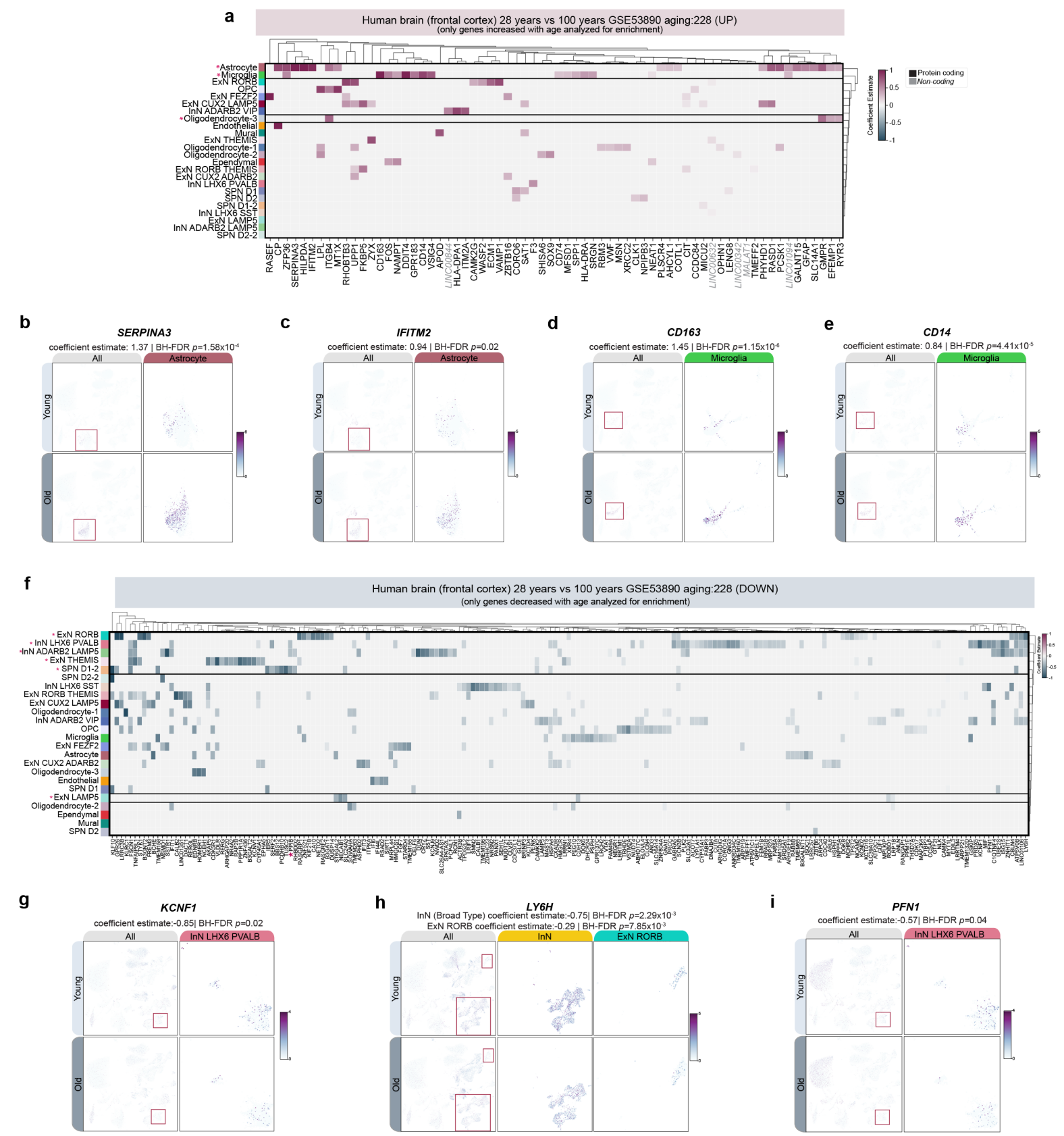
a
Human brain (frontal cortex) 28 years vs 100 years GSE53890 aging:228 (UP)
(only genes increased with age analyzed for enrichment)
Astrocyte
Microglia
ExN RORB
OPC
ExN FEZF2
ExN CUX2 LAMP5
InN ADARB2 VIP
Oligodendrocyte-3
Endothelial
Mural
ExN THEMIS
Oligodendrocyte-1
Oligodendrocyte-2
Ependymal
ExN RORB THEMIS
ExN CUX2 ADARB2
InN LHX6 PVALB
SPN D1
SPN D2
SPN D1-2
InN LHX6 SST
ExN LAMP5
InN ADARB2 LAMP5
SPN D2-2
Protein coding
Non-coding
Coefficient Estimate
b
SERPINA3
coefficient estimate: 1.37 | BH-FDR p=1.58x10-4
c
IFITM2
coefficient estimate: 0.94 | BH-FDR p=0.02
d
CD163
coefficient estimate: 1.45 | BH-FDR p=1.15x10-6
e
CD14
coefficient estimate: 0.84 | BH-FDR p=4.41x10-5
All
Astrocyte
Microglia
Young
Old
f
Human brain (frontal cortex) 28 years vs 100 years GSE53890 aging:228 (DOWN)
(only genes decreased with age analyzed for enrichment)
g
KCNF1
coefficient estimate:-0.85| BH-FDR p=0.02
InN LHX6 PVALB
h
LY6H
InN (Broad Type) coefficient estimate:-0.75| BH-FDR p=2.29x10-3
ExN RORB coefficient estimate:-0.29 | BH-FDR p=7.85x10-3
InN
ExN RORB
i
PFN1
coefficient estimate:-0.57| BH-FDR p=0.04

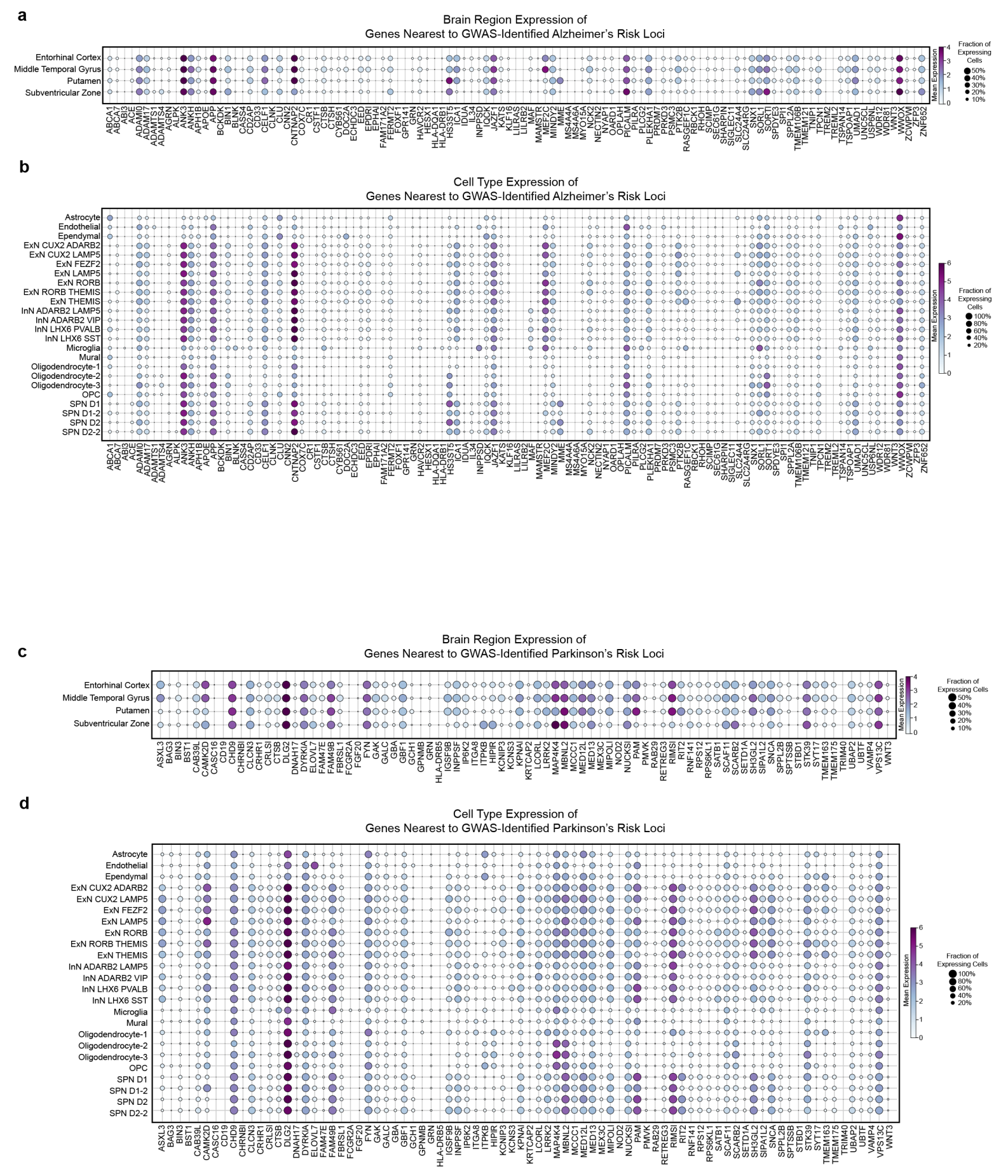
a
Brain Region Expression of
Genes Nearest to GWAS-Identified Alzheimer's Risk Loci
Entorhinal Cortex
Middle Temporal Gyrus
Putamen
Subventricular Zone
Mean Expression
Fraction of Expressing Cells
50%
40%
30%
20%
10%
b
Cell Type Expression of
Genes Nearest to GWAS-Identified Alzheimer's Risk Loci
Astrocyte
Endothelial
Ependymal
ExN CUX2 ADARB2
ExN CUX2 LAMP5
ExN FEZF2
ExN LAMP5
ExN RORB
ExN RORB THEMIS
ExN THEMIS
InN ADARB2 LAMP5
InN ADARB2 VIP
InN LHX6 PVALB
InN LHX6 SST
Microglia
Mural
Oligodendrocyte-1
Oligodendrocyte-2
Oligodendrocyte-3
OPC
SPN D1
SPN D1-2
SPN D2
SPN D2-2
Mean Expression
Fraction of Expressing Cells
100%
80%
60%
40%
20%
c
Brain Region Expression of
Genes Nearest to GWAS-Identified Parkinson's Risk Loci
Entorhinal Cortex
Middle Temporal Gyrus
Putamen
Subventricular Zone
Mean Expression
Fraction of Expressing Cells
50%
40%
30%
20%
10%
d
Cell Type Expression of
Genes Nearest to GWAS-Identified Parkinson's Risk Loci
Astrocyte
Endothelial
Ependymal
ExN CUX2 ADARB2
ExN CUX2 LAMP5
ExN FEZF2
ExN LAMP5
ExN RORB
ExN RORB THEMIS
ExN THEMIS
InN ADARB2 LAMP5
InN ADARB2 VIP
InN LHX6 PVALB
InN LHX6 SST
Microglia
Mural
Oligodendrocyte-1
Oligodendrocyte-2
Oligodendrocyte-3
OPC
SPN D1
SPN D1-2
SPN D2
SPN D2-2
Mean Expression
Fraction of Expressing Cells
100%
80%
60%
40%
20%